Synthesis and Characterization of Saccharinato Complexes of Various Group 9-12 Metals

by

Fezile Siphiwe Wiseman Potwana

Dissertation submitted in fulfilment of the academic requirements for the degree of

Master of Science

School of Chemistry and Physics, University of KwaZulu-Natal, Durban

As the candidate's supervisor I have approved this dissertation for submission.

January 2013

DECLARATION 1: PLAGIARISM

I, Fezile Siphiwe Wiseman Potwana, declare that the experimental work described in this dissertation was carried out at the School of Chemistry and Physics, University of KwaZulu-Natal, Westville campus, between January 2011 and November 2012, under the supervision of Dr. W. E. van Zyl, and that:

1. The research reported in this thesis, except where otherwise indicated, is my original research.
2. This thesis has not been submitted for any degree or examination at any other university.
3. This thesis does not contain other persons' data, pictures, graphs or other information, unless specifically acknowledged as being sourced from other persons.
4. This thesis does not contain other persons' writing, unless specifically acknowledged as being sourced from other researchers. Where other written sources have been quoted, then:
    a. Their words have been re-written but the general information attributed to them has been referenced.
    b. Where their exact words have been used, then their writing has been placed in italics and inside quotation marks, and referenced.
5. This thesis does not contain texts, graphics or tables copied and pasted from the Internet, unless specifically acknowledged, and the source being detailed in the thesis and in the references sections.

Signed

_____

Fezile Siphiwe Wiseman Potwana

DECLARATION 2: PUBLICATIONS

Details of publications:

1. F. S. W. Potwana and W. E. Van Zyl, Acta Cryst. (2011). E**67**, m1635.
2. F. S. W. Potwana and W. E. Van Zyl, Acta Cryst. (2011). E**67**, m1667–m1668.
3. Potwana *et al*., Acta Cryst. (2011). E**67**, m1665.

From all the above publications, my role included carrying out all the experimental work and contributing to the writing of the publications along with my supervisor. The other co-authors contribution was that of an editorial nature and checking on the scientific content and evaluation of my interpretation. Based on their expertise, they have added minor parts to the papers above.

Signed

_____

Fezile Siphiwe Wiseman Potwana

ABSTRACT

The aim of the study was the synthesis and characterization of new mixed ligand saccharinato complexes of various groups 9, 10, 11 and 12 metals, i.e. M = Cd(II), Co(II), Zn(II), Hg(II), Cu(II), and Ni(II) using dimethyl sulfoxide (DMSO) and amine-based ligands such as ethylenediamine (en), N-methyldiethanolamine (MDEA) and 2-(methylamino)ethanol (MEA) from the precursor $[M(C_7H_5SO_3N)_2(H_2O)_4]\cdot 2H_2O$. The new complexes were characterized by elemental analyses, solution Nuclear Magnetic Resonance (NMR), UV–Vis spectroscopy, IR ATR spectroscopy, thermal analysis and single crystal X-ray diffraction. All complexes are mononuclear except complex **(9)** which is a dinuclear Cu(II) complex. A number of the saccharinato complexes are diamagnetic, i.e. *trans*-$[Cd(sac)_2(dmso)_2(H_2O)_2]$ **(1)**, *cis*-$[Zn(sac)_2(dmso)_2]$ **(3)**, $[Hg(sac)_2(dmso)(H_2O)]$ **(4)** and *trans*-$[Cd(sac)_2(en)_2]$ **(11)** and were characterised by NMR. Some of the complexes are paramagnetic, including *trans*-$[Co(sac)_2(dmso)_2(H_2O)_2]$ **(2)**, $[Cu(sac)_2(dmso)(H_2O)_2]$ (**5**), $[Cu(sac)_2(N,O,O\text{-mdea})_2]$ **(7)**, $[Co(sac)_2(N,O,O\text{-mdea})_2]$ **(8)** and $[Ni(sac)_2(en)_2]$ **(10)**. All complexes containing the DMSO ligand were successfully analysed by single crystal X-ray diffraction, i.e. complexes **(1)** to **(5)**. The complexes crystallized in the monoclinic P21/c space group together with complex **(11)**. Complexes $[Ni(N,O,O\text{-mdea})]\cdot 2(sac)$ **(6)**, $[Cu_2(\mu\text{-}O)_2(mea)_4]\cdot 2(sac)$ **(9)**, and $[Co_2(en)_4(CO_3)_2]\cdot 2(sac)3H_2O$ **(12)** were found to crystallize in the triclinic P-1 space group. In DMSO complexes, the metal ion is positioned at the centre of symmetry and complexes **(1)** and **(2)** are octahedrally coordinated by two monodentate DMSO ligands which are *trans* to each other and two aqua-ligands which are also *trans* to each other. The ligands in complex **(3)** are tetrahedrally coordinated to the Zn(II) ion in the *cis* position and in complex **(4)** a distorted trigonal bipyramidal complex was found whereby the DMSO groups are disordered over two places and the site occupancy factors were refined to 0.504(4) and 0.496(4), respectively. Complex **(5)** consisted of Cu(II) ions in a trigonal bipyramidal geometry. Complexes **(6)** and **(12)** have an octahedral coordination geometry with the metal ion positioned at the centre of symmetry. Complex **(9)** is a centrosymmetric binuclear complex containing two strongly distorted square-pyramidal coordinated copper(II) ions bound together by two alkoxo bridges. The bridging oxygen is a deprotonated oxygen of the ethanolic group of MDEA. The MDEA ligand also coordinates to the copper(II) ions through its nitrogen, while the other ethanolic group is not involved in the coordination. For complexes **(6)**, **(9)** and **(12)** the saccharin acts as a weak counter ion and complex **(12)** has a

lattice containing three water molecules of crystallization held together by a hydrogen-bonded network.

The saccharin ligands in the mononuclear complexes are coordinated *via* the N-atom. Thermal behaviour of the complexes was studied using DTA and TGA in nitrogen atmosphere. The complexes are stable below 200 °C and after that they start to show degradation and decomposition characteristics. The complexes lose ligands first and the saccharinate anion at higher temperatures for complexes **(1)** to **(5)** and **(11)**. For complexes **(6)**, **(9)** and **(12)** there is an interchangeable loss of amine ligands with saccharin anions. All the complexes show either endothermic or exothermic DTA peaks at various stages.

DEDICATION

To my father, mother and siblings.

"Everything of importance has been said by someone who didn't invent it. Alfred North Whitehead."

ACKNOWLEDGEMENTS

I would like to give all the praises and glory to God the Almighty, in the name of my Lord and Saviour Jesus Christ, through whose inspiration and divine power has made it possible, for me, to accomplish and finally achieve this academic level and more.

I would like to thank my parents, Michael and Florence, my sisters Phumelele and Nikiwe for their unconditional loving support and encouragement in all spheres of my life.

I would like to thank my supervisor, Dr. Werner van Zyl for his support and guidance during my time as a Masters student and for making this thesis possible through his rich and wealth of knowledge in synthetic chemistry.

I would like to thank the University of KwaZulu-Natal and the School of Chemistry and Physics for accepting me as a Masters student in their campus , to further my studies.

I would like to thank my colleagues and friends Michael Pillay, Vashen Moodley, Sicelo Sithole, Shirveen Sewpersad, Monisola Ikhile and Halliru Ibrahim for all their support and help in my academic career and private life.

I would like to thank the National Research Foundation (NRF) for their financial support during the course of this study and for understanding that young African minds need their support to advance their education, and increase the knowledge of the nation.

I would like to thank everyone who has played a major role in my study career whom I didn't mention by name in my list, my sincere gratitude's.

"Thank you for everything"

LIST OF ABBREVIATIONS

The elements will be annotated on the periodic table.

°C	degree Celsius	nm	nanometre
g ml^{-1}	grams per millilitre	^{1}H	proton NMR
r.t.	room temperature	^{13}C	carbon NMR
ml	milliletre	MHz	mega hertz
g	gram	ppm	part per million
o-	ortho	*trans*-	transatlantic
α	alpha	λ_{max}	maximum wavelength
β	beta	mmol	milimole
Å	Angstrom	Mp	melting point
K	Kelvin	ν	infrared absorption
%	percentage	m	multiplets
M^{2+} or $M^{(II)}$	metal centre	s	singlets
(º) or º	degree	sym	symmetric
cm^{-1}	per centimetre	δ	chemical shift
°C min^{-1}	degree per minute	mg	milligram
cm^{3} min^{-1}	centimetre cube per minute	$SiMe_4$	tetramethylsilane
T	temperature	Calc.	calculated
M^{-1} cm^{-1}	per molar per centimetre	ε	molar absorptiviy
$M^{-1}cm^{-1}$	per molarity per centimetre	asym	asymmetric

pKa	acid dissociation constant at logarithmic scale
$[M(sac)_2(H_2O)_4]\cdot 2H_2O$	tetraaquabis(saccharinato)M^{II} dihydrate

List of Instrumentations

XRD	X-ray diffractometry
FTIR-ATR	Fourier Transform Infrared- Attenuated Total Reflectance
TGA	Thermogravimetric Analyser
UV-Vis	ultraviolet-visible spectrophotometer
NMR	Nuclear Magnetic Resonance

List of Chemicals

HSac	saccharin	MAE	2-(Methylamino)ethanol
en	ethylenediamine	MDEA	N-methyldiethanolamine
DMSO	dimethyl sulfoxide	MeOD	deuterated methanol
Sac	saccharinato anion		

TABLE OF CONTETS

DECLARATION 1: PLAGIARISM ii

DECLARATION 2: PUBLICATIONS iii

ABSTRACT iv

DEDICATION vi

ACKNOWLEDGEMENTS viii

LIST OF ABBREVIATIONS ix

List of Instrumentations x

List of Chemicals x

LIST OF FIGURES xv

LIST OF SCHEMES xviii

LIST OF TABLES xix

CHAPTER 1 1

INTRODUCTION 1

1.1 General Description of Saccharin 1

1.2 The AH-B-X Taste Receptor Theory of Artificial Sweeteners 2

1.3 Artificial Sweeteners 3

1.4 Advantages and Disadvantages of Saccharin 8

1.5 Synthesis of Saccharin 8

1.6 Sodium Saccharinate and Thiosaccharin 10

1.7 Saccharinato Ligand: Metal Complexes of Saccharin and Its Salts 11

1.7.1 Saccharinate Salts 11

1.7.2 Monodentate Coordination of Saccharinato Complexes via the N-atom 12

1.7.3 Saccharinato Mixed Ligand Complexes 13

1.7.4 Metal Complexes of Zn(II) Coordinated to a Mono-or Bidentate Ligand 14

1.7.5 Metal Complexes of M(II) Coordinated to a Monodenate, Bidentate, Tridenate and Bridging Ligand: M(II) = Cu, Co, Cd, Ni and Hg 15

1.7.6 Monodentate Coordination of Saccharinato Complexes via the O-atom 17

1.7.7 Bidentate (N, O) and Tridentate (N, O, O) Coordination of Saccharinato Complexes 19

1.7.8 Unusual Ambidentate Coordination Behaviour of Saccharinato Complexes 20

1.7.9 Bonded and Non-Bonded Saccharinate Anion and Free Saccharin in the Complex 21

1.8 Characteristics of Saccharinato Complexes on Biological Studies 23

1.9 Coordinating Ligand: Dimethyl Sulfoxide 24

1.9.1 Dimethyl Sulfoxide 24
1.9.2 Synthesis of Dimethyl Sulfoxide and Its Reactivity Properties 24
1.10 General Overview of Amines 25
1.10.1 Amines 25
1.11 The Aims and Objectives of this Study 26
1.11.1 Motivation for study 27
1.11.2 Aims of the study 27
1.12 References 28
CHAPTER 2 37
EXPERIMENTAL SECTION 37
2.1 Introduction 37
2.2 Materials and Instrumentation 37
2.2.1 Materials 37
2.2.2 Instrumentation 38
2.3 Synthesis of Saccharinato Complexes of Dimethyl Sulfoxide 39
2.3.1 Synthesis of *trans*-[$Cd(sac)_2(dmso)_2(H_2O)_2$] (**1**) 39
2.3.2 Synthesis of *trans*-[$Co(sac)_2(dmso)_2(H_2O)_2$] (**2**) 39
2.3.3 Synthesis of [$Zn(sac)_2(dmso)_2$] (**3**) 40
2.3.4 Synthesis of [$Hg(sac)_2(dmso)(H_2O)$] (**4**) 40
2.3.5 Synthesis of [$Cu(sac)_2(dmso)(H_2O)_2$] (**5**) 41
2.4 Synthesis of Saccharinato Complexes of N-methyldiethanolamine and 2-(methylamino)ethanol 41
2.4.1 Synthesis of [Ni(*N,O,O*-mdea)$_2$]·2(sac) (**6**) 41
2.4.2 Synthesis of [$Cu(sac)_2$(*N,O,O*-mdea)$_2$] (**7**) 42
2.4.3 Synthesis of [$Co(sac)_2$(*N,O,O*-mdea)$_2$] (**8**) 42
2.4.4 Synthesis of [$(Cu_2(\mu$-*O*$)_2(mea)_4]\cdot 2(sac)$ (**9**) 42
2.5 Synthesis of Saccharinato Complexes of Ethylenediamine 43
2.5.1 Synthesis of [$Ni(sac)_2(en)_2$] (**10**) 43
2.5.2 Synthesis of *trans*-[$Cd(sac)_2(en)_2$] (**11**) 43
2.5.3 Synthesis of [$Co_2(en)_4(CO_3)_2]\cdot 2(sac)3H_2O$ (**12**) 44
2.6 X-ray Crystallography 44
2.6.1 Crystal Structure Determination for Complexes (**2**) and (**6**). 44
2.6.2 Crystal Structure Determination for Complexes (**1**), (**3**), (**4**) and (**9**). 44
2.6.3 Crystal Structure Determination for Complexes (**11**) and (**12**). 45

2.7 References 47
CHAPTER 3 49
SACCHARINATO COMPLEXES WITH A DIRECT M-N BOND 49
3.1 Introduction 49
3.2 Results and Discussion 50
3.2.1 Synthesis of Tetraaquabis(saccharinato)M(II) dihydrate Precursors 50
3.2.2 Synthesis of Mixed Aqua-and Dimethyl Sulfoxide Saccharinato Complexes 51
3.2.3 Synthesis of Amine Saccharinato Complexes 52
3.3 Spectroscopic Properties 53
3.3.1 Nuclear Magnetic Resonance (NMR) Analysis of Complexes 53
3.3.2 Fourier Transform Infrared Spectroscopy (FTIR) Using ATR Spectra 55
3.3.3 UV-Vis spectroscopy 57
3.4 Description of the X-ray Crystal Structures of Saccharinato Complexes 59
3.4.1 Crystal Structures 59
3.4.1.1 *trans*-[$Cd(sac)_2(dmso)_2(H_2O)_2$] and *trans*-[$Co(sac)_2(dmso)_2(H_2O)_2$] 60
3.4.1.2 Hydrogen Bonding of Complexes (**1**) and (**2**) 63
3.4.1.3 [$Zn(sac)_2(dmso)_2$] 65
3.4.1.4 [$Hg(sac)_2(dmso)(H_2O)$] 66
3.4.1.5 Hydrogen Bonding of Complexes (**3**) and (**4**) 68
3.4.1.6 [$Cu(sac)_2(dmso)(H_2O)_2$] 71
3.4.1.7 Hydrogen bonding of complex (**5**) 72
3.4.1.8 *trans*-[$Cd(sac)_2(en)_2$] 73
3.4.1.9 Hydrogen bonding of complex (**11**) 74
3.5 Thermal analysis 75
3.6 References: 79
CHAPTER 4 82
SCARCE CATIONIC COMPLEXES WITH SACCHARINATE AS ANION 82
4.1 Introduction 82
4.2 Results and Discussion 83
4.2.1 Synthesis of Precursors, [$M(sac)_2(H_2O)_4]\cdot 2H_2O$ 83
4.2.2 Preparation of Metal Complexes 83
4.3 Spectral Properties 85
4.3.1 Fourier Transform Infrared spectroscopy (FTIR) Spectral Data of Complexes 85
4.3.2 UV-Vis spectroscopy 86

4.4 Description of the Crystal Structures of Saccharinato Complexes 87
4.4.1 X-ray Structure Determination of the Complexes 87
4.4.2 Crystal structures 88
4.4.2.1 [Ni(*N,O,O*-mdea)$_2$]·2(sac) (**6**) 88
4.4.2.2 [Cu$_2$(μ-*O*)$_2$(mea)$_4$]·2(sac) (**9**) 89
4.4.2.3 Hydrogen bonding of the complexes 90
4.4.2.4 Co$_2$(en)$_4$(CO$_3$)$_2$]·2(sac)3H$_2$O (**12**) 93
4.5 Thermal analysis 95
4.6 References 97
CHAPTER 5 99
CONCLUSION AND FUTURE PROSPECTS 99
5.1 CONCLUSION 99
5.2 FUTURE PROSPECTS 100
APPENDIX 101

LIST OF FIGURES

Figure 1.1 The A-H, B theory of artificial sweeteners. 2
Figure 1.2 The most commonly used artificial sweeteners. 4
Figure 1.3 Schematic diagram of the selected naturally occurring sweeteners 5
Figure 1.4 The schematic structures of saccharin and saccharinato anion. 6
Figure 1.5 Formation of sodium saccharinate from saccharin and sodium hydroxide. 10
Figure 1.6 Contributing resonance structures of saccharinate and thiosaccharin. 10
Figure 1.7 The crystal view of $Na(sac)\cdot 2H_2O$ whereby the Na ions are represented by pink shaded atoms, O atoms red shaded, N atoms blue shaded, S atoms yellow shaded, C atoms grey shaded and H atoms cream shaded. 11
Figure 1.8 Drawing of the structure of the $[M(sac)_2(H_2O)_4]\cdot 2H_2O$ type complexes where M(II) could be Co, Cd, Cu, and Zn. 12
Figure 1.9 The coordination mode of Zn saccharinato complexes, X and Y are donor atoms in mono- or bidentate ligands. 14
Figure 1.10 The possible coordination modes of ligands in Cu(II), Co(II), Cd(II), Ni(II) and Hg(II) metal centres. 16
Figure 1.11 The coordination mode of metal complexes via carbonyl oxygen donor atom. 18
Figure 1.12 Monodentate N ligands of complex $[Cu(sac)_2(iqn)_4]$ with a bulky ligand. 18
Figure 1.13 Monodentate mode via O atom of saccharinato complexes: $[Cu(pyr)_2(sac)_2]$ and $[Co(sac)_2(ppzea)_2]$ with bidentate (N, O) donor atoms and (N, N) donor atoms, respectively 19
Figure 1.14 The molecular view of $[Ag_4(sac)_4(pypr)_2]$ showing a tetranuclear silver(I)-saccharinato complex. 20
Figure 1.15 The molecular view of $[Cu(sac)_2(py)_3]$ showing the ambidentate behaviour of saccharin. 21
Figure 1.16 The complex $[Cd(dipyr)_2(sac)(H_2O)](sac)\cdot(H_2O)$ showing bonded saccharinato ligand and non-bonded saccharinate anion. 23
Figure 1.17 A molecular representation of dimethyl sulfoxide. 24
Figure 1.18 A representation of primary, secondary and tertiary amines. 25
Figure 3.1 NMR labelling scheme for different complexes. 54
Figure 3.2 The ORTEP molecular structure of (**1**) showing the labelling scheme. The dash interactions show intramolecular hydrogen bonding. 61

Figure 3.3 The ORTEP molecular structure of (**2**) showing the labelling scheme. The atom displacement ellipsoids are at 50% probability level. The dashed interactions shows hydrogen bonding. 62
Figure 3.4 The ORTEP crystal packing diagram of (**1**) viewed along the crystallographic c axis. The elements are shown as (C = dark grey, H = light grey, S = yellow, O = red, N = blue and Cd = cream). 64
Figure 3.5 The ORTEP crystal unit cell packing of (**2**) viewed along the crystallographic c axis. The elements are shown as (C = dark grey, H = light grey, S = yellow, O = red, N = blue and Co = grey)..... 64
Figure 3.6 ORTEP molecular structure of (**3**) showing the labelling scheme. The atom displacement ellipsoids are drawn at 50% probability level. The dashed interactions show intramolecular hydrogen bonding. 65
Figure 3.7 The ORTEP molecular structure of **(4)** showing the labelling scheme. The atom displacement ellipsoids are drawn at 50% probability level. 66
Figure 3.8 The ORTEP crystal unit cell packing of (**3**) viewed along the crystallographic c axis. The elements are shown as (C = dark grey, H = light grey, S = yellow, O = red, N = blue and Zn = light blue). 69
Figure 3.9 The ORTEP crystal packing of (**4**) view along the reciprocal cell a* axis, i.e. perpendicular to bc. The elements are shown as (C = dark grey, H = light grey, S = yellow, O = red, N = light blue and Hg = silver). 70
Figure 3.10 The ORTEP molecular structure of (**5**) showing the labelling scheme. The atom displacement ellipsoids are drawn at 50% probability level. The dash interactions show hydrogen bonding. 71
Figure 3.11 The unit cell packing of complex (**5**) viewed down the crystallographic a axis. 72
Figure 3.12 The ORTEP molecular structure of (**11**) showing the labelling scheme. The atoms displacement ellipsoids are drawn at 50% probability level. The dash interactions show hydrogen bonding. 73
Figure 3.13 The ORTEP crystal unit cell packing of (**11**) viewed along crystallographic b axis. The elements are shown as (C = dark grey, H = light grey, S = yellow, O = red, N = light blue and Cd = cream)..... 75
Figure 4.1 Molecular structure of (**6**) showing the atom labelling scheme. The atom displacement ellipsoids are drawn at 50% probability level. Only atoms in the asymmetric unit are labelled and the other half of the complex were generated *via* symmetry code -x, -y, 2-z. The dashed lines indicate hydrogen bonding. 88

Figure 4.2 The ORTEP crystal structure of (**9**) showing the labelling scheme. The atom displacement ellipsoids are drawn at 50% probability level. The atoms in the asymmetric unit are labelled and the other half of the complex was generated via symmetry code 1-x, 1-y, 1-z. The dashed interactions show hydrogen bonding of the complex. 89
Figure 4.3 The ORTEP crystal unit cell packing of (**6**) viewed along the crystallographic b axis. The elements are shown as (C = dark grey, H = light grey, S = yellow, O = red, N = blue and Ni = green). 91
Figure 4.4 The ORTEP crystal packing of (**9**) view down along the crystallographic b axis. The elements are shown as (C = dark grey, H = light grey, S = yellow, O = red, N = blue and Cu = orange). 92
Figure 4.5 The ORTEP crystal structure of (**12**) showing the labeling scheme. The atom displacement ellipsoids are drawn at 50% probability level. The dashed interactions show hydrogen bonding of the complex. 93
Figure 4.6 The ORTEP crystal packing of (**12**) viewed down along crystallographic b axis. The elements are shown as (C = dark grey, H = light grey, S = yellow, O = red, N = blue and Co = light green). 95

LIST OF SCHEMES

Scheme 1.1 The schematic illustration of saccharinate ligand coordination modes. 7
Scheme 1.2 The synthetic scheme of saccharin via the sulfonation of toluene. 9
Scheme 1.3 Synthesis of saccharin via diazotization starting from methyl ester o-aminobenzoic acid..... 9
Scheme 1.4 The oxidation reaction of dimethyl sulfide to yield DMSO. 24
Scheme 3.1 The schematic representation of N-M saccharinato complexes of the present study. 49
Scheme 3.2 Formation of $[M(sac)_2(H_2O)_4]\cdot 2H_2O$ precursor complex. 50
Scheme 3.3 Reactions showing the formation of DMSO saccharinato complexes. 51
Scheme 3.4 Reaction scheme showing the formation of amine saccharinato complexes. 52
Scheme 4.1 Synthesis of $[M(sac)_2(H_2O)_4]\cdot 2H_2O$ precursors. 83
Scheme 4.2 Reactions showing the formation of saccharinato complexes containing amines 84
Scheme 5.1 Reduction of sulfonyl O-donor atom leading to sulfinyl type derivative which can be further coordinated to metals, RA is a reducing agent 100
Scheme 5.2 A possible ring-opening reaction of saccharin..... 100

LIST OF TABLES

Table 1.1 Coordination modes of Zn saccharinato complexes..... 15
Table 1.2 The octahedral complexes of non-bonded saccharinate anion..... 22
Table 3.1 Tabulated analytical results of saccharinato complexes..... 52
Table 3.2 The NMR data of the saccharinato complexes..... 55
Table 3.3 IR spectral data for the metal complexes 56
Table 3.4 Electronic spectra results of saccharinato complexes 58
Table 3.5 Crystal data and structure refinement for complexes (**1**), (**2**), (**3**) and (**4**)..... 59
Table 3.6 Crystal data and structure refinement for complexes (**5**) and (**11**)..... 60
Table 3.7 Tabulated selected bond lengths (Å) and angles (°) for complexes (**1**) and (**2**) and hydrogen bonding coordination geometry for complexes (**1**)[b] and (**2**)[d] 63
Table 3.8 Tabulated selected bond lengths (Å) and angles (°) for complexes (**3**) and (**4**) and hydrogen bonding coordination geometry for complexes (**3**)[f] and (**4**)[k] 68
Table 3.9 Tabulated selected bond lengths (Å) and angles (°) for complex (**5**)[b] 72
Table 3.10 Tabulated selected bond lengths (Å) and angles (°) for complex (**11**)[h] 74
Table 3.11 Thermoanalytical data for selected complexes 76
Table 4.1 Tabulated analytical results of saccharinato complexes..... 84
Table 4.2 IR spectral data for the metal complexes 85
Table 4.3 Electronic spectra results of saccharinato complexes 86
Table 4.4 Crystal data and structure refinement for complexes (**6**), (**9**) and (**12**) 87
Table 4.5 Tabulated selected bond lengths (Å) and angles (°) for complexes (**6**) and (**9**)and hydrogen bonding coordination geometry for complexes (**6**)[b] and (**9**)[e]..... 90
Table 4.6 Tabulated selected bond lengths (Å) and bond angles (°) for complex (**12**) and hydrogen bonding coordination geometry for complex (**12**)[k]..... 94
Table 4.7 Thermoanalytical data for selected metal complexes..... 95

CHAPTER 1

INTRODUCTION

1.1 General Description of Saccharin

This chapter gives an overview of saccharin and focuses on the literature review of saccharinato metal complexes, which are derived from saccharin and its salts. It also gives an overview of the mixed-ligand saccharinato complexes, including dimethyl sulfoxide and ethylenediamine ligands, which are encountered in coordination chemistry. This study entails the synthesis and characterization of new saccharinato coordination complexes.

For the past 20000 years, mankind has realised the necessity of enjoying the "sweet" life by robbing beehives of honey. This attitude shows that humanity presumably had the desire for sweetness as part of their daily food diet, a habit which continues to this day.[1] This became more evident and prominent in the 20th century when the change to machineries and technology became part of life and became advantageous, due to health reasons, for people to have sweetness without extra calories. This idea later led to the discovery of low-calorie sweeteners and one of those sweeteners is called saccharin.[2, 3]

In 1878, a young researcher named Constantin Fahlberg worked in Ira Remsen's laboratory at Johns Hopkins University and accidentally made the magnificent discovery of saccharin when he was working on a project related to coal tar derivatives. As with other discoveries, Fahlberg accidentally spilled a chemical on his hand and later that evening while eating noticed that his bread tasted sweeter than usual. Being naturally curious, he traced the sweetness back to the chemical he used and the artificial sweetener saccharin was discovered.[2, 4]

1.2 The AH-B-X Taste Receptor Theory of Artificial Sweeteners

It is important to understand the relationship between the biological activities and chemical structure of saccharin and other artificial sweeteners. The receptors on the tongue refer to proteins which are responsible for any chemical response or signal recognition and can therefore initiate biological activities. It is one of the reasons that the tongue can differentiate between sweet and bitter. [4-6]

The sweetness of most artificial sweeteners including saccharin can be explained by means of a trifunctional unit system of AH-B-X whereby the units represent an acidic proton, an electronegative atom or centre and the hydrophobic group, respectively. This scheme was explained by Shallenberger and Acree.[7] Their system of explaining sweetness states that sweet tasting compounds consist of a hydrogen bond donor containing group (AH) and a hydrogen bond acceptor containing group (B) which are likely to be separated from each other at a distance of 2.5 to 4.0 angstroms.[8] They also suggested that the receptor must contain a complimentary receptor of B-AH pair that forms two hydrogen bonds when the sweeteners interact with the receptor. Since the formulation of this concept, there has been a number of known exceptions which helps us to understand the ways in which the artificial sweeteners work, see Figure 1.1.[7, 9]

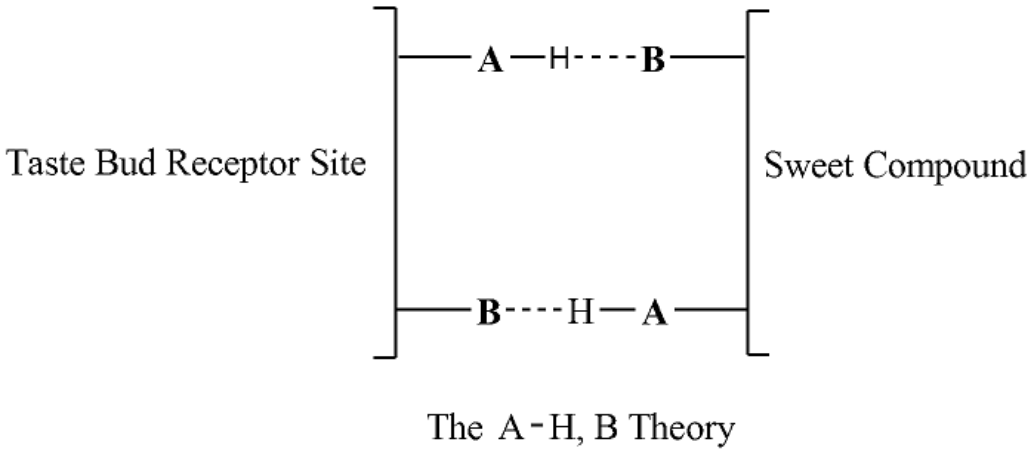

Figure 1. 1 The A-H, B theory of artificial sweeteners.

This theory is very simple and there are numerous known exceptions concerning the ways it works. The model which was proposed served the very important function of stimulating thought about the way sweeteners work. The model was further refined by Shallenberger, Acree and Lee by adding the "steric barrier" to account for many D-amino acids which are said to be sweet and the L-amino acids which are not. Kier also added to the AH-B pair a dispersion binding side of 3.5 Å from the AH group and 5.5 Å from the B. The recalculated distances by van der Heijden and co-workers suggest that there are four different receptor types distinguished by different distances and the three functional groups. From all these exceptions and reasons which explain the realistic and unrealistic view about the model, Nofre and co-workers showed that the model worked successfully. These scientists scored a major breakthrough by combining two known sweeteners of moderate potency to form a compound with higher and remarkable potency.[7,8]

Saccharin is an excellent food additive and it is used in manufactured products since its sweetening power cannot be reduced by heating. It is stable at elevated temperatures and it does not chemically react with other food ingredients. During the manufacture of blended sweeteners, saccharin is used , because it provides stability properties to maintain the product sweetness for a long time as it has a long shelf-life.[2] Saccharin and other low-calorie sweeteners like acesulfame, neotame, sucralose, cyclamate and aspartame, when blended together can either increase or decrease the concentration of the sweet taste depending on the choice and the ratios in which they are mixed together. [1]

1.3 Artificial Sweeteners

Sweetness in simple terms is that desirable sensational taste derived from starch/ carbohydrates such as sugar to bring that prototypical sweet taste. Sugar together with some artificial sweeteners are blended together and added to foods and beverages to enhance taste. It has been demonstrated that sweet taste stimuli originating from sugar and artificial sweeteners is admired by both adults and newborns.[10, 11]

From a long list of existing artificial sweeteners discovered by organic chemists, about five of them are approved by the US Food and Drug Administration (FDA), and these include saccharin, acesulfame potassium, aspartame, neotame and sucralose.[12] Artificial sweeteners are synthetically man-made sugar substitutes which in taste exceed sweetness of normal sugar and they do not occur naturally, although some of which are not in the above list can be derived from nature.[4, 13] Aspartame was discovered in 1965 by Schlatter of the Mazur Pharmaceutical company. This was an important discovery because aspartame is a sweetener that can be metabolised and broken down into natural amino acids and methanol which are present in most of our foods.[14] In 1973, Clauss and Jense of Hoechst AG, discovered acesulfame, in structure more similar to saccharin. It is used in the same way as saccharin in foods and beverages and as a salt or also in its acidic form.[15] Sucralose was discovered in 1976 by Hough and Phadnis, and was obtained when the sugar hydroxyl group of sucrose was substituted with chlorine.[16] Neotame is the sweetest sweetener of these listed and was discovered in 2000 by Nofre and Tinti.[17]

Below are the examples of artificial sweeteners that are currently registered by the FDA:

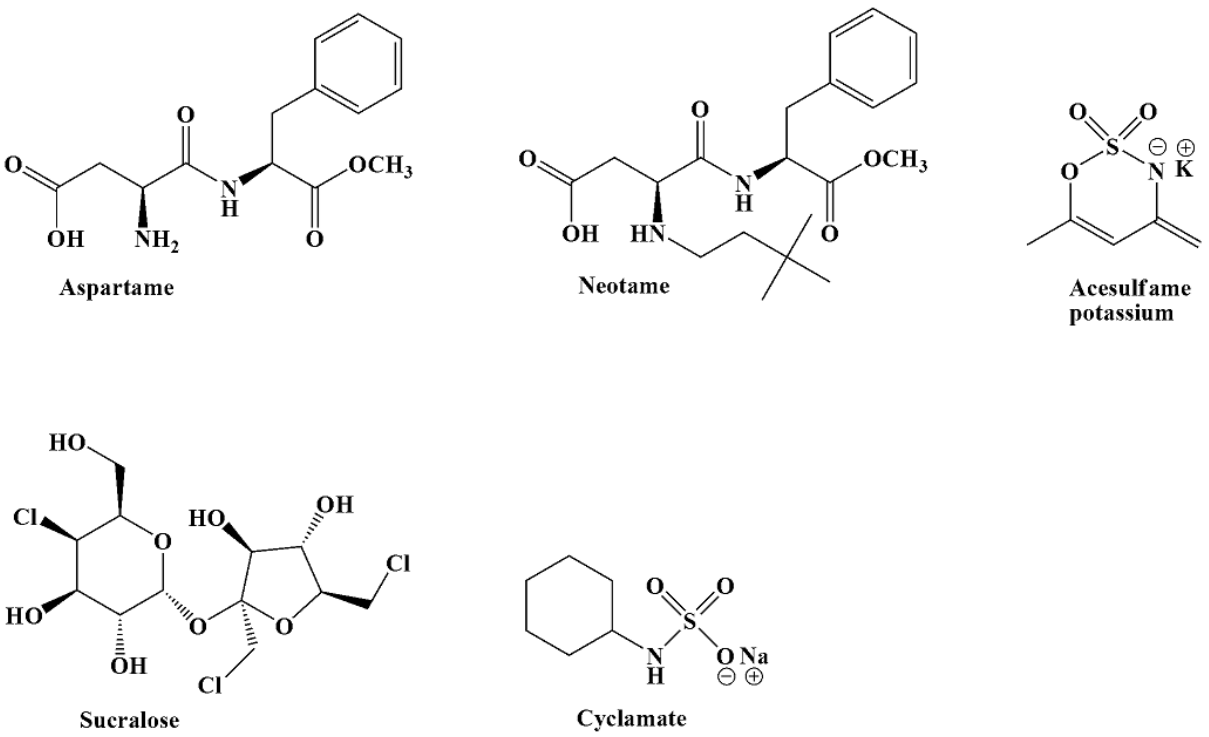

Figure 1. 2 The most commonly used artificial sweeteners.

Aspartame and acesulfame potassium are approximately 200 times sweeter than sucrose, neotame 7000 to 13000 sweeter than sucrose, cyclamate about 30 to 50 times sweeter than sucrose and sucralose about 600 times sweeter than sucrose. Sucrose, xylitol, and steviol, listed below, are naturally occurring sweeteners.[18, 19]

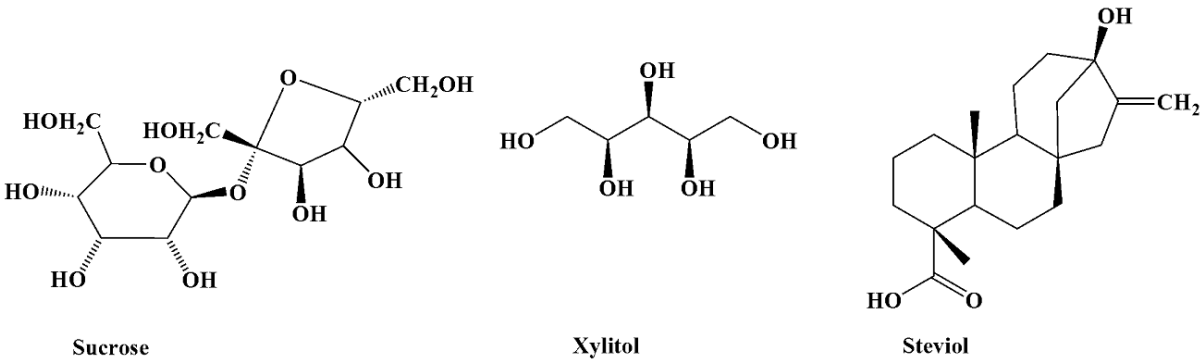

Figure 1. 3 Schematic diagram of the selected naturally occurring sweeteners.

In 1907, saccharin was mostly given to patients with diabetes, who could not take any sweetener containing calories, such as sugar, the source of carbohydrates and energy. Saccharin did not interfere with their lifestyle as it was directly taken into their digestive system without being digested. Another advantage saccharin for diabetics, was that it could produce insulin through simple tasting, as with the other common artificial sweetener, aspartame. Saccharin was also greatly used during the two World Wars when there was shortage of sugar in Europe and the US.[1]

Saccharin is a heterocyclic compound with systematic name o-Sulfobenzimide or 1,2-benzothiazole-3(2H)-one-1,1-dioxide, abbreviated HSac, and it is one of the best known and widely used artificial sweeteners in the world.[20] The chemical structure consists of three functional groups which are carbonyl, imino and sulfonyl, connected to each other *via* a five membered ring attached to a benzene ring. It is a polyfunctional ligand in transition-metal chemistry and can be used as an anion, typically coordinated to metals atoms *via* the nitrogen atom; but potentially also through the oxygen atom of the carbonyl, or two oxygen atoms of the sulfonyl group. As a neutral ligand, the nitrogen atom and the carbonyl oxygen atom can act as donor atoms for the ligand. The coordination modes of the saccharinato ligand is thus varied, and can act as a mono-, bi- and tri-dentate ligand,[20, 21] see scheme 1.1 below. The

crystal structure was first elucidated by Bart and Okaya [22, 23] and Figure 1.4 show the molecular diagram of saccharin and saccharinato anion.

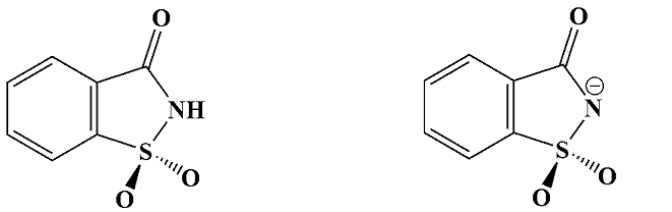

saccharin **saccharinato anion**

Figure 1. 4 The schematic structures of saccharin and saccharinato anion.

Saccharin has a melting point of 228-229.7°C, a pKa value of 1.60 and a density of 0.828 g mL^{-1}, respectively[24] and in its acidic form, HSac is insoluble in water, but dissolves in alcohols such as methanol and ethanol, as well as solvents such as acetone, glycerol and is slightly soluble in ether and chloroform. The sodium and calcium salts of saccharin are both highly soluble in water: 0.67 g mL^{-1} at room temperature, or 1.00 g dissolve in 290 mL of water, or in 25 mL of boiling water.[19] The sweetness of saccharin can be detected in a 1:100000 dilution.[18] The standard molar enthalpies of composition, sublimation- and formation- enthalpies of saccharin have only recently been reported using calorimetric methods.[25-27]

Saccharin has no food energy and it is 300 to 700 times sweeter than sucrose and at high concentrations it leaves a metallic bitterness aftertaste. [2, 18, 28, 29] The reason it is so sweet is still unclear but its molecular structure obviously fit appropriate receptors on the tongue. This idea is further brought forth by the fact that when the hydrogen atom on the N atom is removed and replaced with a methyl group, the sweetness virtually disappears. The alkyl halide derivatives of saccharin class of compounds occur in large variety derived from haloalkane.[30]

Scheme 1.1 is a representation of the different coordination modes of the saccharinato ligand with different metals centres.[31]

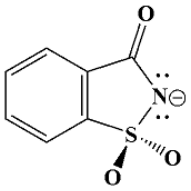

(NH_4^+, Na^+, K^+, Rb^+, Cs^+, Be(II), Mg(II), Ca(II), Sr(II), Ba(II))

I

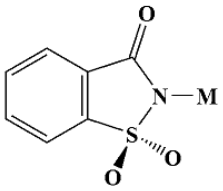

(M = V(II), Cr(II), Mn(II), Fe(II), Co(II), Ni(II), Cu(II), Zn(II), Ag(I), Pt(II), Pd(II), Au(I), Hg(I) and Hg(II))

II

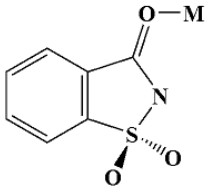

(M = V(II), Ni(II), Cu(II), Co(II), Zn(II), Cd(II), Gd(III), Lu(III))

III

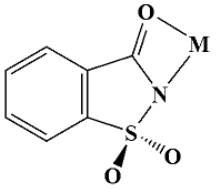

(M = Cr(II), Pb(II), Ag(I), Cd(II), Cu(II))

IV

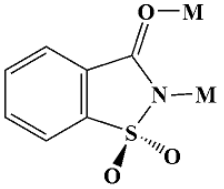

(M = Ba(II), Pb(II), Ag(I), Hg(I) and Hg(II), Cr(II), Cu(II))

V

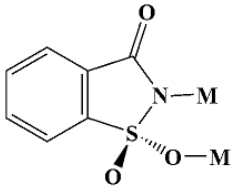

(M = Cr(II), Pb(II), Ag(I), Ba(II), Cd(II), Cu(II), Hg(I) and Hg(II))

VI

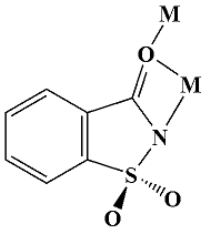

(M = Cr(II), Pb(II), Ag(I), Ba(II), Cd(II), Cu(II))

VII

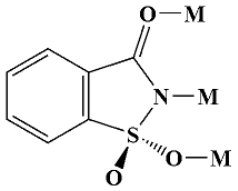

(M = Cr(II), Pb(II), Ag(I), Ba(II), Cd(II), Cu(II))

VIII

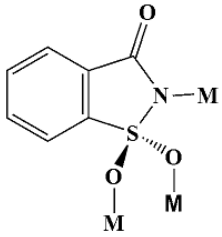

(M = Ba(II), Pb(II), Ag(I), Cr(II))

IX

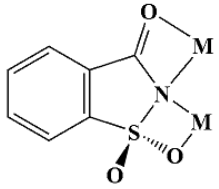

(M = Cr(II), Pb(II), Ag(I), Tl(I))

X

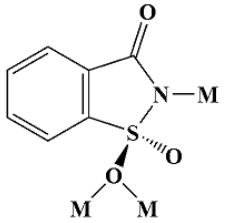

(M = Ag(I))

XI

Scheme 1. 1 The schematic illustration of saccharinate ligand coordination modes.[31, 32]

1.4 Advantages and Disadvantages of Saccharin

Research has shown that saccharin is taken by people to maintain in an excellent health condition and to control their body weight. Regardless of being proven by the health profession to be beneficial for diabetics, it is also proven to reduce dental cavities. This low-calorie sweetener is being used in products such as soft drinks, jams, chewing gums, canned fruits, dessert toppings, baked goods, salad dressing and candy. It is also widely used in health and beauty products such as tooth pastes, mouthwash, cosmetics products, vitamins and pharmaceuticals. Many of us are familiar with saccharin in the pink package of Sweet'N Low.[20, 33]

Saccharin can be synthesised by toluene or ortho-toluenesulfonamide. The starting material ortho-toluenesulfonamide is a main threat to human life because without the correct assessment in the saccharin production, it could be incorporated in the product and cause cancer.[3, 34] Many nitrogen containing compounds are known to be carcinogenic such as aromatic amines, nitrosamines and nitrosamides, nitroquinolines, nitrofurans and mycotoxin.[3, 35, 36] Sodium saccharin is associated with health risks such as allergies and weight gain, but can increase chances of diabetes to non-diabetics. Sodium saccharin is a sugar substitute without calories and is easily absorbed in the human intestines. This is a sweetener which is able to stimulate an endocrinological response like insulin from the pancreas. Sodium saccharin is capable of causing allergies in the human body due to the presence of sulphonamides. These allergies symptoms include headaches, difficulty in breathing, skin rash and diarrhoea.[37]

1.5 Synthesis of Saccharin

There are two synthetic preparations of saccharin which are mostly used by industrial manufactures and in academic laboratories. The first method involves the preparation of saccharin starting from toluene and the second procedure is with methyl ester o-aminobenzoic acid cyclization,[8] see Scheme 1.2.

The first route was reported by Remsen and Fahlberg, whereby toluene is sulfonated by chlorosulfonic acid which results into two isomers namely 4- and 2-toluenesulfonyl chlorides. The isomeric products are separated by chilling the products in an ice-bath. The liquid part is 2-toluenesulfonyl chloride which is separated from the crystallized isomer 4-toluenesulfonyl chlorides and reacted with ammonia to give 2-toluenesulfonylamide. An oxidation of the product with sodium permanganate or chromium(VI) oxide in sulfonic acid gives saccharin.[4]

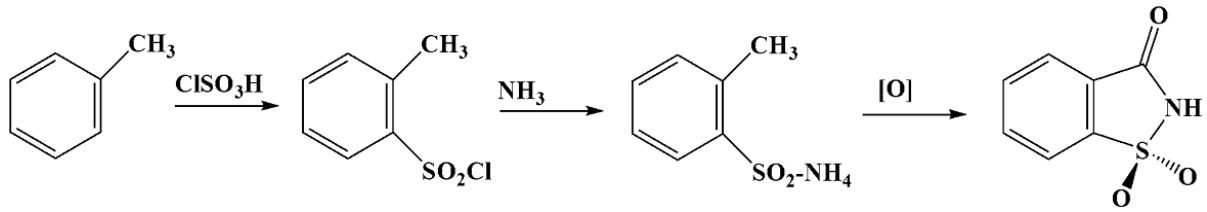

Scheme 1. 2 The synthetic scheme of saccharin via the sulfonation of toluene.

A second route for preparing saccharin is from methyl ester o-aminobenzoic acid cyclization, see scheme 1.3. This is a diazotization reaction whereby nitrous acid is used and the resulting diazonium salt is reacted with sulphur dioxide in the presence of copper dichloride forming the methyl ester o-sulfobenzoic acid. The reaction of the resulting product with chlorine gives o-chlorosulfonylbenzoic acid methyl ester of which upon reaction with ammonia gives o-sulfonylamidobenzoic acid methyl ester. In the presence of hydrogen chloride, the resulting product undergoes cyclization into saccharin.[2]

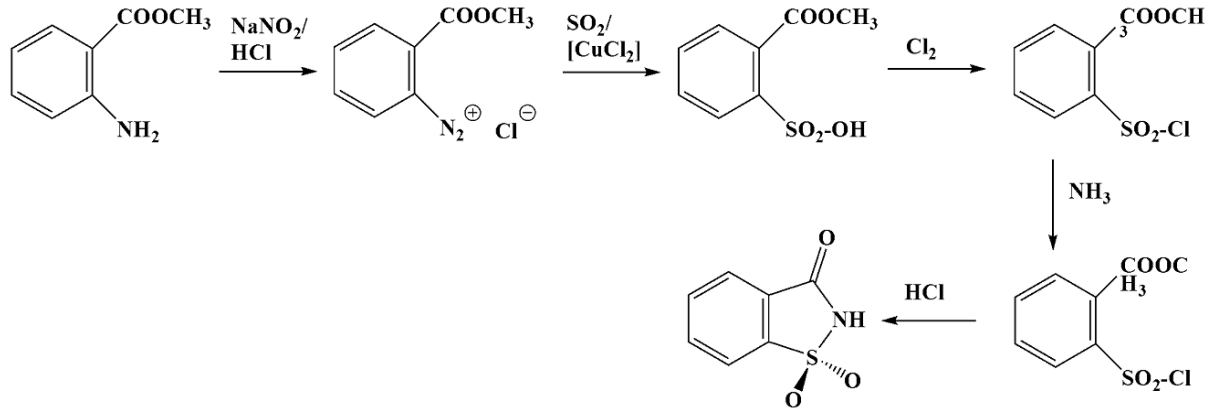

Scheme 1. 3 Synthesis of saccharin via diazotization from methyl ester o-aminobenzoic acid cyclization.

The treatment of saccharin with sodium hydroxide in ethanol results in the substitution of imide hydrogen atom with the sodium ion to give sodium saccharinate.[38]

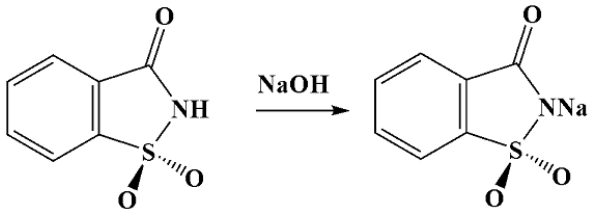

Figure 1. 5 Formation of sodium saccharinate from saccharin and sodium hydroxide.

1.6 Sodium Saccharinate and Thiosaccharin

It exists in an ionised form and can therefore act as a nucleophile. It has been shown to exist in different contributing resonance forms in solution which makes it an ambidentate ligand as it can bind metals through the N or O donor atoms, see figure 1.6. This has been demonstrated by spectroscopic (NMR) and crystallographic data.[39, 40]

Thiosaccharin abbreviated (tsac) with systematic name 1,2-benzisothiazol-3(2H)-thione-1,1-dioxide differs from saccharin by replacing the carbonyl group (C=O) with the thiocarbonyl group (C=S).[41] Thiosaccharin is derived from saccharin and obtained through two thionation methods: i) the treatment of saccharin with phosphorous pentasulfide (P_2S_5)/(structurally P_4S_{10}) in a suitable organic solvent[41, 42], and ii) the reaction of saccharin with Lawesson's reagent in hot toluene.[42]

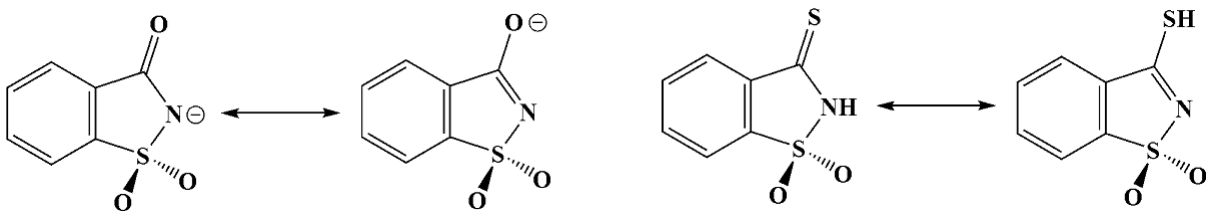

Figure 1. 6 Contributing resonance structures of saccharinate and thiosaccharin.

In general, deprotonation of thiosaccharin causes the negative charge on the N donor atom to decrease and this affects the structural and electronic properties of the ligand making it less effective to bind to the first row transition-metals, while the saccharinato ligand readily binds through the N atom under the same conditions. The thiosaccharin contains the S donor atom which is a soft atom that can readily bind to soft metal centres such as the Cd(II), Hg(II) and Pb(II).[21]

1.7 Saccharinato Ligand: Metal Complexes of Saccharin and Its Salts

1.7.1 Saccharinate Salts

Examples of simple saccharinate salts which behave as cation/ anion species include $Na(sac)\cdot H_2O$, $Mg(sac)_2\cdot 7H_2O$, $K_2Na(sac)_2\cdot H_2O$,[43] $NH_4(sac)$[44] and many others which are presented in the list of coordination modes (see Scheme 1.1 above). Sodium saccharin is of great importance since it is commonly used commercially, whilst the others are not. When sodium saccharin is recrystallized it produces two hydrates. In 95% ethanol, it occurs in the form $Na(sac)\cdot 2/3H_2O$ which appears to crystallized in triclinic space group P1 and when water is used instead, in the process, $Na(sac)\cdot 15/8H_2O$ is afforded.[45, 46]

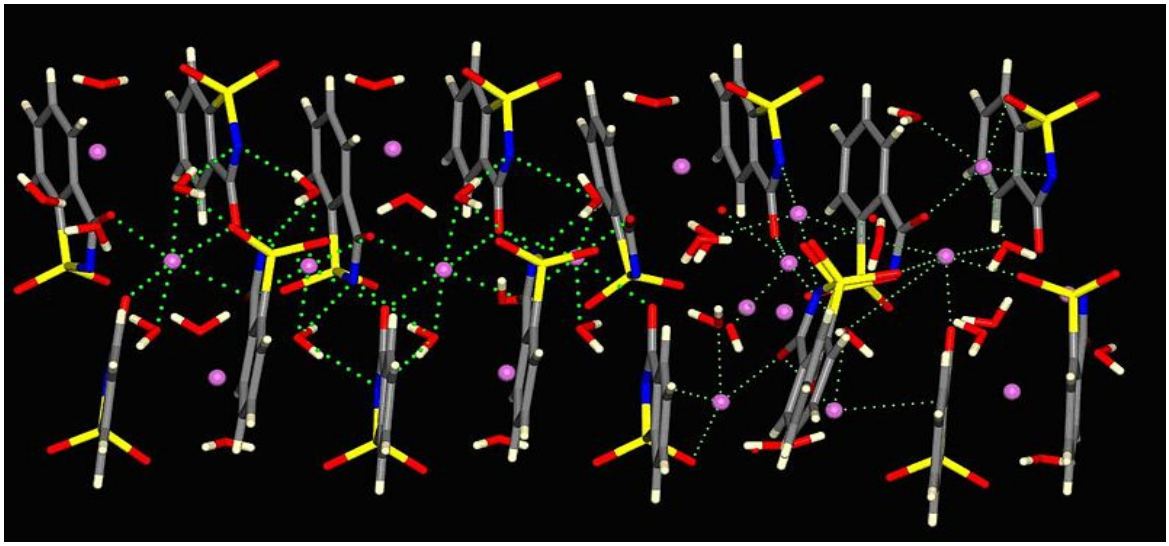

Figure 1.7 The crystal view of $Na(sac)\cdot 2H_2O$ whereby the Na ions are represented by pink shaded atoms, O atoms red shaded, N atoms blue shaded, S atoms yellow shaded, C atoms grey shaded and H atoms cream shaded. [47]

$Na(sac)\cdot 15/8H_2O$ crystallises in a monoclinic space group $P2_{1/n}$. From a crystallographic point of view, the structure has a molecular formula $Na_{64}(sac)\cdot 120H_2O$ and it generates a large unit cell with a cell volume of 15560.0 Å and Z= 64.[47, 48]

The ammonium salt $NH_4(sac)$[44] is the only ionic saccharinate that shows no water of hydration.

The cesium saccharinates, $Cs(sac)\cdot 0.5H_2O$ have only been characterised by IR spectroscopy and their molecular structure remain unknown.[48, 49] This is common to other group 1 salts including $Rb(sac)\cdot 0.5H_2O$ which is obtained by the reaction of saccharin and Rb_2CO_3.[48, 50] $Rb(sac)(Hsac)\cdot H_2O$ is another complex whose analysis is incomplete.[50]

With regard to the alkaline-earth ionic saccharinates, except for Mg(II), none are fully characterised, including $Ca(sac)_2\cdot 4H_2O$, $Sr(sac)_2\cdot 4H_2O$ and $Ba(sac)_2\cdot 8H_2O$. The complexes of Ca(II), Sr(II) and Ba(II) are not soluble in water. The mixed ligand complexes of alkaline earth metals have been synthesised and characterised. [51]

1.7.2 Monodentate Coordination of Saccharinato Complexes via the N-atom

The isomorphous coordination of saccharinato complexes is produced by the reaction of the first row divalent transition metals in aqueous solution and has been extended to the various late transition metal complexes.[52, 53] The complexes are usually prepared from soluble sodium saccharinate in aqueous media as saccharin (Hsac) is only partially soluble in water. The complexes have the following formula: $[M(sac)_2(H_2O)_4]\cdot 2H_2O$, whereby M(II) could be V, Cr, Mn, Fe, Ni, Cu, and Zn. Cadmium also forms part of this list of isomorphous compounds. [53-55] Figure 1.8, demonstrate an octahedral geometry of $[M(sac)_2(H_2O)_4]\cdot 2H_2O$.

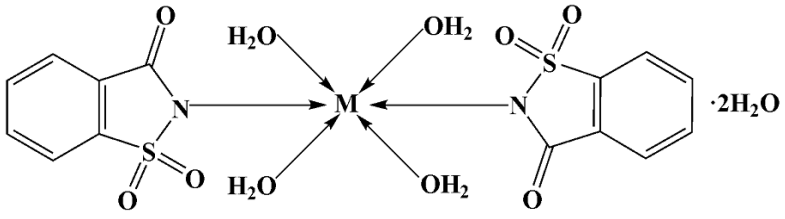

Figure 1. 8 Drawing of the structure of the $[M(sac)_2(H_2O)_4]\cdot 2H_2O$ type complexes where M(II) could be Co, Cd, Cu, and Zn.

Crystallographic data have shown that these complexes possess octahedral coordination geometry. Their structures consist of two saccharin anions *trans* to each other and four aqua ligands, with two waters of crystallisation that form a tetraaquabis(saccharinato)M^{II}dihydrate complex.[49, 55] This is the most established coordination geometry of saccharinate chemistry,[55] see scheme 1.1.

The present study focuses on the following late-transition metal centres: Co, Ni, Cu, and the three group 12 metals Zn, Cd, Hg. All these transition metals have an oxidation state of +2.

1.7.3 Saccharinato Mixed Ligand Complexes

It is common practice in this system to displace the labile aqua ligands in the saccharinato aqua metal complexes (Fig.1.9) with stronger donating, mostly neutral ligands. This is readily accomplished by the direct addition of the neutral ligand into the intermediate aqua saccharinato complexes whereby water is typically used as solvent.[54] The neutral complexes are formed by substitution reactions which lead to new stable mixed-ligand complexes. The complexes can therefore occur as octahedral, tetrahedral, square-planare, trigonal planar and other geometries depending on the metal type used during the reactions.[21, 56]

Copper(I) has shown to be a three coordination metal centre. In some cases copper(I) metal centres have coordinated through the N-saccharinato ligand which upon treatment with PPh_3 gives a three coordinated Cu(I) complex of the type $[Cu(sac)(PPh_3)_2]$ (PPh_3 = triphenylphosphine).[57] Most complexes of silver(I) are dimeric or polymeric in nature, and the structures often display Ag···Ag interactions (argentophilic), for example in $[Ag_2(sac)_2(pyet)_2]$ (pyet = 2-pyridylethanol),[58] $[Ag(sac)(PPh_3)_2]$,[59] $[Ag(sac)(py)_n]$ (py = pyridine),[60] $[Ag(sac)(pym)_n]$ (pym = 2-pridylmethanol)[61] and $[Ag_2(sac)_2(dmen)_2]$ (dmen = *N,N*-dimethylenediamine).[59, 62]

1.7.4 Metal Complexes of Zn(II) Coordinated to a Mono-or Bidentate Ligand

Zinc(II) complexes usually give a tetrahedral coordination geometry. The M-N kind of complexes whereby the labile aqua ligands are displaced by N donor or N,O donor ligands are known. The monodentate and bidentate N-donor atoms usually displace the aqua ligands readily compared to the monodentate and bidentate O-donor ligands. The bidentate ligand containing the N-and O-donor atoms coordinate directly to the empty orbital of the metal to form dative coordinative bonds. There are very few octahedral Zn(II) saccharinato complexes. Figure 1.9 summarizes the coordination geometry of ligands around different metal centres. There are many other examples.

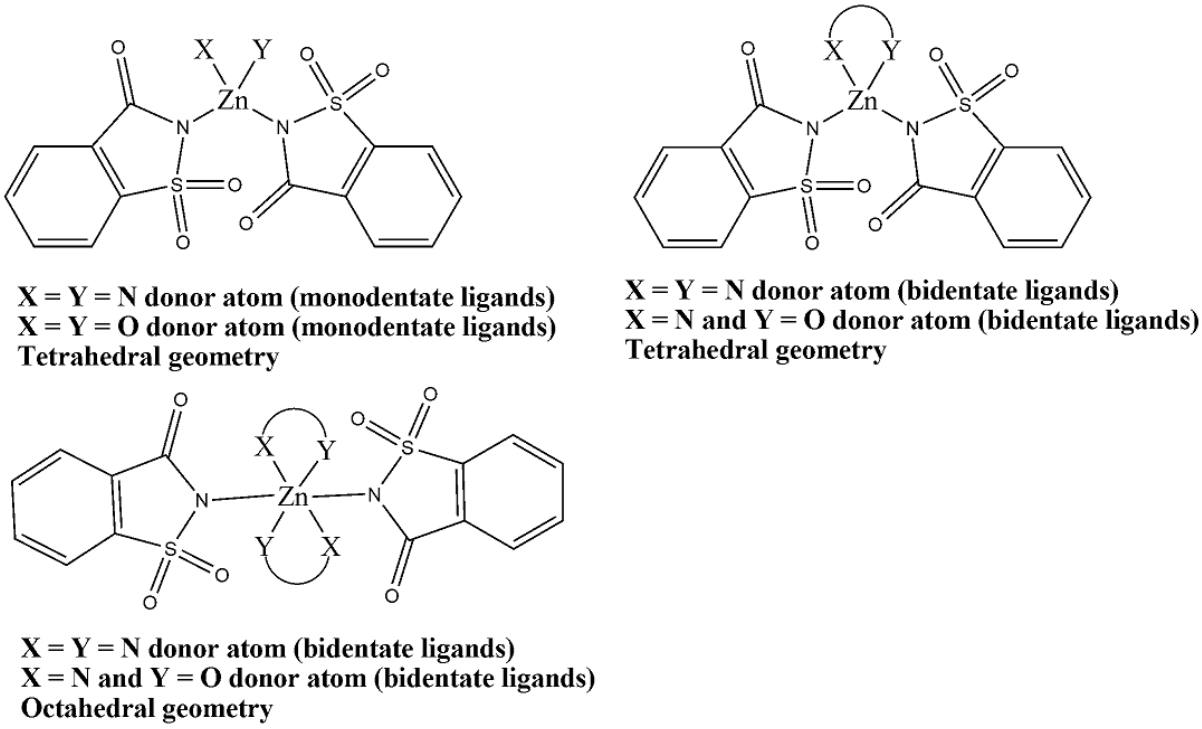

Figure 1. 9 The coordination mode of Zn saccharinato complexes, X and Y are donor atoms in mono- or bidentate ligands.

A tetrahedral coordination mononuclear tris(saccharinato) complex exists for Zn(II) divalent metal centre and is presented by the following structural formula $[Zn(sac)_2(bzim)_2]\cdot 2EtOH\cdot 2H_2O$ (bzim = benzimidazole; EtOH = ethanol).[63] The octahedral complexes observed for the saccharinato complexes are: $[Zn(sac)_2(ea)_2]$(ea = monoethanolamine),[64] $[Zn(sac)_2(ampy)_2]$ (ampy = 2-(aminoethyl)pyridine),[65]

$[Zn(sac)(bpy)_2.(H_2O)]sac$[66] and many others not mentioned in this list. Table 1.1 show the coordination mode of ligands mostly used in the formation of zinc saccharinato complexes.

Table 1. 1 Coordination modes of Zn saccharinato complexes

Type of structural mode	Binding mode of ligand	Examples
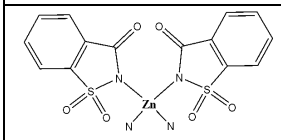	Monodentate *via* N, Tetrahedral	$[Zn(sac)_2(im)_2]$[63]
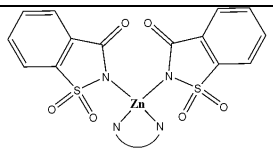	Bidentate *via* N, Tetrahedral	$[Zn(sac)_2(aepy)]$[65]
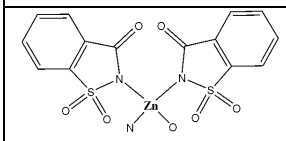	Monodendate *via* N and O, Tetrahedral	$ApyH[Zn(sac)_3(H_2O)]$[67a]
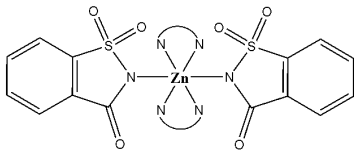	Bidentate *via* N, Octahedral	$[Zn(sac)_2(aepy)_2]$[65]
Abbreviations: (im) = imidazole (aepy) = 2-(2-aminoethyl)pyridine (ApyH)=2-aminopyridinium		

1.7.5 Metal Complexes of M(II) Coordinated to a Monodenate, Bidentate, Tridenate and Bridging Ligand: M(II) = Cu, Co, Cd, Ni and Hg

Copper(II), cobalt(II) and nickel(II) are late -transition metal centres and when complexed with ligands they usually display octahedral, trigonal bipyramidal and square planar coordination geometry. Dimers usually form when the ligand used forms alkoxo-bridges via the O atoms. Cadmium(II) and mercury(II) also form monodentate and bidentate complexes. When labile aqua ligands are displaced by N donor or N,O donor ligands in tetraaquabis(saccharinato)M(II)dihydrate, new complexes readily forms. The saccharinato metal complexes of Cu(II), Pt(II) and Pd(II) possess a square planar coordination geometry. There are two types of saccharinato copper(II) dimer complexes, namely $[Cu_2(sac)_2(dea)_2]$ (dea = diethanolamine anion)[64] and $[Cu_2(sac)_2(\mu\text{-}pypr)_2]$ (pypr = 2-pyridinepropanoxy

anion)[67b]. These two dimers are linked together by two alkoxo-bridges which have relatively short Cu···Cu interactions separated at 2.99 Å for $[Cu_2(sac)_2(dea)_2]$ and 3.04 Å for $[Cu_2(sac)_2(\mu\text{-}pypr)_2]$. These two copper(II) atoms are responsible for antiferromagnetic coupling in the Cu-Cu pair. [67b] The Cu(II) complexes exhibit octahedral coordination geometry. Octahedral complexes observed for the saccharinato ligand include $[M(sac)_2(ea)_2]$ (ea = monoethanolamine) where M(II) = Ni,[68] Cu,[69] Hg(I),[64] $[M(sac)_2(ampy)_2]$ (ampy = 2-(aminoethyl)pyridine) where M(II) = Ni,[70] Cu[71] and Cd[72], $[M(sac)_2(HydEt\text{-}en)_2]$ (HydEt-en = N-2(-hydroxyethyl)-ethyendiamine) where M(II) = Cd and Cu[73] and the complexes of $[M(sac)(bpy)_2(H_2O)]sac$, where M = Co[74] and Ni[75], $[Cd(sac)_2(bpy)_2]$ and $[Hg(sac)_2(bpy)]$[76] (bpy = α, α'-bipyridine). Most of the complexes of the type $[M(sac)_2(NH_3)_4]$ (NH_3 = ammonia) where M(II) = Cd, Co, Cu, Hg(I) have been synthesised but not fully characterised.[57, 77] Figure1.10 show the possible coordination modes of the N or/ and N, O donor atoms which forms in most chemical reactions.

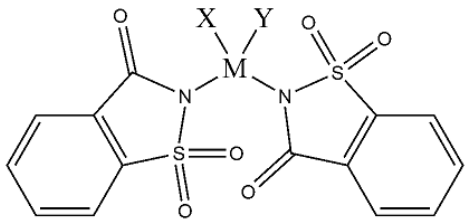

X = Y = N donor atom (monodentate ligands)
X = Y = O donor atom (monodentate ligands)
Tetrahedral geometry: M = Cu^{2+} and Hg^{2+}

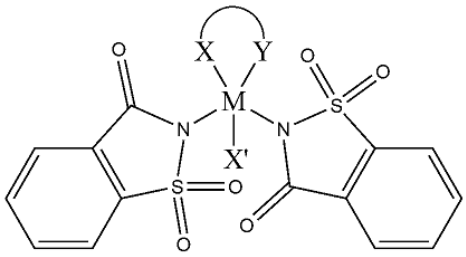

X = Y = N donor atom (bidentate ligands)
X = N and Y = O donor atom (bidentate ligands): X' = H_2O or O or N donor ligands
Trigonal bipyramidal or square planar geometry: M = Cu^{2+}, Co^{2+}, Cd^{2+} and Ni^{2+}

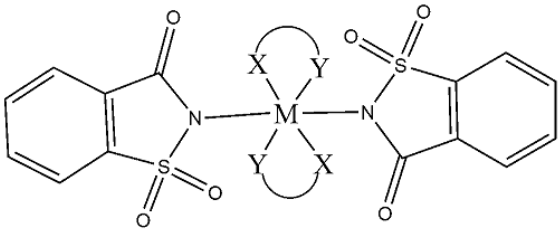

X = Y = N donor atom (bidentate ligands)
X = N and Y = O donor atom (bidentate ligands)
Octahedral geometry:M = Cu^{2+}, Co^{2+}, $Cd^{2+}$and Ni^{2+}

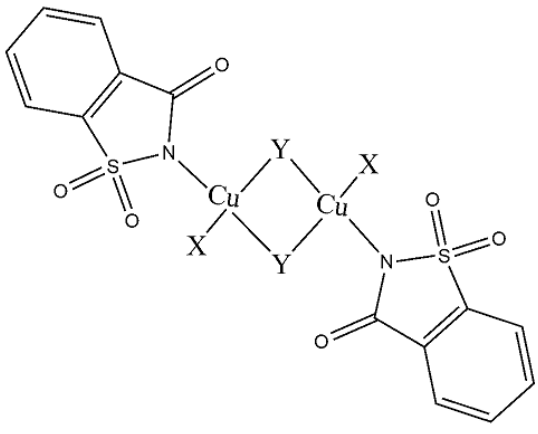

X = N and Y = O donor atom (bidentate ligands)
Dimeric Structure via Cu-Y-Cu

Figure 1. 10 The possible coordination modes of ligands in Cu(II), Co(II), Cd(II), Ni(II) and Hg(II) metal centres.

The trigonal bipyramidal coordination geometry is most likely formed by Cr(II), copper(II), mercury(II) and cadmium (II) depending on the type of ligand. Trigonal bipyramidal coordination geometry for saccharinato complexes include $[Cr(sac)_2(py)]\cdot 2py$[78], $[Cu(ophen)_2(sac)]sac\cdot 2H_2O$ (ophen = o-phenothroline) and $[Cu(bpy)_2(sac)_2(sac)_3\cdot H_2O]$[79,80]. Other examples include $[Hg(Cl)(sac)]$,[81] $[Hg_2(Cl)_2(sac)_2(py)_2]$,[76(a)] $[Hg(sac)_2(pyet)]$, $[Hg(sac)_2(aepy)]$,[82] $[Cd(sac)_2(H_2O)(DMSO)(pyet)]$, $[Cd(sac)_2(pyet)_2]$,[82(a),83] $[Cd(sac)_2(dea)_2]$ and $[Cd(sac)_2(H_2O)_2(nic)_2]$.[84]

Significant saccharinato stretching vibration frequencies of these metal centres occurs in similar regions. The shifts differ according to the binding type and is influenced by the metal type. In general, the IR wavenumbers of Zn saccharinato complexes slightly differ to the IR shifts of other late transition metal complexes. The d^{10}system is not as red shifted as those of the d^6 to d^9 because they have less energy to be excited as compared to d^6 to d^9 systems.

Ag(I) can be coordinated via the N atom of the saccharinato anion to produce T-shaped geometries, for example $[Ag(sac)(ampy)]$ and $[Ag_2(sac)_2(aepy)_2]$.[59, 85, 86]

1.7.6 Monodentate Coordination of Saccharinato Complexes via the O-atom

Although there are two donor atoms of the saccharinate anion to which metals can coordinate differently to form metal complexes, very few saccharinato complexes involve the oxygen atom of the carbonyl group. Coordination through the oxygen atoms of the sulfonyl group is even more scarce. For the saccharinato ligand to engage in M-O bonding, it has to act as a chelating ligand.[21] Below, Figure 1.11 show the coordination modes of the ligands in a saccharinato system engaged in M-O bonding mode.

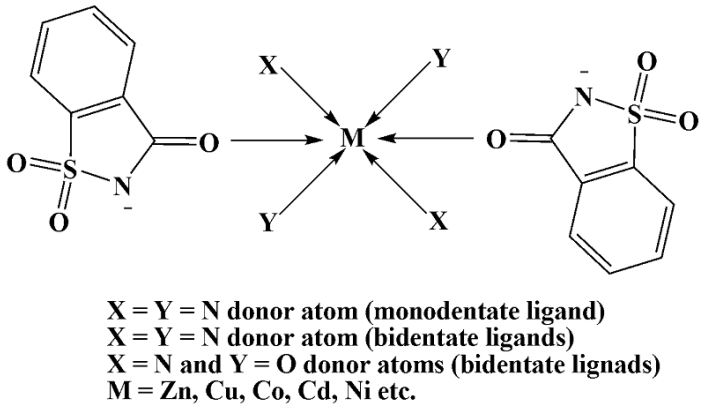

Figure 1. 11 The coordination mode of metal complexes via carbonyl oxygen donor atom.

Coordination chemistry that involves the oxygen donor atom of the carbonyl group is mostly observed when bulky co-ligands are used in the reactions, (e.g. *N,N*-dimethylethylenediamine = dmen). The first complexes of this nature concerned metal centres such as V(II), Ni(II) and Cu(II). The monodentate O-coordinated metal centres complexes reported to date include $[M(sac)_2(py)_4]\cdot 2py$ whereby M(II) = V and Ni, [87, 88] $[V(sac)_2(py)_4]\cdot 2thf$ (thf = tetrahydrofuran),[88] $[VO(OH)(sac)(H_2O)]Hsac$,[89] $[Cu(sac)_2(prz)_4]$ (prz = pyrazole)[90] and $[Cu(pyr)_2(sac)_2]$,[67] $[Cu(sac)(H_2O)_2(mpy)_4]$ (mpy = 4-methylpyridine) [91]and $[Cu(sac)_2(iqn)_4]$ (iqn = isoquinoline).[91] An example is shown in Figure 1.12.

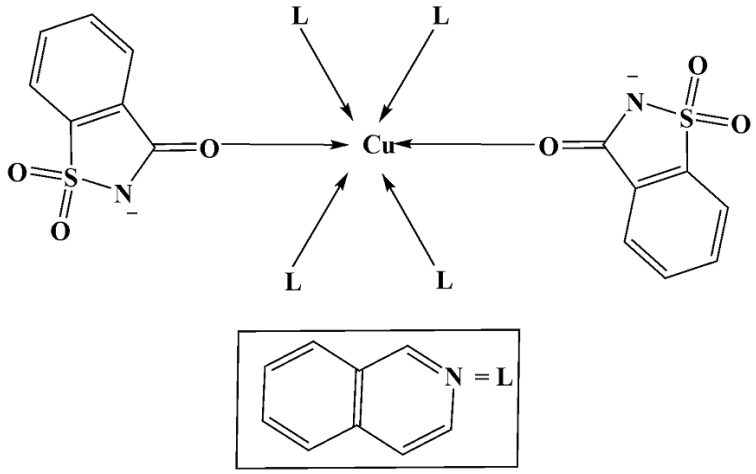

Figure 1. 12 Monodentate N ligands of complex $[Cu(sac)_2(iqn)_4]$ with a bulky ligand.

The following complexes contain the bidentate chelating ligand containing a M-O bond where O atom is from the saccharinate carbonyl group: $[M(pypr)_2(sac)_2]$ (pypr = 2-pyridinepropanol) where M = Cu,[67] Co, Ni[92] and $[Ni(sac)_2(aepy)_2]$[70] and $[M(sac)_2(aeppz)_2]$ (

aeppz = N-(2-aminoethyl)piperazine) where M = Co, Ni,[93] Zn and Cd.[94] These bidentate complexes have shown to crystallise in octahedral coordination geometry. The ligands like pyridine, piperazine derivatives consisting of alkylhydroxy and alkylamino groups have shown to possess similar octahedral geometry.[95] Examples are shown in Figure 1.13.

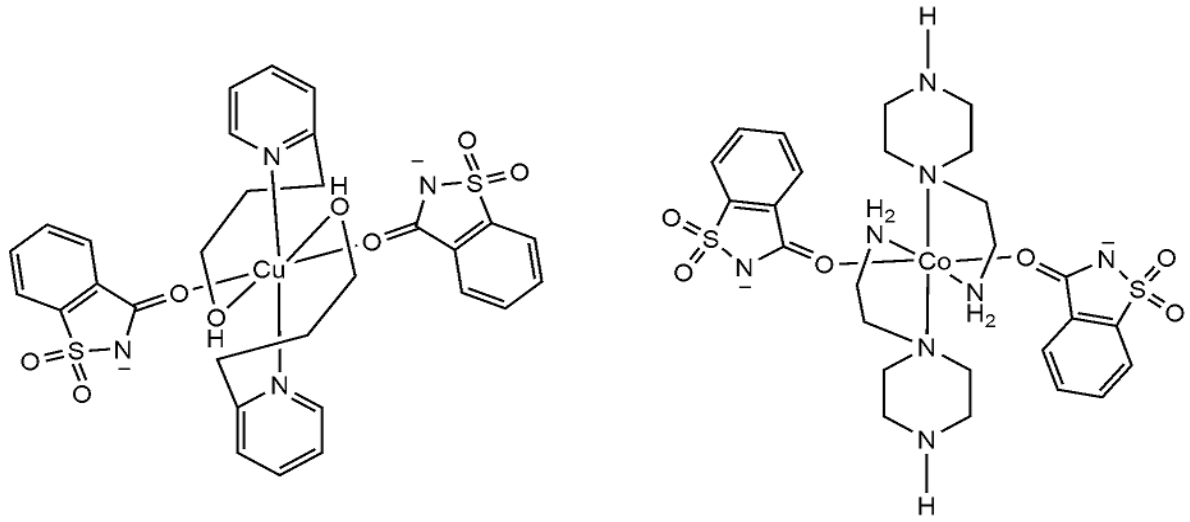

Figure 1. 13 Monodentate mode via O atom of saccharinato complexes: $[Cu(pyr)_2(sac)_2]$ and $[Co(sac)_2(ppzea)_2]$ with bidentate (N, O) donor atoms and (N, N) donor atoms, respectively.

1.7.7 Bidentate (N, O) and Tridentate (N, O, O) Coordination of Saccharinato Complexes

The saccharinate anion can act as a bidentate ligand through the N, O donor atoms and a tetranuclear ligand *via* the N, O, O atoms, Figure 1.14, see previous comment. Amongst those which show this kind of coordination behaviour is the dimeric structure of $[Cr_2(sac)_4]\cdot 2thf$[88] in which the saccharinato moiety coordinates *via* the sulfonyl oxygen donor atoms and also for a polymeric silver(I) complex of the type $[Ag(sac)(dmpy)]_n$ (dmpy = 2,6-dimethanolpyridine). Complexes such as $Na[Ag(sac)_2]$ and the $[Ag(sac)_2]^+$cation[83] have been synthesised and crystallise in a three-dimensional structure leading to bi-and tridentate saccharinato complexes with the chelating agents binding to the Ag(I) and the Na(I) cations. Also, in this kind of coordination chemistry, a few tetranuclear coordination geometries are known such as $[Ag_4(sac)_4(pypr)_2]$[88, 96] which is an interesting structure because of the chelating mode shown by the saccharinato moieties that have coordinated to the four Ag(I) metal centres. There are also the newly discovered coordination mode of saccharinato via the two oxygen atoms of the sulfonyl in complexes of the type $[Ag_2(\mu_3\text{-sac})_2(\mu\text{-nmpen})]_n$ and

$[Ag(sac)(mpr)]_2$[31] (nmpen =N-nitroso-N-methylpentylamine), mpr =2-methyl-1-pyrroline). It shows the saccharinato ligand in a μ_3-coordination mode by means of μ_2-bridging atoms of the two sulfonyl oxygen atoms and the N atoms of the imido group. This structural complex further shows the dimeric structure of the complex linked by the Ag···$C_{sac}(\eta^1)$ interactions of the ions of Ag(I) complex and the phenyl of the adjacent molecule through weak π···π and the Ag···Ag interactions.[21] Other complexes such as $[Tl_2(sac)_2(H_2O)]_n$[21] can either have 8 or 5 coordination resulting in a polymeric structure with both N-and O donor atoms chelating.

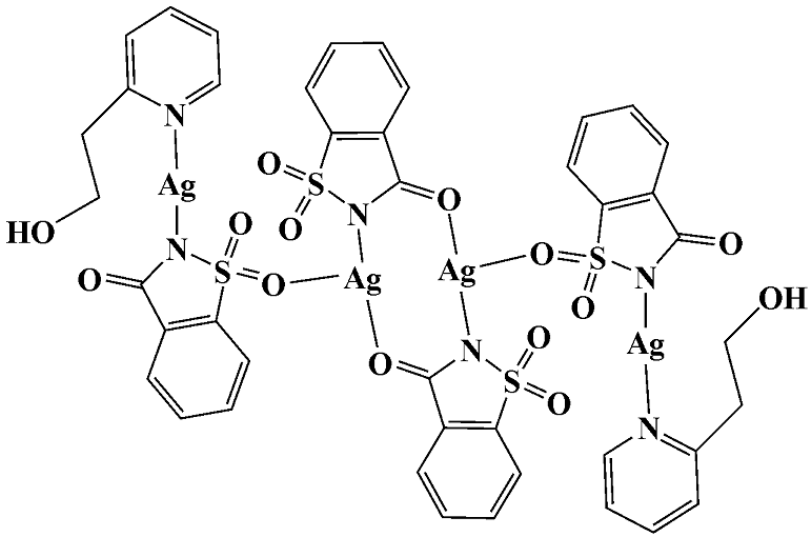

Figure 1. 14 The molecular view of $[Ag_4(sac)_4(pypr)_2]$ showing a tetranuclear silver(I)-saccharinato complex.

1.7.8 Unusual Ambidentate Coordination Behaviour of Saccharinato Complexes

Saccharinato complexes can act as monodentate ligands *via* the N donor atom and as monodentate ligand through the O donor atom (carbonyl). This shows ambidentate behaviour and there are a number of other examples, using the pym ligand, such as $[M(sac)_2(pym)_4]$ whereby M(II) = Co, Zn, Cd and Ni, $[Cu(sac)_2(py)_3]$ and $[Cu(sac)_2(dipy)(H_2O)]$ (dipy = dipyridylamine)[90] and the tris of $ApyH[Cu(H_2O)_2(sac)_3]$.[64] An example is shown in Figure 1.15.

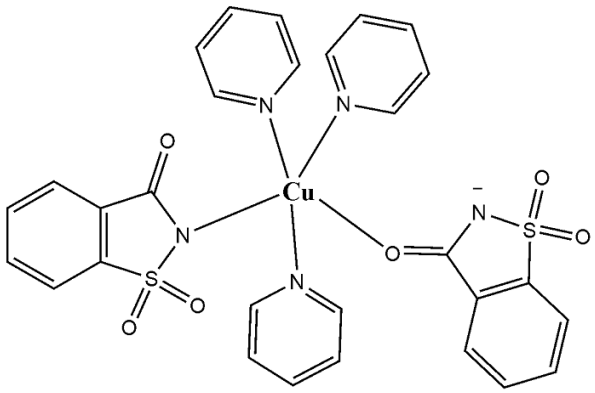

Figure 1. 15 The molecular view of $[Cu(sac)_2(py)_3]$ showing the ambidentate behaviour of saccharin.

1.7.9 Bonded and Non-Bonded Saccharinate Anion and Free Saccharin in the Complex

The saccharinato ligand is multi-functional which can coordinate to metal centres in the inner coordination sphere, but also act as a counter-anion in the outer coordination sphere thus non-bonding to the metal. This feature has been observed in the present study and previously reported for the following complexes: $[Zn(dien)_2](sac)_2$(dien = diethylenetriamine),[97] $[Zn(nic)_2(H_2O)_4](sac)_2$,[98] $[Cd(dien)_2(sac)_2]$,[97] $[Sr(tea)_2(sac)_2]$,[69(a)] $[Zn(H_2O)_2(pyet)_2](sac)_2$,[99] $[Fe(4,4'\text{-bpy})(H_2O)_4](sac)_2$,[100] $[Cd(tea)_2(sac)_2]$,[69] $[Hg(tea)_2(sac)_2]$,[69] $[M(H_2O)_2(pyet)_2](sac)_2$, M = Ni, $[Ba_2S_2(C_{12}H_{24}O_6)_2(H_2O)_2](sac)_2$ ($C_{12}H_{24}O_6$ = the 18-crown-6 ring of 1,4,7,10,13,16-hexaoxaacyclooctadecane),[101] $[Mn(H_2O)_2(phen)_2](sac)_2\cdot H_2O$, $[Cu(H_2O)_2(dmen)_2](sac)_2$,[102] $[Co(im)_4(H_2O)_2](sac)_2$,[95] $[Cu(H_2O)_2(apy)_2](sac)_2$(apy = 4-aminopyridine),[90] $[Zn(tea)_2(sac)_2]$ (tea = triethanolaminate),[69(b)] $[Cu(H_2O)_2(aim)_2]$ $(sac)_2$ (aim = N-alkylimidazole),[103] and $[Zn(dmpy)_2](sac)_2\cdot 2H_2O$.[104]

These metal complexes are non-hygroscopic and stable in air. They are very soluble in DMF and DMSO, and sparingly soluble in warm n-butanol and in methanol isopropanol mixtures. Dissolution of the complexes in water occurs with decomposition. From Table 1.2, not much difference is observed for the different metal-ligand bond lengths.

Table 1. 2 The octahedral complexes of non-bonded saccharinate anion

Complexes	Binding mode of ligand
$[Ni(sac)(H_2O)(bipy)_2](sac)$[66(b)]	Bidentate via N donor
$[Ni(dmpy)_2](sac)_2.2H_2O$[104]	Tridentate via N, O, O donors
$[Ni(H_2O)_2(pyet)_2](sac)_2$[105]	Bidentate via N and O donor
$[Ni(tea)_2(sac)_2]$[106]	Tridentate via N, O, O donors
$[Ni(dien)_2](sac)_2\cdot H_2O$[97]	Tridentate via N, N, N donors
$[Ni(nic)_2(H_2O)_4](sac)$[107]	Monodentate via N and O donors
$[Ni(H_2O)_4(py)_2](sac)_2$[108]	Monodentate via N and O donors
$[Co(sac)(H_2O)(bpy)_2](sac)$[109]	Bidentate via N donor atoms
$[Co(dmpy)_2](sac)_2\cdot 2H_2O$[110]	Tridentate via N, O, O donors
$[Co(H_2O)_2(pyet)_2](sac)_2$[111]	Bidentate via N and O donor
$[Co(tea)_2(sac)_2]$[112]	Tridentate via N, O, O donors
$[Co(nic)_2(H_2O)_4](sac)$[107]	Monodentate via N and O donors
$[Co(H_2O)_4(py)_2](sac)_2$[108]	Monodentate via N and O donors
$[Cu(sac)(byp)_2](sac)\cdot 2H_2O$[66(a)]	Bidentate via N donor atoms
$[Cu(dmpy)_2](sac)_2\cdot 2H_2O$[97]	Tridentate via N, O, O donors
$[Cu(H_2O)_2(pyet)_2](sac)_2$[113]	Bidentate via N and O donor
$[Cu(dien)_2](sac)_2\cdot H_2O$[97]	Tridentate via N, N, N donors

The following complexes are also closely related to those presented in the Table 1.2 $[M(sac)(H_2O)(bpy)_2](sac)$ whereby M(II) = Mn[74] and Zn,[66] $[Mn(sac)(H_2O)(phen)_2](sac)$,[75] $[Cu(sac)(dpy)_2](sac)\cdot 2H_2O$[114] and $[Cu_2(sac)_2(H_2O)_2(bypm)_3](sac)\cdot 2(sac)4H_2O$ (bypm = bipyrimidine)[115]. To reinforce the structural packing of the crystal, hydrogen bonds in the ligands of the complexes exist as supermolecular architectures. An example is shown in Figure 1.16.

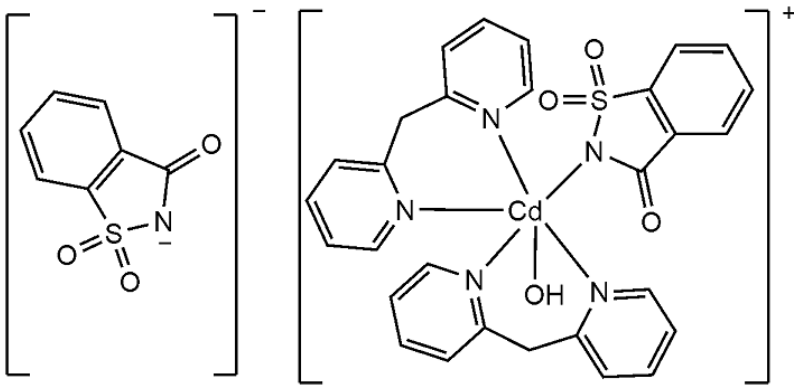

Figure 1. 16 The complex $[Cd(dipyr)_2(sac)(H_2O)](sac)\cdot(H_2O)$ showing bonded saccharinato ligand and non-bonded saccharinate anion.

1.8 Characteristics of Saccharinato Complexes on Biological Studies

The complex $[Zn(sac)_2(H_2O)_4]\cdot 2H_2O$[116, 117] has been shown to have certain inhibitory properties over the carbonic anhydrase enzyme family when they were tested *in vitro*. These types of enzymes are normally referred to as metalloenzymes because they can catalytically convert carbon dioxide and water into bicarbonate and protons. The active side of carbonic anhydrase is usually made of Zn(II) which maintains the balance in the blood and tissues of animals to help with the transportation of carbon dioxide out of the tissue.[118] This complex has the potential to be used as a therapeutic additive for dentifrices.[119] These are the agents to clear and brighten natural teeth. These occur as paste, powder, gels and liquid forms. A similar complex exhibiting inhibitory effects over the carbonic anhydrase is $[Cu(sac)_2(H_2O)_4]\cdot 2H_2O$ except that it cannot be used as a tooth brightening agent, but other complexes with similar properties include dioxouranium (VI), oxovanadium (IV), Ce(IV), Hg(II) and Pb(II).[120]

Most of the Ag(I) saccharinato complexes are polymeric and insoluble in nature, but are of great importance because they have antibacterial activities with sulfadiazine. Due to their insolubility, when examined for biological properties they show a slow liberation of Ag, which makes them a suitable candidate for antibacterial agent. They have been used in pharmaceutical formulation because they can slowly kill and slow down the growth of bacteria.[20, 121]

Studies on lanthanide saccharinato complexes have proven to be important in medical applications. Some of the thiosaccharinato complexes have also showed great potential in antimicrobial activities.[32]

1.9 Coordinating Ligand: Dimethyl Sulfoxide

1.9.1 Dimethyl Sulfoxide

Dimethyl sulfoxide (DMSO) is used considerably in the present study and a brief introduction is presented here. DMSO is a polar aprotic hygroscopic organosulfur compound, a by-product of wood industry and can also dissolve both polar and non-polar compounds. It is a reagent that can act either as a coordinating ligand or a solvent in many chemical reactions. It easily penetrates through the skin of mammalians and human beings. It gives a garlic-like taste in the mouth once it has entered the skin, as a sign of detection.[122, 123]

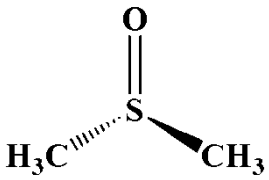

Figure 1. 17 A molecular representation of dimethyl sulfoxide.

1.9.2 Synthesis of Dimethyl Sulfoxide and Its Reactivity Properties

DMSO was first synthesised in 1867 by A. M. Zaitsev. DMSO was obtained by an exothermic oxidative reaction with slow addition of dimethyl sulphide to a concentrated nitric acid to yield the dimethyl sulfoxide.[122]

$$2H_3CSCH_3 + O_2 \longrightarrow 2H_3CSOCH_3 + 66.52kcal.$$

Scheme 1. 4 The oxidation reaction of dimethyl sulfide to yield DMSO.

Nitric acid, oxygen mixed with nitrogen oxides, hydrogen peroxide and many other oxidising reagents can be utilised to oxidise dimethyl sulfide to DMSO.[124]

DMSO is a good Lewis base and can thus act as ligand due to the two pairs lone electrons on the O atom. It also contains two methyl groups which are acidic in nature with a pKa value of 35, as opposed to water which is 15.7. Reactivity properties of DMSO resembles those of the reagents like dimethylformide, dimethylacetamide, N-methyl-2-pyrrolidane and hexamethylphosphoramide. In biochemistry and cell biology it is used as an extracting solvent. In chemistry it is not only used as a reaction solvent by as an important solvent in spectroscopy, i.e. DMSO-d_6 because of its solubilising ability.[125, 126] DMSO is utilised in pharmaceuticals as an anti-inflammatory and an antioxidant.

1.10 General Overview of Amines

1.10.1 Amines

Considerably use of amines was made in the study as coordinating ligands and a brief introduction is presented here. Compounds such as ethylenediamine, 2-(methylamino)ethanol, N-methyldiethanolamine and related compounds are organic amines which are derived from ammonia and are usually characterised by a strong smell of fish. Amines are formed by the process whereby one or more hydrogen atom(s) are replaced by hydrocarbon groups such as alkyl and/ or aryl groups. These are represented by the following formulas: RNH_2, NHR_2 and NR_3, where an electron lonepair resides on the atom.[127, 128]

CH_3NH_2	$(CH_3)NH$	$(CH_3)_2N(C_2H_5)$
methylamine	**dimethylamine**	**ethyldimethylamine**

Figure 1. 18 A representation of primary, secondary and tertiary amines.

The N atoms of amines are basic in nature, although the primary and secondary amines are slightly weak acids with the pKa value of 36. This is due to the influence of degree of solvation of the protonated amines, the steric factor which is more dependent on the group attached to the nitrogen, and the electronic properties of the substituent that replaces hydrogen atom during the synthesis. It should be noted that the same factor that increases the acidity of the amines also decreases their basicity.[128]

Amines are weak hydrogen forming compounds compared to alcohols and this is due to the fact that the N atom is less electronegative than O atom of the alcohols, decreasing the force of attraction between the hydrogen and the nitrogen of the corresponding amine.[129]

1.11 The Aims and Objectives of this Study

Based on the background information provided, that indicates a lack of area not previously investigated, it was felt necessary to further investigate the coordination chemistry of the saccharinato metal complexes. $[M(sac)_2(H_2O)_4]\cdot 2H_2O$ where M(II) represents metal centres such as Co, Cu, Zn, Cd, Hg and Ni, was felt to provide interesting structural motifs and they may also have important biological applications, as indicated. The nucleophilic reaction and the strength of the O donor atom of the DMSO reagent was investigated whereby DMSO was reacted directly at elevated temperature in the presence of the common starting material $[M(sac)_2(H2O)_4]\cdot 2H_2O$. The pKa value of DMSO is greater than water, i.e. 35 and 15.7, respectively, allowing displacement of the labile aqua ligands. Based on the above discussion, amines were used as Lewis bases and bonded to the Lewis acidic metal centres via coordinative dative bonds. This was further investigated with the following amines: ethylenediamine, 2-(methylamino)ethanol and (N-methyldiethanolamine).

1.11.1 Motivation for study

Investigating the coordination patterns of saccharinato complexes and determining the binding modes in late transition metal centres is an interesting study to undertake. A literature search revealed where there is still a number of new areas that could be explored. The polyfunctional nature of saccharin displays different coordination geometry in various complexes thus giving it unique spectral properties. Saccharinato complexes are also of great interest in catalytic studies. These factors combined proved to be a fruitful endeavour to synthesize these complexes which can contribute in the growth and development of the saccharin chemistry.

1.11.2 Aims of the study

- To synthesize several saccharinato complexes of various group 9 to 12 metal complexes with varying neutral auxiliary ligands such as dmso and amines.
- To form a series of stable, isolable complexes with the saccharinato ligand either binding directly to the metal, or in the second coordination sphere forming salts.
- To characterize the synthesized complexes by infra-red, UV-vis and NMR spectroscopy, elemental analyses, determine their melting/decomposition points, thermal studies (TGA and DSC) and to perform single crystal X-ray crystallography on the majority of the new complexes.

1.12 References

1. http://www.saccharin.org/healthy_links.html (Accessed 21 June, 2010).

2. B. Schulze and K. Illgen, *J. Prakt. Chem./Chem-Ztg*, 1997, **339**, 1-14.

3. M. L. Mitchell and R. L. Pearson, *Alternative Sweeteners*, 1991, 127-156.

4. J. W. Ellis, *J. Chem. Educ.*, 1995, **72**, 671-675.

5. D. E. Walters, *J. Chem. Educ.*, 1995, **72**, 680-683.

6. F. M. Assadi-Porter, M. Tonelli, E. Maillet, K. Hallenga, O. Benard, M. Max and J. L. Markley, *J. Am. Chem. Soc.*, 2008, **130**, 7212-7213.

7. R. S. Shallenberger, T. E. Acree and C. Y. Lee, *Nature*, 1969, **221**, 555-556.

8. D. P. P. David, J. Ager, S. A. Henderson, A. R. Katritzky, I. Prakash, D. E. Walters, *Angew. Chem. Int. Ed.*, 1998, **37**, 1802–1817.

9. Y. Nosho, T. Seki, M. Kondo, T. Ohfuji, M. Tamura and H. Okai, *J. Agric. Food. Chem.*, 1990, **38**, 1368-1373.

10. T. R. Scott and J. V. Verhagen, *Nutrition*, 2000, **16**, 874-885.

11. R. S. Shallenberger, *Taste Chemistry*, Blackie Academic & Professional, 1993, 8-16.

12. M. Soffritti, F. Belpoggi, E. Tibaldi, D. D. Esposti and M. Lauriola, *Environ. Health Perspect.*, 2007, **115,** 1293-1297.

13. H. Mitchell, *Sweeteners and Sugar Alternatives in Food Technology*, Blackwell Publishing, Oxford, 2006, 103-129.

14. R. H. Mazur, J. M. Schlatter and A. H. Goldkamp, *J. Am. Chem. Soc.*, 1969, **91**, 2684-2691.

15. K. Clauss and H. Jensen, *Angew. Chem. Int. Ed.*, 1973, **12**, 869-876.

16. L. Hough and S. P. Phadnis, *Nature*, 1976, **263**, 800-800.

17. J.-M. Tinti and C. Nofre, *Chem. Senses*, 2001, **26**, 231-237.

18. M. J. O'Neil, *The Merck index : An Encyclopedia of Chemicals, Drugs, and Biologicals*, Merck & Co., Whitehouse Station, 2001, 440-462.

19. R. Mazur, Sweeteners, Wiley, New York, 1983, **22**, 448-449.

20. E. J. Baran, *Quim. Nova*, 2005, **28**, 326-328.

21. E. J. Baran and V. T. Yilmaz, *Coord. Chem. Rev.*, 2006, **250**, 1980-1999.

22. J. C. J. Bart, *J. Chem. Soc. B*, 1968, 376-382.

23. Y. Okaya, *Acta Cryst.*, 1969, B**25**, 2257-2263.

24. R. Bell, *South. Med. J.*, 1949, **42**, 141-144.

25. L. Williams-Seton, R. J. Davey and H. F. Lieberman, *J. Am. Chem. Soc.*, 1999, **121**, 4563-4567.

26. I. Remsen and C. Fahlberg, *Chem. Ber.,* 1879, **12**: 469–473.

27. V. M. F. Morais, M. S. Miranda, M. A. R. Matos and J. F. Liebman, *Mol. Phys.*, 2006, **104**, 325-334.

28. J. Junge, *Deutsch. Lebensm.-Rundschau*, 1951, **47**, 7.

29. G. A. Iacobucci, *Ing. Quim.*, 1998, **334**, 18.

30. G. H. Hamor and T. O. Soine, *J. Am. Pharm. Assoc.*, 1954, **43**, 120-123.

31. O. Z. Yeşilel, G. Günay and O. Büyükgüngör, *Polyhedron*, 2011, **30**, 364-371.

32. E. J. Baran and V. T. Yilmaz, *Coord. Chem. Rev.*, 2006, **250**, 1980-1999.

33. K. Rosenman, *Environ. Res.*, 1978, **15**, 70-81.

34. D. B. Clayson, Committee on Amines, Assembly of Life Sciences . Board on Toxicology, Environmental Health Hazards, Assembly Of Life Sciences, *Aromatic Amines: An Assessment of the Biological and Environmental Effects*, National Academy Press, 1981, 60-85.

35. L. B. Ellwein and S. M. Cohen, *Crit. Rev. Toxicol.*, 1990, **20**, 311-326.

36. S. M. Cohen, L. L. Arnold and J. L. Emerson, *Agro Food Industry Hi-Tech*, 2008, **19**, 24-28.

37. S. M. Cohen, *Toxicology*, 1995, **102**, 149-159.

38. V. J. H. Ṛuben Vardanyan, ed. V. J. Hruby, Elsevier, 2006, 51-52.

39. J. W. Lehman, *Operational Organic Chemistry: A Problem-Solving Approach to the Laboratory Course*, Pearson Prentice Hall, 2009, 177- 179.

40. *Lehman, J. W. Operational Organic Chemistry: A Problem-Solving Approach to the Laboratory Course, 3rd Ed., Prentice-Hall, Inc., Upper Saddle River, New Jersey, 1999, 150-155.*

41. E. Klingsberg and D. Papa, *J. Am. Chem. Soc.*, 1951, **73**, 4988-4989.

42. J. R. Meadow and J. C. Cavagnol, *J. Org. Chem.*, 1951, **16**, 1582-1587.

43. K. M. A. Malik, S. Z. Haider, M. A. Hossain and M. B. Hursthouse, *Acta Cryst.*, 1984, C**40**, 1696-1698.

44. S. W. Ng, *Acta Cryst.*, 1998, C**54**, 649-651.

45. P. Naumov, G. Jovanovski, O. Grupče, B. Kaitner, A. D. Rae and S. W. Ng, *Angew. Chem. Int. Ed.*, 2005, **44**, 1251-1254.

46. G. Jovanovski and B. Kamenar, *Acta Cryst.*, 1982, C**11**, 247-255.

47. R. Banerjee, P. M. Bhatt, M. T. Kirchner and G. R. Desiraju, *Angew. Chem. Int. Ed.*, 2005, **44**, 2515-2520.

48. P. Naumov, G. Jovanovski, S. Abbrent and L. E. Tergenius, *Thermochim. Acta*, 2000, **359**, 123-130.

49. P. Naumov and G. Jovanovski, *Vib. Spectrosc.*, 2000, **24**, 201-211.

50. P. Naumov and G. Jovanovski, *Spectrochim. Acta PartA Mol. Biomol. Spectrosc.*, 2000, **56**, 1305-1318.

51. P. Naumov and G. Jovanovski, *Curr. Org. Chem.*, 2001, **5**, 1059-1077.

52. S. Z. Haider, K. M. A. Malik and K. J. Ahmed, *J. Bangladesh Acad. Sci.*, 1981, **5**, 81-90.

53. F. A. Cotton, G. E. Lewis, C. A. Murillo, W. Schwotzer and G. Valle, *Inorg. Chem.*, 1984, **23**, 4038-4041.

54. S. Z. Haider, K. M. A. Malik, K. J. Ahmed, G. B. Kauffman and M. Karbassi, in *Inorg. Synth.*, John Wiley & Sons, Inc., 2007, 47-51.

55. S. Z. Haider, K. M. A. Malik, K. J. Ahmed, H. Hess, H. Riffel and M. B. Hursthouse, *Inorg. Chim. Acta*, 1983, **72**, 21-27.

56. S. Z. Haider, K. M. A. Malik, S. Das and M. B. Hursthouse, *Acta Cryst.*, 1984, C**40**, 1147-1150.

57. L. R. Falvello, J. Gomez, I. Pascual, M. Tomás, E. P. Urriolabeitia and A. J. Schultz, *Inorg. Chem.*, 2001, **40**, 4455-4463.

58. V. T. Yilmaz, E. Senel, E. Guney and C. Kazak, *Inorg. Chem. Commun.*, 2008, **11**, 1330-1333.

59. S. W. Ng, *Acta Cryst.*, 1996, C**52**, 1365-1367.

60. S. Hamamci, V. T. Yilmaz and W. T. A. Harrison, *Struct. Chem.*, 2005, **16**, 379-383.

61. S. Hamamci, V. T. Yilmaz, W. T. A. Harrison and C. Thöne, *Solid State Sci.*, 2005, **7**, 423-429.

62. V. T. Yilmaz, S. Hamamci and C. Kazak, *Z. Anorg. Allg. Chem.*, 2005, **631**, 1961-1965.

63. P. A. M. Williams, E. G. Ferrer, M. J. Correa, E. J. Baran, E. E. Castellano and O. E. Piro, *J. Chem. Crystallogr.*, 2004, **34**, 285-290.

64. V. T. Yilmaz, Y. Topcu, F. Yilmaz and C. Thoene, *Polyhedron*, 2001, **20**, 3209-3217.

65. V. T. Yilmaz, S. Caglar and W. T. A. Harrison, *Acta Cryst.*, 2004, C**60**, m35-m38.

66. (a) A. Hergold-Brundic, O. Grupce and G. Jovanovski, *Acta Cryst.*, 1991, C**47**, 2659-2660. (b) V. T. Yilmaz, S. Guney, O. Andac and W. T. A. Harrison, *J. Coord. Chem.*, 2003, **56**, 21-32.

67. (a) V. Yilmaz, F. Yilmaz and C. Kazak, *Transition Met. Chem.*, 2005, **30**, 95-102.

(b) V. Yilmaz, S. Hamamci, O. Andac, C. Thöne and W. A. Harrison, *Trans. Met. Chem.*, 2003, **28**, 676-681.

68. O. Andac, Y. Topcu, V. T. Yilmaz and W. T. A. Harrison, *J. Chem. Crystallogr.*, 2000, **30**, 767-771.

69. O. Andac, Y. Topcu, V. T. Yilmaz and K. Guven, *Acta Cryst.*, 2001, C**57**, 1381-1384.

(a) C. Kazak, S. Hamamci, Y. Topcu, V.T. Yilmaz, *J. Mol. Struct*. 2003, **657**, 351-536.

(b) Y. Topcu, V.T. Yilmaz and C. Thoene, *Acta Cryst*., 2001, **E57**, m600-m602.

70. V. T. Yilmaz, S. Caglar and W. T. A. Harrison, *Transition Met. Chem.*, 2004, **29**, 477-482.

71. V. T. Yilmaz, S. Caglar and W. T. A. Harrison, *J. Coord. Chem.*, 2005, **58**, 549-558.

72. O. Andac, Y. Topcu, V. T. Yilmaz and W. T. A. Harrison, *Acta Cryst.*, 2002, C**58**, m14-m16.

73. V. Yilmaz, A. Karadag and C. Thoene, *J. Coord. Chem.*, 2002, **55**, 609-618.

74. K. B. Dillon, C. Bilton, J. A. K. Howard, V. J. Hoy, R. M. K. Deng and D. T. Sethatho, *Acta Cryst.*, 1999, C**55**, 330-332.

75. R. M. K. Deng, C. Bilton, K. B. Dillon and J. A. K. Howard, *Acta Cryst.*, 2000, C**56**, 142-145.

76. A. Hergold-Brundic, B. Kamenar and G. Jovanovski, *Acta Cryst.*, 1989, C**45**, 556-558. (a) O. Grupče, G. Jovanovski, B. Kaitner and P. Naumov, *Croat. Chem. Acta*, 1999, **72**, 465-476.

77. I. Pascual, *Acta Cryst.*, 1995, C**51**, 2028-2030.

78. N. M. Alfaro, F. A. Cotton, L. M. Daniels and C. A. Murillo, *Inorg. Chem.*, 1992, **31**, 2718-2723.

79. Z. Yugeng, L. Jianmin, W. Jing, W. Xingtao and D. Shaowu, *Cryst. Res. Technol.*, 1994, **29**, 975-980.

80. L. Jianmin, L. Wenbin, Z. Yugeng, L. Shixiong and H. Jinling, *Polyhedron*, 1991, **10**, 403-407.

81. G. Jovanovski, B. Kamenar, G. Ferguson and B. Kaitner, *Acta Cryst.*, 1988, C**44**, 616-618.

82. V. T. Yilmaz, S. Hamamci and C. Thöne, *Cryst. Res. Technol.*, 2002, **37**, 1143-1148. (a) V. T. Yilmaz, S. Hamamci and C. Thöne, *Z. Anorg. Allg. Chem.*, 2003, **629**, 711-715

83. V. T. Yilmaz, S. Hamamci, C. Thoene, *Z. Anorg. Allg. Chem.*, 2004, **630**, 1641-1644.

84. S. Cakir *at al*., *Acta. Cryst.*, 2001, **E57**, m431-m432.

85. S. W. Ng, C. Wei, V. G. Kumar Das and T. C. W. Mak, *J. Organomet. Chem.*, 1989, **373**, 21-27.

86. S. W. Ng, A. J. Kuthubutheen, Z. Arifin, C. Wei, V. G. Kumar Das, B. Schulze, K. C. Molloy, W. H. Yip and T. C. W. Mak, *J. Organomet. Chem.*, 1991, **403**, 101-109.

87. O. V. Quinzani, S. Tarulli, C. Marcos, S. Garcia Granda and E. J. Baran, *Z. Anorg. Allg. Chem.*, 1999, **625**, 1848-1852.

88. V. T. Yilmaz, S. Hamamci, W. T. A. Harrison and C. Thoene, *Polyhedron.*, 2004, **24**, 1693-699.

89. E. G. Ferrer, S. B. Etcheverry and E. J. Baran, *Monatsh. Chem.*, 1993, **124**, 355-366.

90. P. Naumov, G. Jovanovski, M. G. B. Drew and S. W. Ng, *Inorg. Chim. Acta*, 2001, **314**, 154-162.

91. P. Naumov, G. Jovanovski, M. Ristova, I. A. Razak, S. Çakir, S. Chantrapromma, H. K. Fun and S. W. Ng, *Z. Anorg. Allg. Chem.*, 2002, **628**, 2930-2939.

92. S. Hamamci, V. T. Yilmaz and W. T. A. Harrison, *J. Coord. Chem.*, 2003, **56**, 1033-1039.

93. V. T. Yilmaz, S. Hamamci and C. Thöne, *Cryst. Res. Technol.*, 2003, **38**, 992-995.

94. S. Guney, V. T. Yilmaz and W. T. A. Harrison, *J. Coord. Chem.*, 2005, **58**, 1667-1674.

95. L. Jianmin, Z. Yugeng, L. Wenbin and L. Shixiong, *Polyhedron*, 1992, **11**, 419-422.

96. V. T. Yilmaz, S. Hamamci and O. Büyükgüngör, *Polyhedron*, 2008, **27**, 1761-1766.

97. C. A. Johns and K. M. Abdul Malik, *Polyhedron*, 2002, **21**, 395-401.

98. B. S. Parajón-Costa, E. J. Baran, O. E. Piro and E. E. Castellano, *Z. Naturforsch.,B: Chem. Sci.*, 2002, **57**, 43-46.

99. S. Hamamci, V. T. Yilmaz and C. Thone, *Acta Cryst.*, 2002, E**58**, m369-m371.

100. P. D. L. Williams, *J. Navig.*, 2002, **55**, 405-418.

101. S. Chantrapromma, A. Usman and H. K. Fun, *Acta Cryst.*, 2002, C**58**, m534-m536.

102. H. Icbudak, H. Olmez, O. Z. Yesilel, F. Arslan, P. Naumov, G. Jovanovski, A. R. Ibrahim, A. Usman, H.-K. Fun, S. Chantrapromma and S. W. Ng, *J. Mol. Struct.*, 2003, **657**, 255-270.

103. P. Naumov, G. Jovanovski, M. Ristova, I. A. Razak, S. Cakir, S. Chantrapromma, H. K. Fun and S. W. Ng , *Z. Anorg. Allg. Chem.*, 2002, **628**, 2930-2939.

104. V. T. Yilmaz, S. Guney, O. Andac and W. T. A. Harrison, *J. Coord. Chem.*, 2003, **56**, 21-32.

105. V. T. Yilmaz, S. Guney, O. Andac and W. T. A. Harrison, *J. Coord. Chem.*, 2003, **56**, 21-32.

106. Y. Topcu, O. Andac, V. T. Yilmaz and W. T. A. Harrison, *Acta Cryst.*, 2001, E**57**, m82-m84.

107. E. E. Castellano, O. E. Piro, B. S. Parajón-Costa and E. J. Baran, *Z. Naturforsch.,B: Chem. Sci.*, 2002, **57**, 657-660.

108. G. Jovanovski, P. Naumov, O. Grupče and B. Kaitner, *Eur. J. Solid State Inorg. Chem.*, 1998, **35**, 579-590.

109. R. M. K. Deng, C. Bilton, K. B. Dillon and J. A. K. Howard, *Acta Cryst.*, 2000, C**56**, 142-145.

110. O. Andac, S. Guney, Y. Topcu, V. T. Yilmaz and W. T. A. Harrison, *Acta Cryst.*, 2002, C**58**, m17-m20.

111. V. T. Yilmaz, S. Hamamci and C. Thone, *Acta Cryst.*, 2002, **58**, m702-m704.

112. Y. Topcu, O. Andac, V. Yilmaz and W. Harrison, *J. Coord. Chem.*, 2002, **55**, 805-815.

113. V. T. Yilmaz, S. Hamamci and C. Thöne, *J. Coord. Chem.*, 2003, **56**, 787-795.

114. A. Hergold-Brundic, O. Grupce and G. Jovanovski, *Acta Cryst.*, 1991, C**47**, 2659-2660.

115. G. A. van Albada, I. Riggio, J. Reedijk, I. Mutikainen and U. Turpeinen, *Trans. Met. Chem.*, 2002, **27**, 341-345.

116. C. T. Supuran and I. Puscas, *Helicon: Timisoara*, 1994, 29-111.

117. F. Mincione, L. Menabuoni, F. Briganti, G. Mincione, A. Scozzafava and C. T. Supuran, *J. Enzym Inhib. Med. Chem.*, 1998, **13**, 267-284.

118. M. R. Badger and G. D. Price, *Ann. Rev. Plant Physiol. Plant Mol. Biol.*, 1994, **45**, 369-392.

119. G. L. Christie, D. Cummins, J. R. Duffield, S. R. Hurford, C. R. Morris, P. I. Riley, J. A. Vesey and D. R. Williams, *J. Inorg. Biochem.*, 1991, **42**, 273-287.

120. C. T. Supuran, J. Y. Winum and B. Wang, *Drug Design of Zinc-Enzyme Inhibitors: Functional, Structural, and Disease Applications*, John Wiley & Sons, 2009, 15-35.

121. R. Weber, M. Gilles and G. Bergerhoff, *Z. Kristallogr.*, 1993, **206**, 273-274.

122. K.-M. Roy, in *Ullmann's Encyclopedia of Industrial Chemistry*, Wiley-VCH Verlag GmbH & Co. KGaA, 2000, 716-717.

123. F. G. Bordwell, *Acc. Chem. Res.*, 1988, **21**, 456-463.

124. M. V. Gavrilin, G. V. Sen'chukova and E. V. Kompantseva, *Pharm. Chem. J.*, 2000, **34**, 490-493.

125. K. V. Balakin, N. P. Savchuk and I. V. Tetko, *Curr. Med. Chem.*, 2006, **13**, 223-241.

126. G. Kvakovszky, A. McKim and J. C. Moore, *ECS Trans.*, 2007, **11**, 227-234.

127. C. W. Hoerr, H. J. Harwood and A. W. Ralston, *J. Org. Chem.*, 1944, **09**, 201-210.

128. M. A. Fox and J. K. Whitesell, *Organic Chemistry*, Jones and Bartlett Publishers, 2004, 64-74.

129. F. A. Bettelheim and J. M. Landesberg, *Laboratory Experiments for Introduction to General, Organic and Biochemistry*, Cengage Learning, 2012, 341-345.

CHAPTER 2

EXPERIMENTAL SECTION

2.1 Introduction

This chapter outlines the experimental methods and conditions used to prepare the complexes described in this thesis. The synthetic methods are generalized for a similar series of complexes. The complexes are represented in bold in the experimental procedure. The TGA results will be tabulated in the discussion section for those complexes in which the TGA was performed.

2.2 Materials and Instrumentation

2.2.1 Materials

All chemicals and solvents used were Analytical Grade purchased from Sigma-Aldrich and were used without further purification. Double distilled water was utilized. All reactions were performed under atmospheric conditions. Crystals which were used for single crystal X-ray crystallographic studies were obtained by slow evaporation of the solvent.

As suggested on the preparation procedures below of $[M(sac)_2(H_2O)_4]\cdot 2H_2O$ whereby M represent the metal centre, complexes were prepared as per literature method.[1-6]

2.2.2 Instrumentation

IR spectra were recorded on an ATR spectrophotometer in the range of 380-4000 cm^{-1} using Perkin-Elmer® Precisely, Universal ATR Sampling Accessory.

UV-Vis spectrophotometry, were performed at different concentration ranges and were recorded on a Shimadzu, UV-3600, UV-VIS-NIT spectrophotometer in the range of 250-900 nm for complexes (**2**), (**5**), (**6**)-(**10**) and (**12**) and 200-700 nm complexes (**1**), (**3**), (**4**) and (**11**). All complexes were run in DMF except (**6**) and (**10**) which were analysed in DMSO.

^{1}H and ^{13}C NMR spectra of complexes (**1**), (**3**), (**4**) and (**11**) were recorded in deuterated solvents on a Bruker Ultra-Shield™ spectrometer AVANCE^{III} operating at 400 MHz. The chemical shifts were recorded as δ values in reference to $SiMe_4$ at 0.00 parts per million (ppm) at 25°C (298.15K).

The purity of the complexes was determined by melting point on a SMP3, Stuart Scientific melting point apparatus/hot stage, made in UK.

The CHN elemental analyses were carried out using Thermo Scientific Flash 2000 Elemental Analyser at the Mass Spectrometry laboratory, School of Chemistry and Physics, UKZN.

Thermal analysis curves (TG, DTA and DTG) were obtained using TA instruments SDT Q600, second generation simultaneous TGA/ DSC thermal analyzer in a dynamic nitrogen atmosphere with the flow rate of 80 cm^3 min^{-1} at the temperature range of 25 to 1000 °C . A sample size of 5-10 mg and a heating rate of 10 °C min^{-1} were used.

2.3 Synthesis of Saccharinato Complexes of Dimethyl Sulfoxide

Complexes (**1**) to (**5**) were synthesized using the same general procedure as described below where DMSO = (dimethyl sulfoxide).

2.3.1 Synthesis of *trans*-$[Cd(sac)_2(dmso)_2(H_2O)_2]$ (**1**)

Colourless microcrystals of $[Cd(sac)_2(H_2O)_4]\cdot 2H_2O$ (1.13 g; 2.10 mmol) were placed in a 100 mL beaker and dissolved in excess amounts of dimethyl sulfoxide (20 mL). The reaction mixture was gently heated on a heating plate with stirring to reduce the volume of DMSO to ~7 mL. The beaker was removed from the heat source and allowed to stand for 6 days during which time large colourless blocky crystals of complex were obtained. Yield (1.30 g, 92%); Mp 114°C; Anal. Calc. for $C_{18}H_{24}CdN_2O_{10}S_4$: C, 32.3; H, 3.6; N, 4.5. Found: C, 33.2; H, 3.7; N, 4.8 %. ^{1}H NMR (CD_3OD, 400MHz) δ(ppm):3.36 (m, 4H, H_2O), 2.53 (s, 12H, DMSO), 7.57-7.67 (m. 8H, C_6H_4); ^{13}C NMR (MeOD, 101MHz) d(ppm.): 40.36 (CH_3-dmso), 119.15 (C_6-ring), 122.54 (C_6-ring), 131.46 (C_6-ring), 131.15 (C_6-ring), 134.46 (C_6-ring), 145.14 (C_6-ring) 167.86 (C=O); IR (ATR) 3481, 3016 ν(OH), 1646, 1609 ν(C=O), 1583, 1460 ν(C=C), 1271, 1256 ν(O=S=O); 1054, 1036 ν(S=O).

2.3.2 Synthesis of *trans*-$[Co(sac)_2(dmso)_2(H_2O)_2]$ (**2**)

Red microcrystals of $[Co(sac)_2(H_2O)_4]\cdot 2H_2O$ (0.932 g; 1.80 mmol) were used in the reaction. The crystals grew to convenient size after 10 days in a beaker by slow evaporation of DMSO solvent yielding large light red blocky crystals of (**2**). Yield (1.00 g, 93.0%); Mp 120°C. Anal. Calc. for $C_{18}H_{24}CoN_2O_{10}S_4$: C, 35.1; H, 3.9; N, 5.0. Found: C, 35.5; H, 4.0; N, 5.1 %. IR-ATR (cm^{-1}): 3486, 3005 ν(OH); 1618 ν(C=O); 1584, 1460 ν(C=C); 1256 ν(O=S=O); 1141 ν(S=O).

2.3.3 Synthesis of $[Zn(sac)_2(dmso)_2]$ (**3**)

Colourless microcrystals of $[Zn(sac)_2(H_2O)_4]\cdot 2H_2O$ (1.60 g; 2.82 mmol) were used in the reaction. The crystals grew to convenient size after 6 days in a beaker by the method of slow evaporation of DMSO solvent yielding colourless blocky crystals of (**3**). Yield (1.51 g, 92%); Mp 190°C; Anal. Calc. for $C_{18}H_{20}ZnN_2O_6S_4$: C, 36.8; H, 4.1; N, 4.5. Found: C, 36.6; H, 4.0; N, 4.6 %. ^{1}H NMR (MeOD, 400MHz) δ(ppm): 2.56 (s, 12H, DMSO), 7.62-7.76 (m. 8H, C_6H_4); ^{13}C NMR (MeOD, 101 MHz) δ(ppm.): 40.37 (CH_3-DMSO), 121.23 (C_6-ring), 124.89 (C_6-ring), 133.32 (C_6-ring), 134.21 (C_6-ring), 134.27 (C_6-ring), 144.80 (C_6-ring) 171.57 (C=O); IR (ATR) 1687 ν(C=O), 1596, 1419ν(C=C), 1274, 1245 ν(O=S=O); 1138 ν(S=O).

2.3.4 Synthesis of $[Hg(sac)_2(dmso)(H_2O)]$ (**4**)

Colourless microcrystals of $[Hg(sac)_2(H_2O)_4]\cdot 2H_2O$ (2.00 g; 2.97 mmol) were used in the reaction. The crystals grew to convenient size after 9 days in a beaker by the method of slow evaporation of DMSO solvent yielding colourless blocky crystals of (**4**). Yield (1.75 g, 80 %); Mp 135°C; Anal. Calc. for $C_{16}H_{24}HgN_2O_8S_3$: C, 32.8; H, 3.9; N, 4.5. Found: C, 30.5; H, 3.5; N, 4.1 %. ^{1}H NMR (CD_3OD, 400MHz) δ(ppm): 2.49 (m, 2H, H_2O), 2.53 (s, 6H, DMSO), 7.87-8.09 (m. 8H, C_6H_4); ^{13}C NMR (CD_3OD, 101MHz) d(ppm.): 40.38 (CH_3-dmso), 120.74 (C_6-ring), 124.42 (C_6-ring), 128.96 (C_6-ring), 134.03 (C_6-ring), 134.68 (C_6-ring), 142.34 (C_6-ring) 163.87 (C=O); IR (ATR) 3414ν(OH), 1674, 1674ν(C=O), 1594, 1458 ν(C=C), 1310, 1285, 1302 $\nu(CNS)_{sym}$; 1284, 1243 $\nu(O=S=O)_{asym}$; 1154, 1170 $\nu(O=S=O)_{sym}$; 947 $\nu(CNS)_{asym}$; 1121, 1138 ν(S=O).

2.3.5 Synthesis of $[Cu(sac)_2(dmso)(H_2O)_2]$ (**5**)

Blue microcrystals of $[Cu(sac)_2(H_2O)_4]\cdot 2H_2O$ (1.13 g; 2.10 mmol) were used in the reaction. The crystals grew after 9 days in a beaker by the method of slow evaporation of DMSO solvent yielding deep blue crystals of (**5**). Yield (1.02g, 90%); Mp 184-185°C; Anal. Calc. for $C_{16}H_{24}HgN_2O_8S_3$: C, 35.8; H, 3.3; N, 5.2. Found: C, 35.5; H, 3.4; N, 5.2 %. ^{13}C NMR (CD_3OD, 101MHz) d(ppm.): 40.39 (CH_3-dmso), 121.20 (C_6-ring), 124.91 (C_6-ring), 133.42 (C_6-ring), 134.21 (C_6-ring), 134.24 (C_6-ring), 144.90 (C_6-ring) 171.90 (C=O); IR (ATR) 3275 ν(OH), 1651, 1619 ν(C=O), 1586 ν(C=C), 1256, 1300 $\nu(O{=}S{=}O)_{asym}$;1161 $\nu(O{=}S{=}O)_{sym}$, 1345 $\nu(CNS)_{sym}$, 951$\nu(CNS)_{asym}$, 1147 ν(S=O). Single crystals were obtained by slow evaporation of DMSO solvent.

2.4 Synthesis of Saccharinato Complexes of N-methyldiethanolamine and 2-(methylamino)ethanol

Complexes (**6**) to (**9**) were synthesized using the same general procedure as described below where mdea = (N-methyldiethanolamine) and mea = (2-(methylamino)ethanol).

2.4.1 Synthesis of $[Ni(\textit{N,O,O}\text{-mdea})_2]\cdot 2(sac)$ (**6**)

Green coloured microcrystals of $[Ni(sac)_2(H_2O)_4]\cdot 2H_2O$ (0.350g; 0.659 mmol) were placed in a 250 mL beaker and dissolved in methanol (30 mL) and N-methyldiethanolamine (1 mL) was added and the reaction mixture was gently stirring for 15 minutes at 80°C. The beaker was removed from the heat source and allowed to stand for 3 days during which time large violet block crystals of (**6**) were obtained. Yield (0.325 g, 75%); Mp 225°C (decompose); Anal. Calc. for $C_{24}H_{34}CoN_4O_{10}S_2$: C, 43.3; H, 4.8; N, 8.4. Found: C, 43.0; H, 4.6; N, 8.6 %. IR (ATR) 2917 $\nu(N\text{-}CH_3)$, 2690 $\nu(CH_2)$,1613 ν(C=O), 1580, 1441 ν(C=C), 1336 $\nu(CNS)_{sym}$; 1286 $\nu(S{=}O)_{asym}$,1155 $\nu(S{=}O)_{sym}$, 979 $\nu(CNS)_{asym}$, 535 ν(Co-N). Single crystals were obtained by slow evaporation of methanol solvent.

2.4.2 Synthesis of [Cu(sac)$_2$(*N,O,O*-mdea)$_2$] (**7**)

Green crystals of [Cu(sac)$_2$(H$_2$O)$_4$]·2H$_2$O (0.350g; 0.651 mmol) were used in the reaction. The crystals grew after 3 days in a beaker by the method of slow evaporation of water/ methanol solvent yielding large blue block crystals of (**7**). Yield (0.375 g, 86%); Mp 195°C; Anal. Calc. for $C_{24}H_{34}CuN_4O_{10}S_2$: C, 43.3; H, 5.1; N, 8.4. Found: C, 44.3; H, 5.2; N, 8.7 %. IR (ATR) 3407 ν(OH), 2921 ν(CH), 1638 ν(C=O), 1454 ν(C=C), 1347 $\nu(CNS)_{sym}$; 1295 $\nu(S=O)_{asym}$,1168, 1144 $\nu(S=O)_{sym}$, 965 $\nu(CNS)_{asym}$, 554 ν(Co-N). Single crystals were obtained by slow evaporation of water solvent.

2.4.3 Synthesis of [Co(sac)$_2$(*N,O,O*-mdea)$_2$] (**8**)

Red crystals of [Co(sac)$_2$(H$_2$O)$_4$]·2H$_2$O (0.350g; 0.653 mmol) were used in the reaction. The crystals grew to convenient size after 3 days in a beaker by the method of slow evaporation of methanol solvent yielding large light orange block crystals of (**8**). Yield (0.367 g, 87%); Mp 210°C (decompose); Anal. Calc. for $C_{24}H_{34}CoN_4O_{10}S_2$: C, 43.6; H, 5.2; N, 8.4. Found: C, 43.3; H, 5.1; N, 8.0 %. IR (ATR) 2917, 2858 $\nu(N\text{-}CH_3)$, 2672 ν(CH), 1620 ν(C=O), 1580, 1453 ν(C=C), 1346 $\nu(CNS)_{sym}$; 1284 $\nu(S=O)_{asym}$,1146 $\nu(S=O)_{sym}$, 962 $\nu(CNS)_{asym}$, 533 ν(Co-N). Single crystals were obtained by slow evaporation of methanol solvent.

2.4.4 Synthesis of [(Cu$_2$(μ-*O*)$_2$(mea)$_4$]·2(sac) (**9**)

Blue crystals of [Cu(sac)$_2$(H$_2$O)$_4$]·2H$_2$O (0.350g; 0.653 mmol) were placed in a 250 mL beaker and dissolved in double distilled water (30 mL) and 2-(methylamino)ethanol (1 mL) was added and the reaction mixture was gently stirred on a hotplate for 15 minutes at 80°C. The beaker was removed from the heat source and allowed to stand for 3 days during which time large blue plate crystals of (**9**) were obtained. Yield (0.390 g. 76%); Mp 165°C; Anal. Calc. for [($C_{12}H_{34}Cu_2N_2O_4$)].2($C_7H_4NO_3S$): C, 39.5; H, 5.4; N, 10.6. Found: C, 39.2; H, 5.0; N, 10.2 %.IR (ATR) 3187 ν(NH), 2823, 2876 ν(NH), 1627 ν(C=O), 1583, 1456 ν(C=C), 1330 $\nu(CNS)_{sym}$; 1255 $\nu(S=O)_{asym}$,1147 $\nu(S=O)_{sym}$, 947 $\nu(CNS)_{asym}$, 527 ν(Cu-N). Single crystals were obtained by slow evaporation of water solvent.

2.5 Synthesis of Saccharinato Complexes of Ethylenediamine

Complexes (**10**) to (**12**) were synthesis using the same general procedure as described below where en = (ethylenediamine).

2.5.1 Synthesis of $[Ni(sac)_2(en)_2]$ (**10**)

Green crystals of $[Ni(sac)_2(H_2O)_4]\cdot 2H_2O$ (0.350g; 0.653 mmol) were placed in a 250 ml beaker and dissolved in methanol (15 mL) and ethylenediamine (1 mL) was added and the reaction mixture was gently stirred for 15 minutes at 80°C. The beaker was removed from the heat source and allowed to stand for two days during which time large purple block crystals of (**10**) were obtained. The same complex was prepared in double distilled water and the crystals grew within a week. Yield (0.348 g, 98%); Mp 154°C (decompose); Anal. Calc. for $C_{18}H_{24}NiN_6O_6S_2$: C, 39.8; H, 4.4; N, 15.5. Found: C, 39.5; H, 4.2; N, 15.8 %. IR (ATR) 3330, 3266 ν(NH for en), 2928, 2884 ν(CH), 1621 ν(C=O), 1571, 1455 ν(C=C), 1339 $\nu(CNS)_{sym}$; 1262, 1275 $\nu(S=O)_{asym}$, 1134 $\nu(S=O)_{sym}$, 94 6 $\nu(CNS)_{asym}$, 515 ν(Ni-N). Single crystals were obtained by slow evaporation of methanol solvent.

2.5.2 Synthesis of *trans*-$[Cd(sac)_2(en)_2]$ (**11**)

Colourless microcrystals of $[Cd(sac)_2(H_2O)_4]\cdot 2H_2O$ (0.350g; 0.653 mmol) were used in the reaction. The crystals grew to convenient size after 4 days in a beaker by the method of slow evaporation of methanol solvent yielding large colourless block crystals of (**11**). The crystal can be grown in water as well. Yield (0.361 g, 93%); Mp 189°C (decompose); Anal. Calc. for $C_{18}H_{24}CdN_6O_6S_2$: C, 36.2; H, 4.0; N, 14.0. Found: C, 36.0; H, 3.9; N, 14.3 %. ^{1}H NMR (CD_3OD, 400MHz) d(ppm): 2.61 (s, 8H, NH_2), 2.76(s, 8H, CH_2 of en), 7.58-7.68 (m. 8H, C_6H_4). ^{13}C NMR (CD_3OD, 101MHz) δ(ppm.): 40.00 (C-en), 119.19 (C_6-ring), 122.58 (C_6-ring), 131.22 (C_6-ring), 131.71 (C_6-ring), 134.44 (C_6-ring), 144.96 (C_6-ring) 167.78 (C=O); IR (ATR) 3365, 3296 ν(NH for en), 3070, 2883 ν(CH), 1654 ν(C=O), 1565, 1457 ν(C=C), 1324 $\nu(CNS)_{sym}$; 1251 $\nu(S=O)_{asym}$, 1137 $\nu(S=O)_{sym}$, 943 $\nu(CNS)_{asym}$, 476 ν(Cd-N).

2.5.3 Synthesis of $[Co_2(en)_4(CO_3)_2]\cdot 2(sac)3H_2O$ (12)

Red microcrystals of $[Co(sac)_2(H_2O)_4]\cdot 2H_2O$ (0.350g; 0.653 mmol) were used in the reaction. The crystals grew after a week in a beaker by the method of slow evaporation of methanol solvent yielding needle red crystals of (**12**). Yield (0.339 g, 95%); Mp 135°C decomposes; Anal. Calc. for $C_{18}H_{24}CoN_6O_6S_2$: C, 33.2; H, 4.4; N, 15.0. Found: C, 33.5; H, 4.9; N, 15.3 %. IR (ATR) 3458 ν(OH); 3235, 3096 ν(NH for en), 2954 ν(CH for en), 1577 ν(C=O), 1457 ν(C=C), 1331 $\nu(CNS)_{sym}$; 1248 $\nu(S=O)_{asym}$, 1141 $\nu(S=O)_{sym}$, 949 $\nu(CNS)_{asym}$, 464 ν(Co-N). Single crystals were obtained by slow evaporation of methanol and water solvent.

2.6 X-ray Crystallography

2.6.1 Crystal Structure Determination for Complexes (2) and (6).

X-ray single crystal intensity data was collected on a Nonius Kappa-CCD diffractometer using graphite monochromated Mo-Kα radiation (λ = 0.71073 Å). The temperature was controlled by an Oxford Cryostream cooling system (Oxford Cryostat). The data collection was evaluated using the Bruker Nonius "Collect" program. Data were scaled and reduced using DENZO-SMN software.[8] Absorption corrections were performed using SADABS.[9]
The structure was solved by direct methods and refined employing full-matrix least-squares with the program SHELXL-97[9] refining on F^2. A molecular diagram was initially produced using the program Pov-Ray and graphic interface X-seed.[7] The crystal structures were re-drawn using 50% probability ellipsoids on the ORTEP program. The software program used for crystal packing diagrams was Mercury 3.0.

2.6.2 Crystal Structure Determination for Complexes (1), (3), (4) and (9).

Single-crystal X-ray diffraction data was collected on a Bruker KAPPA APEX II DUO diffractometer using graphite-monochromated Mo-Kα radiation (χ = 0.71073 Å). Data were

carried out at 173(2) K. The temperature was controlled by an Oxford Cryostream cooling system (Oxford Cryostat). Cell refinement and data reduction were performed using the program SAINT.[10] The data was scaled and absorption correction performed using SADABS.[11]

The structure was solved by direct methods using SHELXS-97[11] and refined by full-matrix least-squares methods based on F^2 using SHELXL-97[11] and using the graphics interface program X-Seed.[12] The programs X-Seed and POV-Ray[13] were both used to prepare molecular graphic images. The crystal structures were re-drawn using 50% probability ellipsoids on the ORTEP program. The software program used for crystal packing diagrams was Mercury 3.0.

2.6.3 Crystal Structure Determination for Complexes (**11**) and (**12**).

The crystal was mounted in a stream of cold nitrogen at 100(1) K and centred in the X-ray beam using a video camera.[14, 16, 17, 19, 20]

The crystal evaluation and data collection were performed on a Bruker Smart APEXII diffractometer with Mo-Kα radiation (λ = 0.71073 Å). The diffractometer to crystal distance was set at 4.00 cm. The initial cell matrix was obtained from three series of scans at different starting angles. Each series consisted of 12 frames collected at intervals of 0.5º in a 6º range with the exposure time of 10 seconds per frame. The reflections were successfully indexed by an automated indexing routine built in the APEXII program suite.[15] The final cell constants were calculated from a set of 6460 strong reflections from the actual data collection for (**11**).

Data collection method involved ω scans of width 0.5°. Data reduction was carried using the program *SAINT*+.[15] The structure was solved by direct methods using SHELXS[18] and refined.[15] Non-H atoms were first refined isotropically and then by anisotropic refinement with full-matrix least-squares calculations based on F^2 using SHELXS. All H atoms were positioned geometrically and allowed to ride on their respective parent atoms. The carboxyl H atoms were located from the difference map and allowed to ride on their parent atoms. All

H atoms were refined isotropically. The absorption correction was based on fitting a function to the empirical transmission surface as sampled by multiple equivalent measurements.[15]

The final least-squares refinement of 151 parameters against 2754 data resulted in residuals *R* (based on *F*2 for $I \geq 2\sigma$) and *wR*(based on F^2 for all data) of 0.0526 and 0.0186, respectively, for (**11**). The final difference Fourier map was featureless. The molecular diagrams were drawn with 50% probability ellipsoids using ORTEP program.

2.7 References

1. K. J. Ahmed, A. Habib, S. Z. Haider, K. M. A. Malik and M. B. Hurthouse, *Inorg. Chim. Acta*, 1981, **56**, L37.

2. S. Z. Haider, K. M. A. Malik, K. J. Ahmed, H. Hess, H. Riffel and M. B. Hursthouse, *Inorg. Chim. Acta*, 1983, **72**, 21-27.

3. S. Z. Haider, K. M. A. Malik, S. Das and M. B. Hursthouse, *Acta Crystallogr. Sect. C: Cryst. Struct. Commun.*, 1984, **40**, 1147-1150.

4. F. A. Cotton, G. E. Lewis, C. A. Murillo, W. Schwotzer and G. Valle, *Inorg. Chem.*, 1984, **23**, 4038-4041.

5. F. A. Cotton, E. Libby, C. A. Murillo, G. Valle, M. Bakir, D. R. Derringer and R. A. Walton, in *Inorg. Synth.*, John Wiley & Sons, Inc., 2007, 306-310.

6. S. Z. Haider, K. M. A. Malik, K. J. Ahmed, G. B. Kauffman and M. Karbassi, in *Inorg. Synth.*, John Wiley & Sons, Inc., 2007, 47-51.

7 L. J. Barbour, *X-Seed: A Software Tool for Supramolecular Crystallography*, *J. Supramol. Chem.*, 2001, **1**, 189-191.

8. Z. Otwinowski and W Minor, *Methods in Enzymology, Macromolecular Crystallography*, ed. Carter Jr, C. W. & Sweet, R. M., part A, Academic Press, 1997, **276**, 307-326.

9. G. M. Sheldrick, SHELXL-97, SHELXS-97 and SADABS, University of Göttingen, Germany, 1997.

10. SAINT Version 7.60a, Bruker AXS Inc., Madison, WI, USA, 2006.

11. G. M. Sheldrick, SHELXS-97, SHELXL-97 and SADABS version 2.05, University of Göttingen, Germany, 1997.

12. (a) L. J. Barbour, *J. Supramol. Chem.*, 2001, **1**, 189-191; (b) J. L. Atwood and L. J. Barbour, *Cryst. Growth Des*., 2003, **3**, 3.

13. Bruker-AXS, APEX2, SADABS, and SAINT Software Reference Manuals. Bruker AXS, Madison, Wisconsin, USA, 2009.

14. G. M. Sheldrick, SHELXL. *Acta Cryst.,* 2008,**A64**, 112-122.

15. L.J. Farrugia, *J. Appl. Cryst*., 1999, **32**, 837-838.

16. ORTEP3 for Windows - L. J. Farrugia, *J. Appl. Crystallogr*. 1997, **30**, 565.

17. SHELX [Includes SHELXS86, SHELXS97, SHELXL97, CIFTAB (and SHELXA)] - G. M. Sheldrick, *Acta Cryst*., 2008, A**64**, 112-122.

18. ORTEP-III - M. N. Burnett and C. K. Johnson, Report ORNL-6895. Oak Ridge National Laboratory, Oak Ridge, Tennessee, 1996.

19. SAINT: Area-Detector Integration Software.; Siemens Industrial Automation, Inc.: Madison, WI, 1995.

20. SADABS: Area-Detector Absorption Correction; Siemens Industrial Automation, Inc.: Madison, WI, 1996

CHAPTER 3

SACCHARINATO COMPLEXES WITH A DIRECT M-N BOND

3.1 Introduction

The chemistry of saccharin (1,2-benzisothiazoline-3-(2*H*)one 1,1-dioxide or *o*-sulphobenzimide) has attracted attention during the past decade partly because of its biological significance.[1, 2] Saccharine exhibits a number of diverse coordination bonding modes with a combination of potential donor atoms such as (N or O)-monodentate, (N,O)-bidentate and (N, O, O)-tridentate chelating and bridging ligands. The coordination is capable of forming different complexes, ranging from monomers, coordination polymers to alkoxo-bridging dinuclear complexes.[3, 4, 35] The chemistry of M-N_{sac} varies with small changes in the complexes' composition and configurations, i.e. the XRD data of previously reported complexes differs in coordination geometries, tetrahedral for Zn(II) metal centres and octahedral for Cd(II), Co(II) and Cu(II) complexes.[5] The study herein focuses on the bonding of M-N saccharinato complexes and the ligand coordination modes containing the O donor atoms and the N donor atoms. The neutral complexes obtained from dimethyl sulfoxide, N-methyldiethanolamine and ethylenediamine are reported and discussed in Chapter 3, together with the characterization methods.

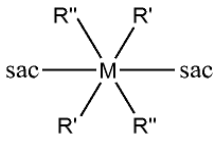

Complexes **1** and **2** : R'' = $(CH_3)_2SO$ and R' = H_2O
1 (Cd) and **2** (Co)

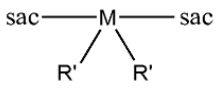

Complex **3** : R' = $(CH_3)_2SO$
3 (Zn)

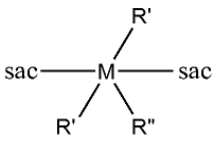

Complex **4** : R' = $(CH_3)_2SO$
R'' = H_2O
4 (Hg)
Complex **5** : R' = H_2O
R'' = $(CH_3)_2SO$
5 (Cu)

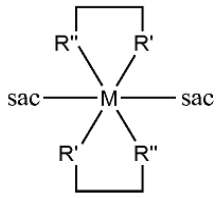

Complexes **7** and **8** : R'' = $N(CH_3)(CH_2)_2OH$ and R' = OH
7 (Cu) and **8** (Co)
Complexes **10** and **11**: R'' = R' = NH_2
10 (Ni) and **11** (Cd)

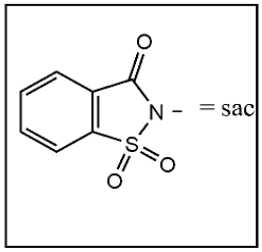

Scheme 3.1 The schematic representation of N-M saccharinato complexes of the present study.

The complex $[Cd(sac)_2(H_2O)(dmso)(pyet)]$[6] consists of both M-N and M-O ligating function of DMSO. Other important complexes are discussed in the crystal structure section. $[M(3,5\text{-}DNB)_2(dmso)_2(H_2O)_2]$, (M(II) is Zn, Cu, Ni or Co, 3,5-DNB is the 3,5-dinitrobenzoato)[7], is a complex that shows similar coordination mode to ones previously reported.

3.2 Results and Discussion

3.2.1 Synthesis of Tetraaquabis(saccharinato)M(II) dihydrate Precursors

The tetraaquabis(saccharinato)M(II) dihydrate metal complexes, $[M(sac)_2(H_2O)_4]\cdot 2H_2O$, were synthesised using an aqueous metathesis reaction at a temperature of 80°C, see Scheme 3.2. This involved the addition of 2 molar equivalents of sodium saccharin aqueous solution (50 mL) to an aqueous solution of 1 molar equivalent metal salt (50 mL). Upon heating the reaction mixture the volume of water eventually reduced to 50 mL and by allowing the solution to stand undisturbed, $[M(sac)_2(H_2O)_4]\cdot 2H_2O$ crystals were formed from the solution. The crystals are obtained by filtration using a Buchner funnel with suction. The products typically have similar colours to the metal salts. The structures of these starting metal complexes have been previously determined and characterised by Fourier Transform Infrared spectroscopy (FTIR), UV-Vis spectroscopy, thermal analysis curves (TG, DTA, DSC and DTG).[8, 9]

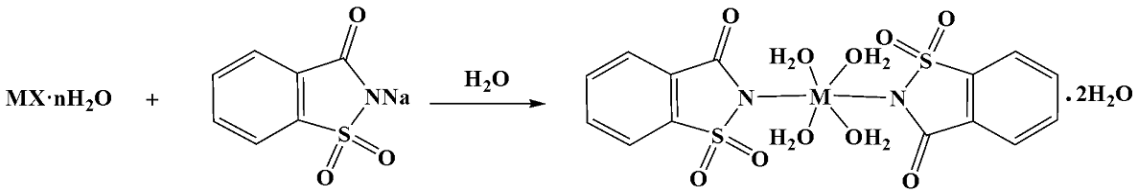

$MX\cdot nH_2O$: $Cd(NO_3)_2\cdot 4H_2O$, $CoCl_2\cdot 6H_2O$, $Zn(NO_3)_2\cdot 6H_2O$, $HgCl_2$ and $CuSO_4\cdot 5H_2O$

Scheme 3.2 Formation of $[M(sac)_2(H_2O)_4]\cdot 2H_2O$ precursor complex.

The above reaction produces a variety of complexes in satisfactory to good yields, ranging from 60 to 90%.

3.2.2 Synthesis of Mixed Aqua-and Dimethyl Sulfoxide Saccharinato Complexes

According to the literature, the aqua ligands from the $[M(sac)_2(H_2O)_4]\cdot 2H_2O$ complexes are easily displaced by strong neutral ligands when the reaction is performed in polar protic solvents like water, methanol and ethanol because they are weakly coordinated to the metal centres. $[M(sac)_2(H_2O)_4]\cdot 2H_2O$ complexes of M = Cd, Co, Zn, Hg and Cu were prepared.[8] The precursor complexes were reacted by refluxing each complex in excess DMSO. The reaction mixture was heated until the volume of DMSO was reduced from 20 ml to 7 ml. This readily allowed the crystallization process to occur. The resulting solutions of the complexes were allowed to stand at room temperature from a few days to two weeks for slow evaporation of the solvent to take place. The crystals which formed were collected by filtration and are air-stable which is very convenient. The $[Ni(sac)_2(H_2O)_4]\cdot 2H_2O$ complex failed to give the desired product. The IR data showed the complex co-crystallized with the starting material yielding a micro-crystalline material. The IR data was inconclusive because it showed a mixture of the product and the starting material. The products which were obtained from the above outlined brief method were complexes (**1**) to (**5**) which had a good percentage yield which ranged from 80 to 93 % and the micro-analysis confirms the formation of the products (see Chapter 2 and Scheme 3.3 for chemical properties). Table 3.1 shows a list of physical properties of the complexes.

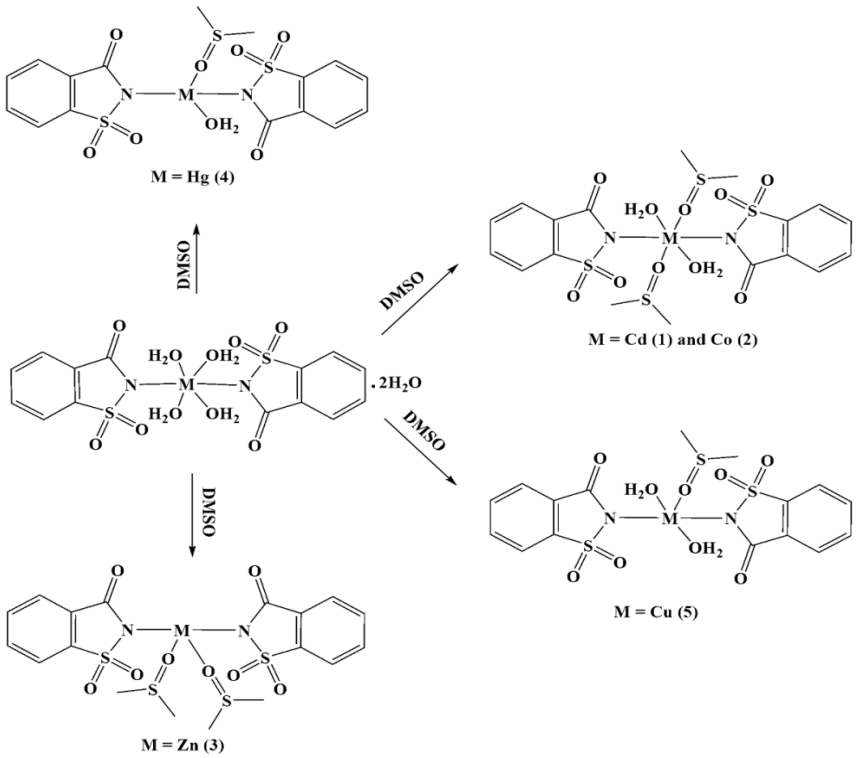

Scheme 3.3 Reactions showing the formation of DMSO saccharinato complexes.

3.2.3 Synthesis of Amine Saccharinato Complexes

The four mixed-ligand amine containing complexes were synthesised from the $[M(sac)_2(H_2O)_4]\cdot 2H_2O$ complexes for M = Cd(II), Co(II) and Cu(II) which were prepared according to the reaction in Scheme 3.4.

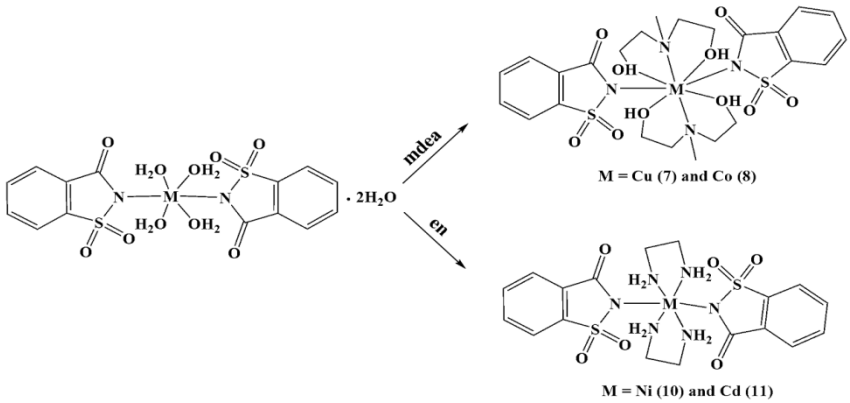

Scheme 3.4 Reaction scheme showing the formation of amine saccharinato complexes

The complexes (**7**) and (**8**) and (**10**) and (**11**) were isolated in excellent yield, which ranged from 86 to 98 %. The CHN micro-analysis confirmed the formation of the bulk products (see Chapter 2 and Scheme 3.3 for chemical properties). Table 3.1 shows a list physical properties of the complexes.

Table 3. 1 Tabulated analytical results of saccharinato complexes

Complexes	Colour	Melting point (°C)	Molecular weight	Yield (%)
1	Colourless	112-115	669.03	92.0
2	Pink	110[*, a]	615.56	93.0
3	Colourless	190-191	585.97	92.0
4	Colourless	135	1322.22	80.0
5	Blue	145[a]	538.05	90.0
7	Blue	195	665.10	86.0
8	Light orange	210[a]	661.10	87.0
10	Violet	154[a]	543.23	98.0
11	Colourless	189[a]	596.95	93.0

[*] change colour to blue, [a] decomposes

3.3 Spectroscopic Properties

3.3.1 Nuclear Magnetic Resonance (NMR) Analysis of Complexes

For complexes (**1**), (**3**), (**4**) and (**11**), shown in Figure 3.1, the ^{1}H and ^{13}C NMR spectral data is presented in Table 3.2. The ^{1}H NMR demonstrated that the H atoms of the H_2O ligand for complexes (**1**) and (**4**) varies with solvent. The aqua-ligand protons of complex (**4**) appears at 2.50 ppm which appears to overlap with the deuterated DMSO peak and for complex (**1**) the aqua-ligand proton peak resonate at 3.36 ppm in deuterated DMSO. Both the aqua-ligand peaks in complexes (**1**) and (**4**) integrate to a multiplet of 4H for complex (**1**) and 2H for complex (**4**). The ambiguous behaviour of this peak and the overlapping are due to the hygroscopic and the hydrophilic nature of the deuterated solvent when the complexes are in solution which led to hydrogen bonding interaction that alter the peak intensity and proton numbers in the spectra.[10, 11] The amine protons show a similar feature which have strong hydrogen bonding that result in broader peaks in NMR spectra. Another multiplet was attributed to the peaks of the saccharinate protons in the range of 7.56 to 8.00 ppm which integrate to 8 protons for all four complexes. A singlet proton of the monodentate coordinated DMSO for complexes (**1**), (**3**) and (**4**) was noted to be in the range 2.53 to 2.56 ppm which integrate to 12 protons of the methyl protons of all DMSO ligands for complexes (**1**) and (**3**), and 6 protons of the methyl protons for complex (**4**). The NMR protons of (**11**) show that the amine protons integrate to 8H which appears resonate at 2.76 ppm and the protons of CH_2 of the amine ligand integrate to 8H which appears at 2.61 ppm. The proton signal intensities in the NMR spectra corresponds with the proposed structure. In general, the H signals of all the new complex was shifted slightly downfield compared with the signal of the starting material. The ^{13}C NMR spectra accounted for all the C atoms of the complexes to be present, further supporting the solution structures.

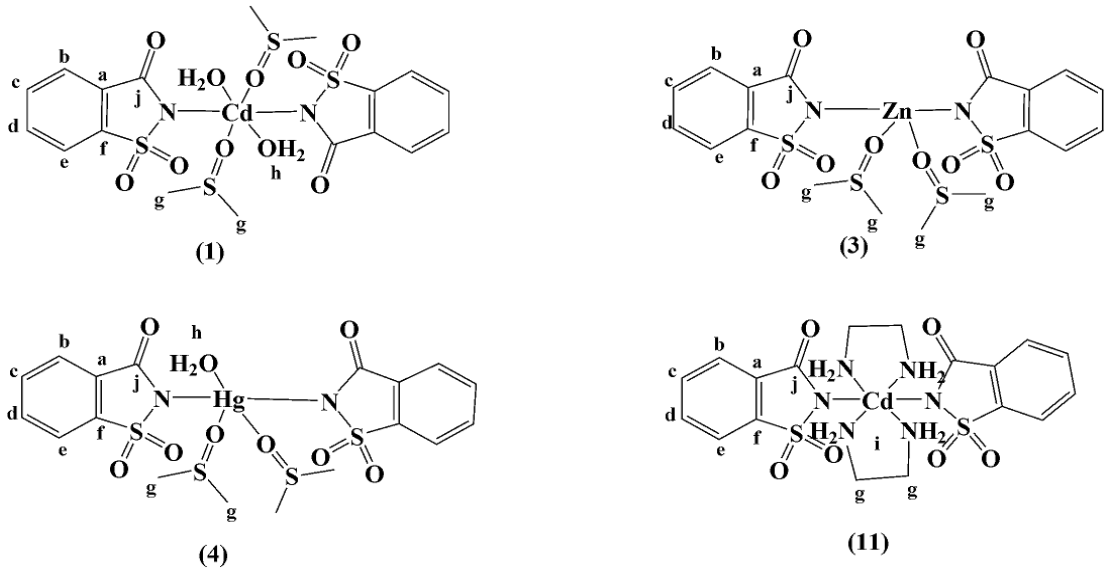

Figure 3. 1 NMR labelling scheme for different complexes

The ^{13}C NMR spectra of complexes (**1**), (**3**), (**4**) and (**11**) showed chemical shifts very similar to saccharinate anion. The difference is observed in the C atoms present in the ligands of the coordinating species to the metal centres, see Table 3.2. The signal in the range of 163.86 to 171.90 ppm was attributed to the carbonyl carbon. The C atom chemical shifts in the range of 142.34 to 144.95 ppm correspond to the carbon atom on the benzene ring, labelled (a). These are shifted further downfield due to the electron withdrawing C=O group of the ligand so are shielded. In the range 122.56 to 124.96 ppm, the chemical shift of C atoms, (c), on the benzene ring next to the carbon labelled (a) was observed with low intensity of the peak. In the range 133.24 to 134.67 ppm, the chemical shift of the carbon atom labelled (c), was observed. The signal in the range of 131.71 to 134.21 ppm was assigned and labelled (d), which is in-between carbon atoms (c) and (e). The chemical shift of the carbon atom in the range of 119.19 to 121.23 ppm belongs to the carbon atom labelled (e). And the carbon labelled (f) have the chemical shift signals which ranges from 128.96 to 133.42 ppm and it is attributed to the carbon atom which is adjacent to the sulfonyl group of the saccharinate anion. The chemical shifts observed at the signal shift between 40.36 to 40.39 ppm are assigned to the methyl groups of DMSO in (**1**), (**3**) and (**4**). Their presence are important as it means the aqua ligands had been displaced. This chemical shift for complex (**4**) is incorporated within the carbons of the solvent peaks, see appendix. Complex (**11**) consists of the amine carbon atoms at 40.00 ppm which is also incorporated in the solvent peak. The reference chemical shifts are reported.[12]

No NMR data was recorded due to the paramagnetic nature of Co(II), Ni(II) and Cu(II) complexes. However, this is the result of Oh geometry in the Ni(II) and Co(II) complexes, as Oh geometry of

these complexes are paramagnetic. It should be indicated that not all Ni(II) complexes are paramagnetic as square planar Ni(II) complexes are not.

Table 3. 2 The NMR data of the saccharinato complexes

^{1}H and ^{13}C NMR Positions		The NMR of complexes and their frequencies (ppm)							
^{1}H***	^{13}C****	1*		3**		4*		11*	
		^{1}H	^{13}C	^{1}H	^{13}C	^{1}H	^{13}C	^{1}H	^{13}C
a	a	–	145.14	–	144.80	–	142.34	–	144.95
b, c , d and e	b	8H, m, 7.57-7.67	122.54	8H, m, 7.62-7.76	124.88	8H, m, 7.87-8.09	128.96	8H, m, 7.58-7.68	122.57
	c		131.65		134.27		134.67		134.44
	d		134.46		134.21		134.03		131.71
	e		119.15		121.23		120.74		119.19
	f	–	131.15	–	133.32	–	128.96	–	131.21
g	g	12H, s, 2.53	40.36	12H, s, 2.56	40.36	6H, s, 2.53	40.38	8H, s, 2.76	40.00
h		4H, m, 3.36	–		–	2H, m,2.49	–		
i			–		–		–	8H, s, 2.61	–
	j		167.86		171.57		163.86		167.77

*Solvent: DMSO-d_6, **Solvent: MeOH, ***^{1}H NMR (400MHz) and ****^{13}C NMR (101MHz)

Complexes (**2**) and (**5**), (**7**) and (**8**), and (**10**) have paramagnetic metal centres and no attempt was made to record their NMR spectra. There were no experimental determined values for the ferromagnetic nature of complexes in this thesis, hence paramagnetic compounds were simply compared with the literature for related metals and oxidation states.[23, 41]

3.3.2 Fourier Transform Infrared Spectroscopy (FTIR) Using ATR Spectra

The IR spectra of saccharinato complexes are displayed in Table 3.3, where key wavenumbers of the complexes can be seen. The wavenumbers for the starting $[M(sac)_2(H_2O)_4]\cdot 2H_2O$ complex was reported.[8, 13] The current complexes possess much similar infrared properties. The important infrared peaks are observed at the following frequencies: 3500 to 3100 cm^{-1} for different types of the aqua-ligands which are present in the complexes; 1610 cm^{-1} for carbonyl group; 1280 cm^{-1} for $SO_{2(asym)}$;

1150 cm^{-1} for $SO_{2(sym)}$;1570 to 1479 cm^{-1} for C=C and 942 cm^{-1} for $CNS_{(asym)}$ and 1327 cm^{-1} for $CNS_{(sym)}$.[9, 14]

Table 3. 3 IR spectral data for the metal complexes

Complexes	ν(OH)	ν(NH)/ N-CH	ν(C=O)	ν(SO_2)		ν(CNS)		ν(C=C)	ν(SO)
				asym	sym	asym	sym		dmso
1	3481, 3016	–	1646, 1609	1271, 1256	1152, 1141	953	1330	1583, 1460	1054, 1036
2	3486, 3005	–	1618	1256	1141	949	1317	1584, 1460	1141
3	–	–	1687	1274, 1245	1153	941	1324	1596	1138
4	3414	–	1697	1284	1154	947	1302	1594, 1458	1138, 1138
5	3275	–	1651, 1619	1256, 1300	1161	951	1345	1586, 1460	1147
7	3407	2921	1635	1262, 1295	1144	965	1347	1590, 1454	–
8	–	2858, 2672	1620	1264, 1284	1146	957	1346	1580, 1453	–
10	–	2948, 2928	1621	1262, 1275	1134	946	1339	1571, 1455	–
11	–	2882, 2949	1654	1272, 1254	1137	943	1324	1565, 1457	–

The high energy broad absorption band at the range of 3005 to 3486 cm^{-1} shows the characteristics of ν(OH) vibration intensity which can be attributed to the hydroxyl group of the aqua ligands for complexes (**1**), (**2**), (**4**) and ν(OH) vibration intensity for complex (**7**) correspond to the hydroxyl group of alcohol of the ligand. The bands at 2672 to 2949 cm^{-1} which are observed in complexes (**7**) to (**8**) and (**10**) to (**11**) are attributed to ν(NH) and ν(N-CH) stretches, respectively, as indicated in Table 3.3. The distinct strong absorption vibration band of the ν(C=O) band for complexes (**1**) to (**5**) and (**7**) to (**8**) and (**10**) to (**11**), appears in the range 1609 to 1697 cm^{-1}. There has been a slight increase in wavenumber of the C=O of all complexes compared to that of the starting material. The free saccharin ligand has a vibration band at 1720 cm^{-1}. The band which is observed to be at the range 1453 to 1594 cm^{-1} is assigned to the ν(C=C) stretch in the saccharin ring. For pure saccharin this band occur at 1600 to 1462 cm^{-1}.[5] The vibration stretch at 1289 to 1347 cm^{-1} and 941 to 977 cm^{-1} vibration intensity are assigned to $(CNS)_{sym}$ and $(CNS)_{sym}$ moieties, respectively. These CNS vibration bands correlate with those of the starting material which are in the region of 942 and 1327 cm^{-1} for $(CNS)_{sym}$ and $(CNS)_{sym}$. There are closely related intensity peaks in the range 1248 to 1300 and 1134 to 1161 cm^{-1} which are assigned to ν_{asym}(O=S=O) and ν_{sym}(O=S=O) stretches, respectively. The most important absorption bands are those observed at the range of 1036 to 1147 cm^{-1} for ν(S=O) corresponding to the complexes containing DMSO as ligands, complexes (**1**), (**2**), (**3**), (**4**) and (**5**). The frequencies in this range 300 to 550 cm^{-1} are due to M-O and M-N vibration bands.[15, 16] These

are not listed in Table 3.3, see Appendix. Although IR is a secondary characterization tool, the functional groups identified for the complexes support and confirm the formation of the relevant complexes.

3.3.3 UV-Vis spectroscopy

The behaviour of complexes (**1**) to (**5**) and (**7**) to (**8**) and (**10**) to (**11**) in the different solvents DMF and DMSO, were analysed by UV-Vis absorption spectroscopy under normal atmospheric conditions in the range of 900 nm to 200 nm. The spectral data of the complexes are shown in Table 3.4, listing with the λ_{max} values and molar absorptivity in parenthesis. The λ_{max} values of complexes (**1**) to (**5**) and (**7**) to (**8**) and (**10**) to (**11**) are compared with those that have been previously reported for sodium saccharinate which exhibit two absorption bands at λ_{max} = 220 nm, ε = 10166 L mol^{-1} cm^{-1} and at λ_{max} = 268nm, ε = 1628 L mol^{-1} cm^{-1} which are assigned to the ligand-to-ligand charge-transfer intraligand L-L* transition,[17] and $[M(sac)_2(H_2O)_4]\cdot 2H_2O$ complexes at λ_{max} = 525 nm and 280 nm for Co(II), λ_{max} = 680 nm, 400 nm and 280 nm for Ni(II), and λ_{max} = 780 nm and 355 nm for Cu(II).[13, 18] Amongst these complexes, colourless complexes of (**1**), (**3**), (**4**) and (**11**) show similar λ_{max} values compared to Na(sac) whereby the absorption peak appears in the range 260 to 374 nm. These absorption bands are due to the strong conjugated $\pi\cdots\pi$ interaction in the benzene ring. These are accompanied by small absorption peaks at the shoulder of the broad peaks in the similar region of the UV-vis which is observed at lower concentrations of the sample. These are attributed to the intraligand L-L* transition of the saccharinate anion. Similar absorption peaks are observed for the complex $[M(sac)_2(H_2O)_4]\cdot 2H_2O$.[5] The peaks which are visible at the shoulders of the broad ones are in ranges 260 to 374 nm which are also observable at very low concentration. Complexes **(2)** and **(8)** are two different complexes that possess the same metal centres, Co(II) and they show similar UV-visible absorption behaviour at slightly different region of the spectra. These complexes display three absorption bands. The intraligand L-L* transition observed in these complexes appears to be slightly red shifted compared to the starting $[M(sac)_2(H_2O)_4]\cdot 2H_2O$ complexes,[8] presumably due to the different ligands involved which can influence the spectral shift. The intraligand L-L* transition of the saccharinate anion of the complexes are observed in the ranges 259 to 287 nm. In the visible region, in the ranges 379 to 871 nm, small absorption peaks are noted due to d-d transition, usually observed in an octahedral coordination geometry of the metal centre. For complexes containing a Co(II) centre, the metal-to-ligand charge transfer is photostable. The molar extinction (absorptivity), ε, of complexes having d-d transitions are known to fall in the range 5 to 500 $M^{-1}cm^{-1}$ (where M = mol dm^{-3}).[19, 20] The molar absorptivity range of these complexes is 19.2 to 164 $M^{-1}cm^{-1}$. These values are within the known range mentioned above. The Cu(II) complexes (**5**) and (**7**) present three absorption bands. In the range 255 to 374 nm, complexes (**5**) and (**7**) consist of two peaks corresponding to the saccharinate anion of the complexes. These absorption peaks are associated with

intraligand L-L* transition due to ligand-to-metal-charge-transfer (LMCT) arising from an un-occupied ligand π -orbital to the empty d-orbital of Cu(II). A low energy intensity from 638 to 802 nm resulting from the d-d transition is noticed due metal-to-ligand-charge-transfer (MLCT) transition which occurs when the saccharinato complexes and other related complexes are in a low oxidation state and this shows the activity whereby the ligands are easily reduced in solution. This is also similar to the behaviour seen with the Co(II) and Ni(II) systems due to the paramagnetism of the metal centres which arises because of the influence of the LMCT transition. The range of the molar absorptivity of the Cu(II) complexes is from 77 to 137 $M^{-1}cm^{-1}$. These values correspond with the ranges ε of octahedral complexes.[19, 21] Complex (**10**) has three absorption bands. These bands appear at 273, 588 and 774 nm close to the values of one's reported earlier. The d-d transition state of the two octahedral coordination geometry metal centred complexes are the a range of 419 to 774 nm. The values of λ_{max} of the complexes (**1**) to (**5**) and (**7**) to (**8**) and (**10**) to (**11**) are slightly shifted at the red-shift region compared to those of the starting material of these complexes. Molar absorptivities of the ligands that participates in the charge-transfer absorption are normally larger than 10,000 L mol^{-1} cm^{-1},[17] see Table 3.4. The region which indicates the presence of intraligand L-L* transition in the complexes is greater than 500 $M^{-1}cm^{-1}$ and less than 10, 000 $M^{-1}cm^{-1}$ which indicates the formation of the sacharinato complexes. The complexes, which include a variety of metal centres such as Zn(II), Cd(II) and Hg(II), do not show absorption activities in the visible region of the spectra because of the nature of the d^{10} metal system which has a fully occupied electron system decreasing the HOMO-LUMO energy gap for excitation of electron to radiate coloured properties. Only ligand transitions are shown due to the saccharinate anion.

Table 3. 4 Electronic spectra results of saccharinato complexes

Complexes	λ_{max} (nm), ε (M^{-1} cm^{-1})[x]		
	Ligands		d–d
1	260(3274)	262(3923)	–
2	259(1879)	262(3541)	536(36.9)
3	259(2176)	277(2321)	–
4	253(2867)	261(3628)	–
5	255(3850)	260(4472)	802(104)
7	287(7028)	374(1339)	719(137)
8	272(3752)	–	598(21.6),871(31.3)
10	273(2576)	–	558(19.2),774(21.9)
11	275(2815)	–	–

[x] ε Values given in parentheses.

Complexes (**2**), (**5**) to (**8**) and (**10**) have paramagnetic properties. Copper(II), (**5**), complex have weak antiferromagnetic interaction due a spin-orbit coupling contribution and high spin ligand coordinated to the metal centre.[22,23] Nickel(II), (**10**), is a (d^8) system and cobalt(II),(**2**) is a (d^7) complex which show a strong antiferromagnetism due to an increase in the size of the saccharin π systems observed in the packing of the complexes which then produces a stabilisation of the low spin case resulting in a strong antiferromagnetic coupling for both metal centres.[23,24] Other reasons are that the spin polarisation is usually predominant in extended π systems and a ligand to metal electron-transfer appears to be large enough for π systems. This must be kept in mind because it is an influence of strong antiferromagnetic which lead to unresolved NMR spectra's.[41]

3.4 Description of the X-ray Crystal Structures of Saccharinato Complexes

3.4.1 Crystal Structures

Table 3. 5 Crystal data and structure refinement for complexes (**1**), (**2**), (**3**) and (**4**)

	1	**2**	**3**	**4**
Formula	$C_{18}H_{24}CdN_4O_{10}S_4$	$C_{18}H_{24}CoN_2O_{10}S_4$	$C_{18}H_{20}N_2O_8S_4Zn$	$C_{32}H_{32}Hg_2N_4O_{16}S_6$
M_r	669.08	615.60	586.03	1322.22
Crystal system	Monoclinic	Monoclinic	Monoclinic	Monoclinic
Space group	*P21/c (No.14)*	*P21/c (No.14)*	*P21/c (No.14)*	*P21/c (No.14)*
a, Å	10.2613(5)	10.2304(3)	19.2506(7)	8.0133(4)
b, Å	15.4294(8)	15.1418(6)	8.2855(3)	10.5317(5)
c, Å	7.9951(4)	7.8615(3)	14.8880(5)	23.8346(11)
α, deg	90	90	90	90
β, deg	98.8890(10)	98.068(2)	103.4600(10)	90.0010(10)
γ, deg	90	90	90	90
V	2384.2(3)	2421.0(2)	1900.7(2)	1905.9(5)
Z	2	2	4	2
ρcalcd, g cm^{-3}	1.777	1.696	1.686	2.183
M, mm^{-1}	1.262	1.115	1.473	8.012
F(000)	604	634	1200	1272
Crystal size (mm^3)	0.08x0.11x0.14	0.10x0.15x0.27	0.05x0.11x0.14	0.08x0.08x0.17
Θ Range (º)	2.0,28.4	2.4,28.3	2.2,28.4	2.5,28.4
Index range (*h,k,l*)	-13/13, -20/19, -10/10	-13/13, -20/20, -10/10	-25/25, -11/11, -19/19	-10/10, -14/14, -31/31
T, K	173(2)	173(2)	173(2)	173(2)
Reflections collected	12452	5888	44984	18460
Independent reflections	3121	3000	5730	4998
R_{int}	0.038	0.018	0.047	0.028
Completeness to	Θ = 26.4º 100%	Θ = 28.4º 100%	Θ = 28.4º 100%	Θ = 28.4º 100%
Goodness-of-fit on *F*2	1.03	1.06	1.02	1.33
Final *R* indices [I > 2σ(*I*)]	*R*1 = 0.0272, w*R*2 = 0.0657	*R*1 = 0.0207 w*R*2 = 0.0459	*R*1 = 0.0518 w*R*2 = 0.1251	*R*1 = 0.0637 w*R*2 = 0.1473
R indices (all data)	*R*1 = 0.0253 wR2 = 0.0608	*R*1 = 0.0304 w*R*2 = 0.0814	*R*1 = 0.0268 w*R*2 = 0.0668	*R*1 = 0.0315 w*R*2 = 0.0668
Largest diff. peak and hole, e / Å	-0.41 and -0.41	-0.49 and -0.071	-0.30 and -0.42	-1.78 and -1.08

Table 3. 6 Crystal data and structure refinement for complexes (**5**) and (**11**)

	5	**11**
Formula	$C_{16}H_{14}CdN_2O_9S_3$	$C_{18}H_{24}CdN_6O_6S_2$
M_r	538.05	596.95
Crystal system	Monoclinic	Monoclinic
Space group	*P21/c (No.14)*	*P21/c*
a, Å	7.763(2)	11.4307(2)
b, Å	10.889(3)	6.93280(10)
c, Å	24.420(6)	15.1437(3)
α, deg	90	90
β, deg	98.221(5)	112.2700(10)
γ, deg	90	90
V	2043.0(9)	1110.57(3)
Z	4	2
ρcalcd, g cm^{-3}	1.749	1.785
M, mm^{-1}	1.429	1.221
F(000)	1029	604
Crystal size (mm^3)	0.02x0.04x0.08	0.51x0.24x0.30
Θ Range (°)	1.7,28.3	2.2,26.4
Index range (*h,k,l*)	-10/10, -14/14, -32/31	-12/15, -9/17, -18/20
T, K	173(2)	173(2)
Reflections collected	18859	21415
Independent reflections	5052	2764
R_{int}	0.059	0.0192
Completeness to	Θ = 26.4° 100%	Θ = 26.4° 100%
Goodness-of-fit on *F*2	1.08	1.144
Final *R* indices [I > 2σ(*I*)]	*R*1 = 0.0916, w*R*2 = 0.2504	*R*1 = 0.0184 w*R*2 = 0.0523
R indices (all data)	*R*1 = 0.0916, w*R*2 = 0.2504	*R*1 = 0.0186 w*R*2 = 0.0526
Largest diff. peak and hole, e / Å	-0.81 and 5.27	0.370 and -0.663

w = 1/[\s^2^(Fo^2^)+(0.0260P)^2^+0.4033P] where P=(Fo^2^+2F for complex (**1**), w = 1/[\s^2^(Fo^2^)+(0.0497P)^2^] where P=(Fo^2^+2Fc^2^)/3 for complex (**2**), w = 1/[\s^2^(Fo^2^)+(0.0289P)^2^+1.4252P] where P=(Fo^2^+2Fc^2^)/3 for complex (**3**) ,w = 1/[\s^2^(Fo^2^)+(0.0000P)^2^+9.9656P] where P=(Fo^2^+2Fc^2^)/3 for complex (**4**), w = 1/[\s^2^(Fo^2^)+(0.1487P)^2^+8.2144P] where P=(Fo^2^+2Fc^2^)/3 for complex (**5**)

3.4.1.1 *trans*-$[Cd(sac)_2(dmso)_2(H_2O)_2]$ and *trans*-$[Co(sac)_2(dmso)_2(H_2O)_2]$

A view of the molecular structure of complexes (**1**) and (**2**) is shown in Figure 3.2 and Figure 3.3, respectively. The selected bond distances and angels are tabulated in Table 3.7. The unit cell dimensions of the crystal structure are shown in Table 3.5.

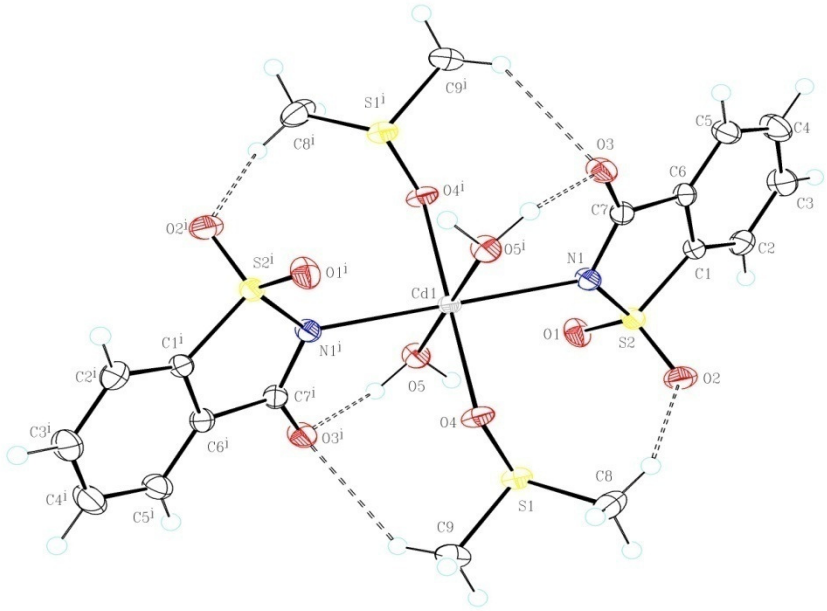

Figure 3. 2 The ORTEP molecular structure of (**1**) showing the labelling scheme. The dash interactions show intramolecular hydrogen bonding.

The two molecular structures differ from one another by the metal centres, i.e. complex (**1**) has Cd(II) and complex (**2**) has Co(II) as a metal centre. The structures are isomorphous (isostructures), all non-hydrogen atoms were refined anisotropically. All hydrogen atoms could be found in the different electron density maps. All, except H5A and H5B on O5, were placed in idealised positions refining in riding models with U_{iso} set at 1.2 or 1.5 times those of their parent atoms. The water hydrogen atoms H5A and H5B were located in the different electron density maps and refined with independent isotropic temperature factors and simple bond length constraints of d(O-H) = 0.980(2) Å. The structure was refined to R factor of 0.0253 and 0.0304, respectively, for complexes (**1**) and (**2**). For parameters for crystal data collection and structure refinements, the bond lengths, angles and torsion angles are contained in file of complexes (**1**) and (**2**), see Appendix.

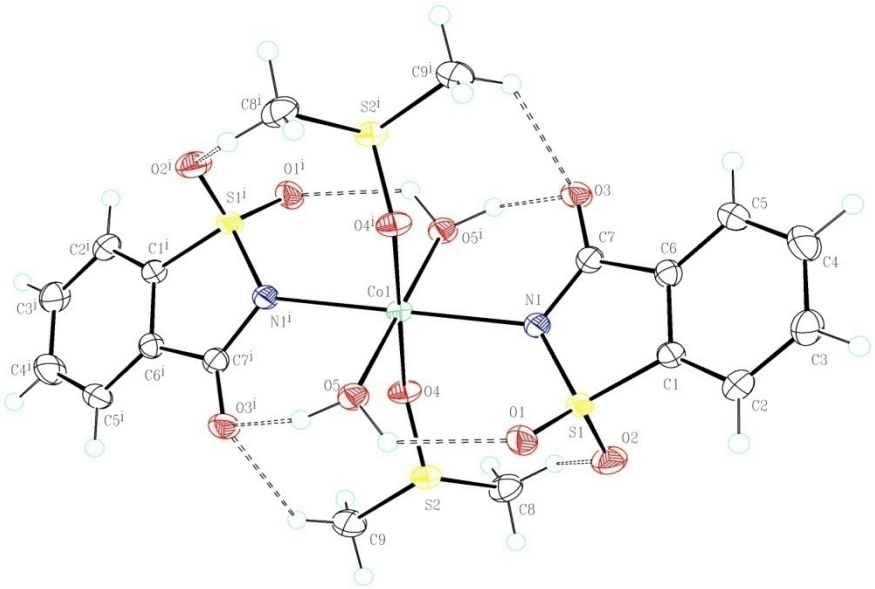

Figure 3. 3 The ORTEP molecular structure of (**2**) showing the labelling scheme. The atom displacement ellipsoids are at 50% probability level. The dashed interactions shows hydrogen bonding.

The structure of complexes (**1**) and (**2**) comprises ligands of aqua and neutral dmso, as well as the saccharinato ligands. The crystallographic data for both complexes indicates the crystallization of the single X-ray crystal structure, in the monoclinic system in the space group P21/c. For both complexes the metal centre is positioned at the centre of the ligand. The metal centre in each complex is coordinated to the six-coordinating ligands which all act as monodentate ligands. The complexes have an octahedral coordination geometry through which the two saccharinate anion ligands are bonded to the metal centre *via* the nitrogen atoms. The two aqua and DMSO ligands have coordinated in the *trans* position to each other. There are many examples of these closely related complexes which illustrate the ranges of the bond distances and angles that could be used to compare with those of complexes, (**1**) and (**2**).[6] The Cd1-O4, Cd1-O5 and the Cd1-N1 have the bond lengths of 2.2817(15), 2.2817(15) and 2.2366(18) Å, respectively. The bond length of Cd-O of M-OH_2 and Cd-N of the starting material is 2.2755(17) and 2.2612(14) Å,[25] respectively. The bond lengths of Cd1-O4 and Cd1-O5 are thus longer whilst Cd1-N1 of the complex (**1**) is shorter. Complex (**2**) shows that the Co1-O4, Co1-O5 and the Co1-N1 have a bond distance of 2.0932(12), 2.0620(12) and 2.2396(15) Å, respectively, which are all shorter than those of (**1**). The difference of Co1-O4 and Co1-O5 is caused by the relative bulkiness of the $(CH_3)_2SO$ ligand present, compared to the less bulky H_2O ligand. A comparison of the bond distances show that the M-O bond distance of the $(CH_3)_2SO$ is

longer than the H_2O ligand. The bond distances of Cd–Nsac and Cd–Osac are similar to those reported for $[Cd(sac)_2(pym)_2]$ which are 2.2612(14) and 2.2755(17) Å,[23] respectively.[26, 27]

3.4.1.2 Hydrogen Bonding of Complexes (**1**) and (**2**)

The tables below contains selected bond lengths and angels of both complexes (**1**) and (**2**).

Table 3. 7 Tabulated selected bond lengths Å and angles° for complexes (**1**) and (**2**) and hydrogen bonding coordination geometry for complexes (**1**)[b] and (**2**)[d]

	M = Cd	M = Co		M = Cd	M = Co
M1-N1	2.2366(18)	2.2396(15)	O4-M1-O5	91.14(6)	91.94(5)
M1-O4	2.2817(15)	2.0932(12)	O4-M1-N1	94.42(6)	94.77(5)
M1-O5	2.2817(15)	2.0620(12)	O4-M1-O4a	180.00	180.00
S1-O4	2.2864(15)	1.572(13)	O5-M1-N1	98.14(5)	95.03(5)
M1-O4a	2.2864(15)	2.0932(12)	N1-M1-N1a	180.00	180.00
			O4a-M1-O5a	91.14(6)	91.94(5)

Hydrogen bonding for complex (**1**)

D-H···A	d(D-H) (Å)	d(H···A) (Å)	d(D···A) (Å)	<(DHA) (°)
O(5)-H(5A)···O(3)[a]	0.979(18)	1.78(3)	2.685(2)	153(3)
O(5)-H(5B)···O(1)	0.980(18)	2.35(3)	2.904(2)	114.8(19)
O(5)-H(5B)···O(1)[d]	0.980(18)	1.934(16)	2.866(2)	158(3)
N(8)-H(8B)···O(5)[i]	0.980	2.5700	2.363(3)	128.00
C(8)-H(8B)···O(4)[g]	0.980	2.4700	3.328(3)	145.00
C(9)-H(9B)···O(4)[g]	0.980	2.5700	3.393(3)	142.00

[b] Translation of Symmetry Code: (a); 1-x,2-y,-z (g) x,y,-1+z; (d) 1-x,2-y,1-z; (i) 1-x,-1/2+y,1/2-z.

Hydrogen bonding for complex (**2**)

D-H···A	d(D-H) (Å)	d(H···A) (Å)	d(D···A) (Å)	<(DHA) (°)
O(5)-H(5A)···O(3)[a]	0.980(17)	1.73(2)	2.6458(17)	155(3)
O(5)-H(5B)···O(1)	0.981(19)	2.09(3)	2.8028(17)	127.9(19)
O(5)-H(5B)···O(1)[d]	0.981(19)	2.058(16)	2.9036(17)	143(2)
N(8)-H(8B)···O(5)[i]	0.980	2.5400	3.277(2)	132.00
C(8)-H(8B)···O(4)[g]	0.980	2.5100	3.383(2)	148.00
C(9)-H(9B)···O(3)[g]	0.980	2.5800	3.363(2)	137.00
C(9)-H(9B)···O(4)[g]	0.980	2.5800	3.432(2)	146.00

[d] Translation of Symmetry Code: (a); 1-x,1-y,-z ; (b) 1-x,1-y,1-z ; (c) x,3/2-y,1/2+z (i) 1-x,1/2+y,1/2-z.

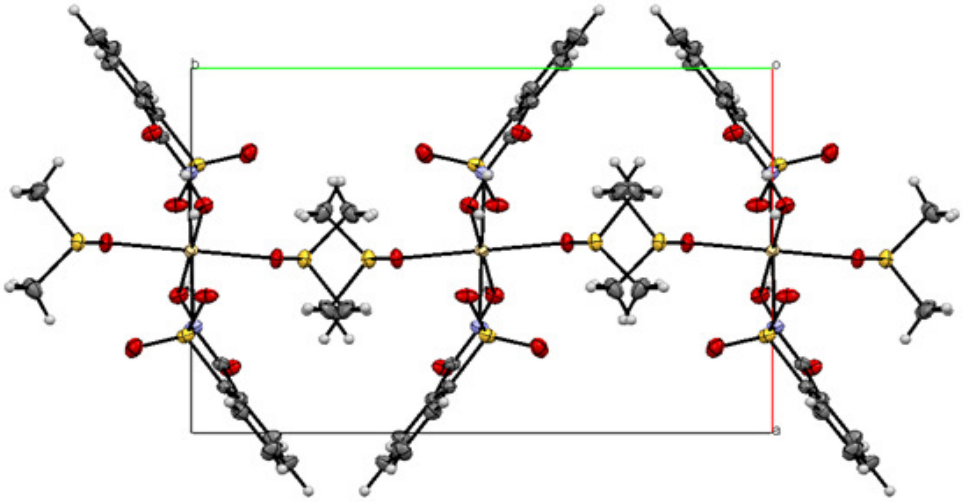

Figure 3. 4 The ORTEP crystal packing diagram of (**1**) viewed along the crystallographic c axis. The elements are shown as (C = dark grey, H = light grey, S = yellow, O = red, N = blue and Cd = cream).

The main interactions within the complexes are shown in the structure representations as *dash lines*. The hydrogen bonding of complex (**1**) and (**2**) is illustrated in Table 3.7 and illustrated by the crystal packing displayed in Figure 3.4 and Figure 3.5, respectively. This shows that the crystal packing of the complex is stabilised throughout by the intra- and intermolecular hydrogen bonding together with weak van der Waals interactions which result in three dimensional framework lattices of the complexes.

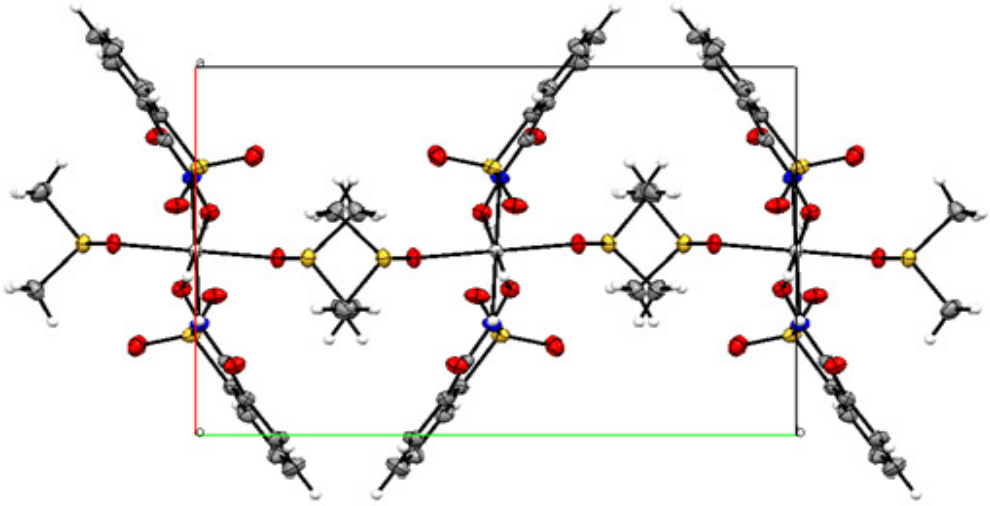

Figure 3. 5 The ORTEP crystal unit cell packing of (**2**) viewed along the crystallographic c axis. The elements are shown as (C = dark grey, H = light grey, S = yellow, O = red, N = blue and Co = grey).

The aqua ligand H atoms which form strong hydrogen bonding with the carbonyl group and sulfonyl group of the saccharinate anion, see Table 3.7 and Figure 3.4, respectively, e.g. O(5)-H(5A)···O(3) and O(5)-H(5B)···O(1), 153(3) and 158(3)º respectively for complex (**1**). The O(7)-H(7A)···O(1) angle is 167(7)º for complex (**2**). These have a contact distance of 2.904(2) Å between atoms O1···O5 and a contact distance of 2.866(2) Å between O1···O5d, respectively. H-bonding of the $(CH_3)_2SO$ ligand is C(8)-H(8B)···O(4) and C(9)-H(9B)···O(4) each with an angle of 145 and 142º, respectively. There are weak hydrogen bonds which involves the sulfonyl oxygen atom with the adjacent molecule in a weak intermolecular C-H···O interaction with the aqua-ligands. The aqua ligand H atoms which are involved in strong hydrogen bonding with the carbonyl group of the saccharinate anion and helps to stabilize the 3-D lattice which is observed in Figure 3.4 and Figure 3.5.

3.4.1.3 $[Zn(sac)_2(dmso)_2]$

The molecular structure of complex (**3**) consists of direct Zn-N and Zn-O bonds, as shown in Figure 3.4. The selected bond distances and angles are shown in Table 3.8. The unit cell dimensions of the crystal structure are shown in Table 3.5. The parameters for crystal data collection and structure refinements, the bond lengths, angles, and torsion angles are contained in the file of complex (**3**) see Appendix.

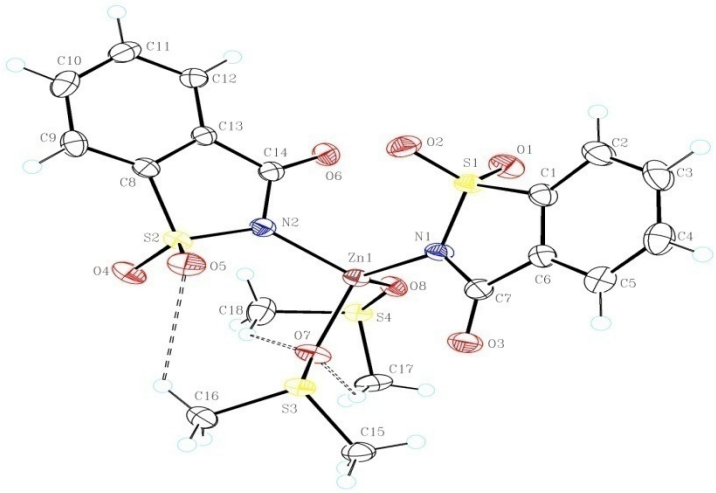

Figure 3. 6 ORTEP molecular structure of (**3**) showing the labelling scheme. The atom displacement ellipsoids are drawn at 50% probability level. The dashed interactions show intramolecular hydrogen bonding.

The structure is formed from two neutral DMSO ligands and two anionic sac ligands. The crystallographic data indicates that the single X-ray structure of complex (**3**) crystallises in a monoclinic system with the space group of P21/c whereby the metal centre is positioned at the centre. The metal centre is coordinated to four ligands which all act as monodentate ligands in the tetrahedral complex. The N-M-N bond angles fall within the range 105.6(1) to 114.8(1)º,[30] and the one reported for this complex is 113.85(7)º. There are many examples of closely related complexes to (**3**). The Zn-N bond distances are 1.996(3) and 2.000(3) Å reported for $[Zn(sac)_2(NH_3)_2]$[28] for the two Zn-N saccharinate anions, and 2.006(3) and 2.007(3) Å for the two ammonia ligands. For complex $[Zn(C_7H_4NO_3S)_2(C_2H_6OS)_2]$[29], it is observed that the Zn-N bond distances are 1.9742(16) and 2.0025(16)Å. These bond distances are comparable to the Zn-N bond distances observed for $[Zn(sac)_2(NH_3)_2]$. Other complexes have shown that the bond distance of Zn-O and Zn-N is 2.1642(3) and 2.0873(9) Å, respectively, and that the Zn-O of the H_2O ligands in the starting $[M(sac)_2(H_2O)_4]\cdot 2H_2O$ complex is 2.2423(9) Å.[30] These lengths are longer than those of (**3**) which is Zn1-O8 = 1.9807(13) and Zn1-O7 = 1.9468(13) Å. This correlates well with other Zn saccharinato complexes.[28, 31]

3.4.1.4 $[Hg(sac)_2(dmso)(H_2O)]$

The ORTEP molecular structure of complex (**4**) is shown in Figure 3.7, together with the numbering scheme of the atoms present in the structure. The selected bond distances and angels are in Table 3.8.

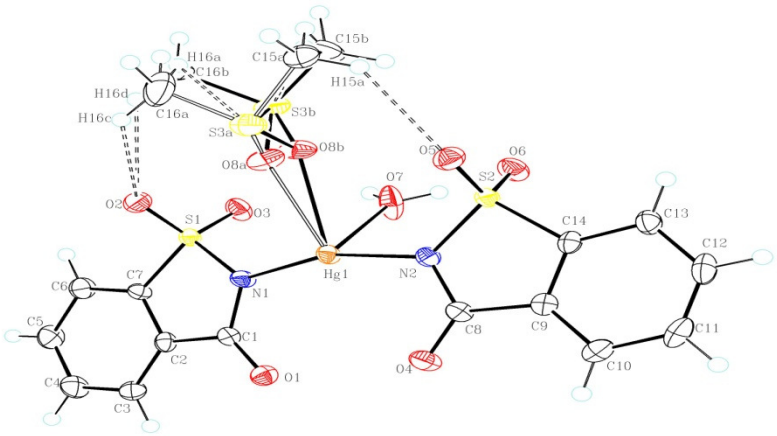

Figure 3. 7 The ORTEP molecular structure of **(4)** showing the labelling scheme. The atom displacement ellipsoids are drawn at 50% probability level.

The unit cell dimensions of the crystal structure are shown in Table 3.5.

The crystallographic data indicate that complex (**4**) crystallizes in a monoclinic system within the space group P21/c, see Table 3.5. In this structure the $(CH_3)_2SO$ groups caused disorder over two sites and the site occupancy factors were refined to 0.504(4) and 0.496(4), respectively. The metal centre is coordinated to four ligands that act as monodentate ligands. This gives the complex a distorted trigonal pyramidal coordination geometry through which the two saccharinate anion ligands are bonded to the metal centre *via* the nitrogen atoms which forms a neutral complex to metal centre which has a +2 oxidation state.

The angles of the tetrahedral complexes of this type falls within the range of 105.6(1) to 114.8(1)º and due to the molecular strain in (**4**), the angles are smaller than 109º, which indicates ideal tetrahedral geometry. Key bond angles for (**4**) include O7-Hg1-O8A = 89.2(3), O7-Hg1-N1 = 84.77(14), O7-Hg1-N2 = 100.77(14), O7-Hg1-O8B = 76.5(3), O8A-Hg1-N1 = 99.7(3), O8B-Hg1-N1 103.8(3) and O8B-Hg1-N2 = 94.2(3)º, which supports a distorted trigonal pyramidal geometry, see Table 3.8.

Bond lengths of 2.614(4) for Hg1-O7, 2.457(11) for Hg1-O8A, 2.076(4) for Hg1-N1, 2.068(4) for Hg1-N2, and 2.452(11) Å for Hg1-O8B were obtained. These selected bond distances of (**4**) for Hg-N saccharinate are related to those of the previously reported $[Hg(sac)_2]$ complexes which are 2.037, 2.049, 2.029 and 2.058 Å.[32] Other reported bond length examples include: 2.019 Å for [Hg(Cl)(sac)][33] 2.120 and 2.140 Å for $[Hg(sac)_2(bipy)]$ which are shorter than $[Hg(sac)_2(ampy)_2]$[34] and $[Hg(ea)_2(sac)_2]$[25] at 2.739(3) and 2.7955(16)Å, respectively. The bond distance of M-OH_2 for **(4)** is 2.614(4) for Hg1-O7 which is slightly shorter than that of Hg–OW (W= H_2O) which is 2.820(9) which has been shown to have weaker interaction with the mercuric metal centre.[35]

3.4.1.5 Hydrogen Bonding of Complexes (**3**) and (**4**)

Table 3. 8 Tabulated selected bond lengths Å and angles° for complexes (**3**) and (**4**) and hydrogen bonding coordination geometry for complexes (**3**)[f] and (**4**)[k]

Zn1-N1	1.9742(16)
Zn1-N2	2.0025(16)
Zn1-O7	1.9468(13)
Zn1-O8	1.9807(13)

O7-Zn1-O8	98.92(8)
O7-Zn1-N1	116.96(6)
O7-Zn1-N2	103.92(2)
O8-Zn1-N1	113.93(6)
N1-Zn1-N2	113.85(7)

Hg1-O7	2.614(4)
Hg1-O8A	2.457(11)
Hg1-N1	2.076(4)
Hg1-N2	2.068(4)
Hg1-O8B	2.452(11)
S3A-O8A	1.231(11)
S3A-C16A	1.805(15)
O8B-S3B	1.805(15)

O7-Hg1-O8A	89.2(3)
O7-Hg1-N1	84.77(14)
O7-Hg1-N2	100.77(14)
O7-Hg1-O8B	76.5(3)
O8A-Hg1-N1	99.7(3)
O8A-Hg1-N2	99.5(3)
N1-Hg1-N2	161.94(16)
O8B-Hg1-N1	103.8(3)
O8B-Hg1-N2	94.2(3)
H7A-O7-H7B	103(5)
Hg1-N1-S1	127.0(2)
Hg1-N2-S2	125.3(2)
Hg1-N2-C8	120.1(3)

Hydrogen bonding for complex (**3**)

D-H···A	d(D-H) (Å)	d(H···A) (Å)	d(D···A) (Å)	<(DHA) (°)
C(3)-H(3)···O(1)[m]	0.9500	2.5900	3.480(3)	155.00
C(4)-H(4)···O(8)[a]	0.9500	2.5100	3.318(3)	142.00
C(9)-H(9)···O(4)[d]	0.9500	2.399	3.318(3)	167.00
C(15)-H(15A)···O(1)[c]	0.9500	2.4800	3.231(3)	134.00
C(15)-H(15C)···O(3)	0.9800	2.5400	3.156(3)	121.00
C(16)-H(16B)···O(2)[b]	0.9800	2.5500	3.221(3)	125.00
C(16)-H(16C)···O(6)[l]	0.9800	2.4900	3.438(3)	163.00
C(18)-H(18B)···O(5)[c]	0.9800	2.5600	3.2500(3)	127.00

[f] Translation of Symmetry Code: (a) 1-x,1-y,1-z ; (b) x,1/2-y,-1/2+z; (c) x,1+y,z; (d) x,3/2-y,1/2+z ;(l) 1-x,-1/2+y,3/2-z; (m) x,3/2-y,-1/2+z.

Hydrogen bonding for complex (**4**)

D-H···A	d(D-H) (Å)	d(H···A) (Å)	d(D···A) (Å)	<(DHA) (°)
O(7)-H(7A)···O(1)[c]	0.87(4)	1.96(5)	2.815(5)	167(7)
O(7)-H(7B)···O(3)	0.86(5)	2.39(4)	2.937(5)	122(4)
O(7)-H(7B)···O(4)[c]	0.86(5)	2.39(5)	3.082(6)	138(6)
C(4)-H(4)···O(3)[i]	0.9500	2.5500	3.373(6)	145.00
C(13)-H(13)···O(2)[h]	0.9500	2.5800	3.282(2)	131.00
C(15A)-H(15A)···O(5)	0.9800	2.4200	3.231(12)	139.00
C(15A)-H(15B)···O(8A)[a]	0.9800	2.5600	3.375(16)	141.00

[k] Translation of Symmetry Code: (a) -x,1-y,1-z ; (c) 1-x,-y,1-z; (h) x,1/2-y,1/2+z; (i) 1-x,-1/2+y,1/2

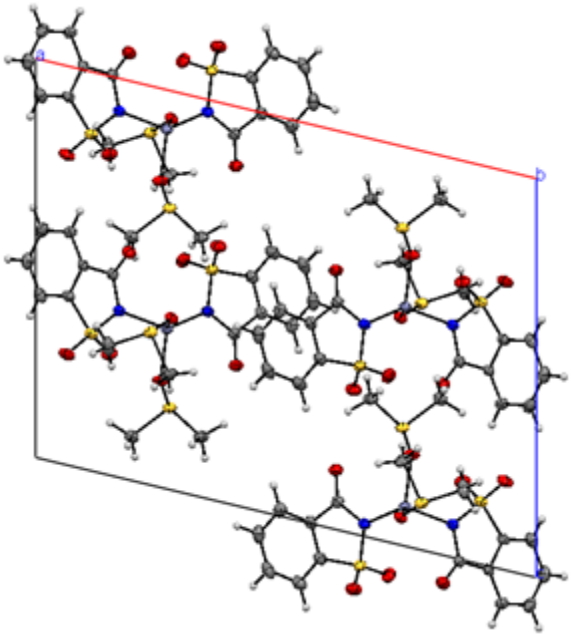

Figure 3. 8 The ORTEP crystal unit cell packing of (**3**) viewed along the crystallographic c axis. The elements are shown as (C = dark grey, H = light grey, S = yellow, O = red, N = blue and Zn = light blue).

The hydrogen bonding of complex (**3**) is shown in Table 3.8. The results show that the crystal packing of the complex is stabilised throughout by the intra-and intermolecular hydrogen bonding together with weak van der Waals interactions which results in a 3D framework lattice, see Figure 3.8. The DMSO ligands consists of the hydrogen atoms which forms a strong hydrogen bonding with the carbonyl group of the adjacent saccharinate anion of the complex which involves the intermolecular C-H···O interaction of 155º for C(3)-H(3)···O(1) and 167º for C(9)-H(9)···O(4) and 163º for C(16)-H(16C)···O(6). The contact distance between these intermolecular hydrogen bonds of the carbonyl group and hydrogen atoms of DMSO, H16C-O6_1 is 2.490, sac(π)···sac(π) stacking interactions between the two saccharinate anions of the adjacent molecules is 3.384 Å, the π···O-S is 2.514 Å, the

sulfonyl oxygen atoms interactions with H-atoms of the benzene and adjacent $(CH_3)_2SO$ molecule is 2.593Å and 2.475Å, respectively. The interaction between the atom of H-dmso and S-atom of the adjacent dmso is non-bonding due to a 3.000 Å (S4-H16B_d) contact distance. The sulfonyl oxygen atoms of the adjacent molecule are interacting with the S-atoms of the adjacent $(CH_3)_2SO$ molecule at a contact distance of 3.115(16) Å (O2-S3). The crystal packing of complex (**3**) shows that the angle between the two saccharinate anions on the complex has a dihedral angle of 73.08 °. These interactions help in stabilizing the complex so that it forms the 3D-lattice system shown in Figure 3.8.

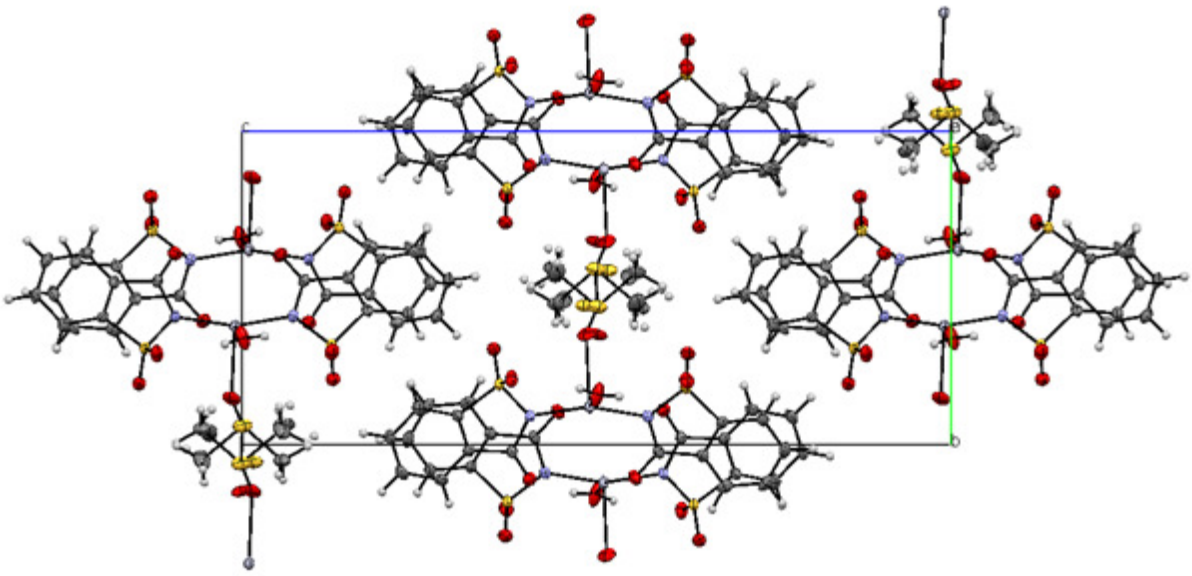

Figure 3. 9 The ORTEP crystal packing of (**4**) view along the reciprocal cell a* axis, i.e. perpendicular to bc. The elements are shown as (C = dark grey, H = light grey, S = yellow, O = red, N = light blue and Hg = silver).

The hydrogen bonding of complex (**4**) is shown in Table 3.8. This shows that the crystal structure packing of the complex is stabilised throughout by the intra-and intermolecular hydrogen bonding together with weak van der Waals interactions which results in 3D framework lattice of the complexes. The hydrogen atom in the dmso ligand forms a strong hydrogen bond with the sulfonyl group of the saccharin anion of the same atoms in the molecular structure and the adjacent molecular structure, see Figure 3.9. This is also observed in the aqua-ligands with the sulfonyl oxygen atoms. There are weak hydrogen bonds which involves the conjugated π electrons of atom of the adjacent phenyl hydrogen atom with the hydrogen atoms of the π molecule system that involves a weak intermolecular sac(π)···sac(π) interaction. The saccharinato ligands of the complexes are calculated to lie planar. These ligands possesses the dihedral angle of 8.00º that result into the 3D system observed in Figure 3.9.

3.4.1.6 $[Cu(sac)_2(dmso)(H_2O)_2]$

A view of the molecular structure of complex (**5**) is shown in Figure 3.10, together with the numbering scheme of the atoms. The selected bond distances and angels are givenin Table 3.9. The unit cell dimensions of the crystal structure are shown in Table 3.6.

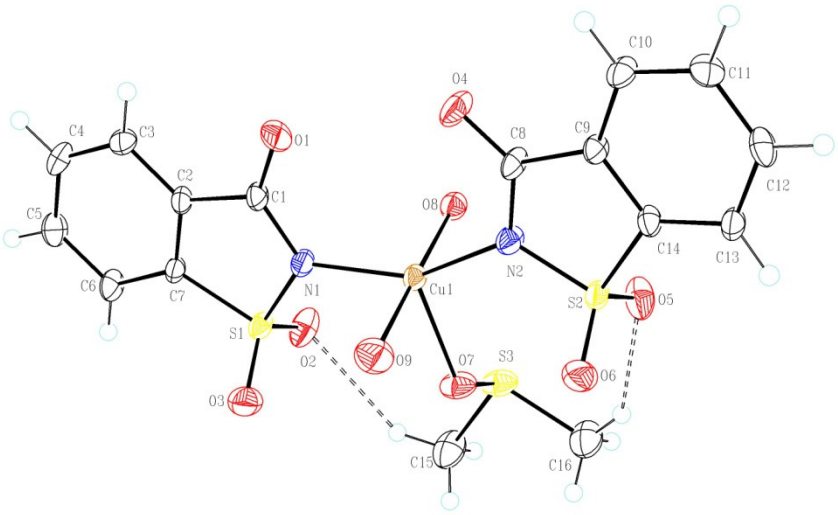

Figure 3. 10 The ORTEP molecular structure of (**5**) showing the labelling scheme. The atom displacement ellipsoids are drawn at 50% probability level. The dash interactions show hydrogen bonding.

The molecular structure of complex (**5**) is composed of two H_2O and one $(CH_3)_2SO$ monodentate ligands. The Cu(II) metal centre is directly bonded to the saccharinato ligand *via* the N donor atom. The crystallographic data reveals that complex (**5**) crystallises in a monoclinic system within the space group of P21/c (14). The crystal is twinned and forms a distorted trigonal bipyramidal coordination geometry with the metal centre centrosymmetric to the ligands. These complexes and many others are used to compare the bond lengths and angles with those of complex (**5**): $[Cu(sac)_2(H_2O)(eapy)]$[36] and $[Cu(sac)_2(H_2O)(bzim)_2]$[37]. From Table 3.9, the N-O(W) bond distances are similar for Cu-O7 and lesser for Cu-O8 and Cu-O9 at 1.967(4) and 1.953(5), respectively. This might be due to twinning of the complex which resulted in the ellipsoid of the O8 and O9 to be slightly larger than expected. The average range M-N bond of complexes $[Cu(sac)_2(H_2O)(eapy)]$ and $[Cu(sac)_2(H_2O)(bzim)_2]$ is 2.012 to 2.058Å, refer to Table 3.9 for complex **(5)**. The bond angels of **(5)**

are also presented in Table 3.9, which are 150.2(2) ° for N1-Cu1-N2, 178.3(2)º for O8-Cu1-O9, 84.0(2)º for O7-Cu1-O9, 94.4(18)º for O7-Cu1-O8 and 124.4(3)º for Cu1-O7-S3.

3.4.1.7 Hydrogen bonding of complex (**5**)

The hydrogen bonding of complex (**5**) is presented in Figure 3.10 as *dashed lines*.

Table 3. 9 Tabulated selected bond lengths Å and angles° for complex (**5**)[b]

Cu1-N1	2.032(5)	N1-Cu1-N2	150.7(2)
Cu1-N2	2.030(5)	O8-Cu1-O9	178.3(2)
Cu1-O8	1.967(4)	O7-Cu1-O9	84.0(2)
Cu1-O7	2.174(4)	O7-Cu1-O8	94.41(18)
Cu1-O9	1.953(5)	Cu1-O7-S3	124.4(3)

D-H···A	d(D-H) (Å)	d(H···A) (Å)	d(D···A) (Å)	<(DHA) (°)
C(4)-H(4)···O(3)[e]	0.9500	2.5200	3.271(9)	137.00
C(15)-H(15A)···O(7)[i]	0.9800	2.5800	3.510(10)	159.00
C(15)-H(15C)···O(2)	0.9800	2.5200	3.362(9)	144.00
C(16)-H(16A)···O(5)	0.9800	2.5500	3.404(9)	146.00

[b] Translation of Symmetry Code: (e) ;1-x,2-y,-z; (i) -x,-1/2+y,-1/2-z.

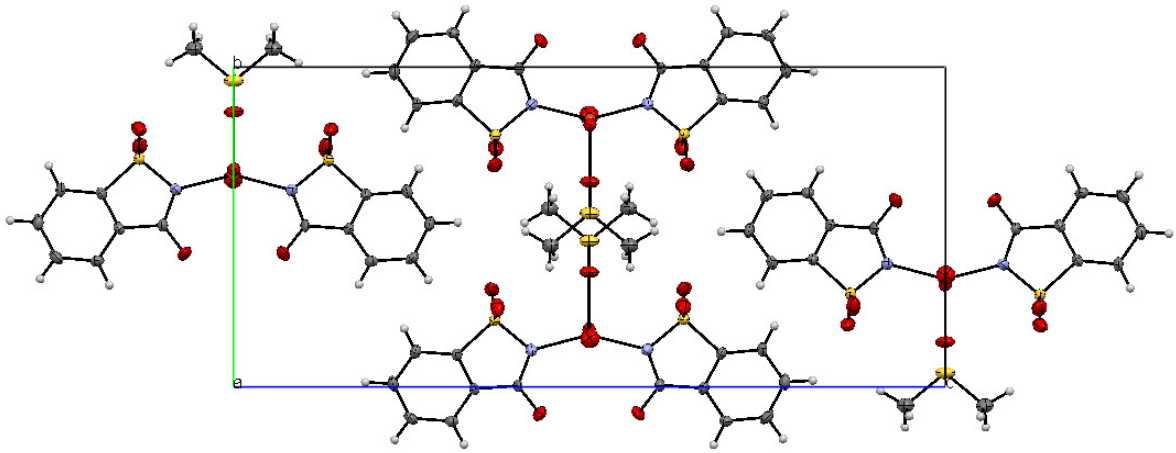

Figure 3. 11 The unit cell packing of complex (**5**) viewed down the crystallographic a axis.

Complex (**5**) is stabilized by intermolecular hydrogen bonding together with weak van der Waals interactions. This structure forms a polymeric 3D framework *via* the O8, O9, O4 and O1 atoms which create an intermolecular hydrogen bonding network with the adjacent molecules *via* (C-H···O) interactions, see Table 3.9 and Figure 3.11.

3.4.1.8 *trans*-[Cd(sac)$_2$(en)$_2$]

A view of the molecular structure of complex (**11**) is shown in Figure 3.12, together with selected bond distances and angels which are in Table 3.6.

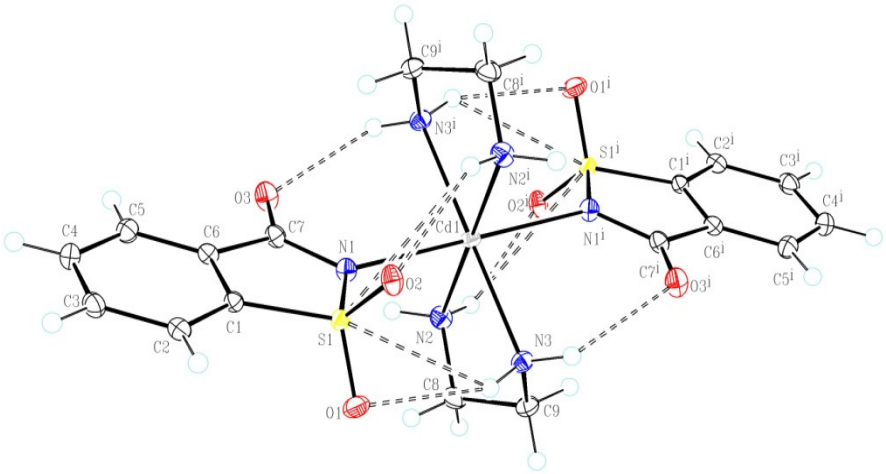

Figure 3. 12 The ORTEP molecular structure of (**11**) showing the labelling scheme. The atoms displacement ellipsoids are drawn at 50% probability level. The dash interactions show hydrogen bonding.

The crystallographic data indicates that the single X-ray structure of complex (**11**) crystallises in a monoclinic system within the space group of P21/c. The metal centre is coordinated to the six-coordinating ligands in which the ethylenediamine acts as a bidentate chelating ligand and the saccharinato ligand is monodentate. The complex has an octahedral coordination geometry through which the two saccharinato ligands are bonded to the metal centre *via* the N atoms which forms a neutral complex. The saccharinato ligands are coordinated *trans* to each other. There are many examples of closely related complexes which illustrate the ranges of bond distances and angles that could be used to compare with those of the complex (**11**). It is noted from the previously reported complexes that the Cd1-N1 have the bond distance of 2.2366(18). The bond distance of Cd-N saccharinate of the starting material is 2.2612(14) Å. Herein, the bond distance of Cd1-N1 is

2.4157(11), Cd1-N2 is 2.3440(11) and Cd1-N3 is 2.4720(17) Å. The bond distance of complex (**11**), i.e. Cd1-N1 is 2.4157(11), Cd1-N2 is 2.3440(11) and Cd1-N3 is 2.4720(17) Å are longer than that of those previously reported, but is similar to those of Cdl-N2 which is 2.324 (11), Cd-N is 2.423(8), Cd-N is 2.338 (11) of the complex $[Cd(sac)_2(NH_3)_4]$[38] ,$[Cd(sac)_2(bpy)_2]$[39]and $[Cd(sac)_2(ampy)_2]$[40] and the N2-Cdl-N3 is 93.6 (4), N3-Cdl-N1 is 88.5 (4) and N2-Cdl-N1 is 94.6 (3). The bond angles of (**11**) are as follows: N1-Cd1-N3 is 90.75(4) and N1-Cd1-N2 is 91.89(4), and these are similar to $[Cd(sac)_2(NH_3)_4]$[38] ,$[Cd(sac)_2(bpy)_2]$[39]and $[Cd(sac)_2(ampy)_2]$.[40]

3.4.1.9 Hydrogen bonding of complex (11)

Table 3.10, below shows the bond lengths and angles of complex (**11**). The atoms which show interactions within the complexes are shown in the main structures Figure 3.12.

Table 3. 10 Tabulated selected bond lengths Å and angles° for complex (**11**)[h]

Cd1-N1	2.4157(11)	N1-Cd1-N3	90.75(4)
Cd1-N2	2.3440(11)	N1-Cd1-N3o	89.25(4)
Cd1-N3	2.4720(17)	N2-Cd1-N3	77.11(4)
C9-N3	1.4720(17)	N2-Cd1-N3o	102.89(4)
C8-C9	1.523(2)	N1-Cd1-N1o	180.0

Hydrogen bonding for complex (**11**)

D-H···A	d(D-H) (Å)	d(H···A) (Å)	d(D···A) (Å)	<(DHA) (°)
1 N(2)-H(2B)···O(2)[a]	0.92	2.39	3.1627(17)	141
1 N(3)-H(3A)···O(2)[b]	0.92	2.29	2.9497(16)	128
1 N(3)-H(3A)···O(3)[c]	0.92	2.34	2.9966(18)	128
1 N(3)-H(3B)···O(1)	0.92	2.46	3.2964(16)	151
1 C(2)-H(2)···O(3)[b]	0.92	2.52	3.1697(18)	128
1 C(8)-H(8A)···O(3)[d]	0.92	2.46	3.4225(18)	173

[h] Translation of Symmetry code: (a) 1-x,-y,1-z ;(b) x,1+y,z;(c) 1-x,1-y,1-z;(d) x,-1/2-y,1/2+z.

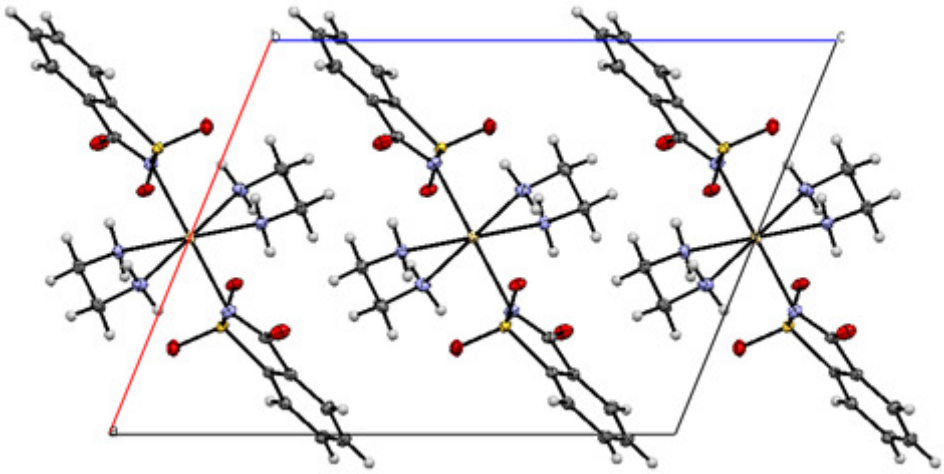

Figure 3. 13 The ORTEP crystal unit cell packing of (**11**) viewed along crystallographic b axis. The elements are shown as (C = dark grey, H = light grey, S = yellow, O = red, N = light blue and Cd = cream).

The hydrogen bonding of complex (**11**) is shown in Table 3.10. The crystal packing of the complex is stabilised throughout by the intra-and intermolecular hydrogen bonding together with weak van der Waals interactions which result in three dimensional framework lattice of the complexes. The ethylenediamine ligand hydrogen atoms which form a mono-, bi- and trifurcated intra-and intermolecular strong hydrogen bonding with the carbonyl group oxygen atom and sulfonyl oxygen atoms of the adjacent saccharinate ligands, see Table 3.10. There are strong hydrogen bonding which involves the sulfonyl oxygen atom with the adjacent molecule resulting in a strong intermolecular of N-H···O interaction. The phenyl and ethylene hydrogen atoms are also showing a weak interaction with the oxygen atoms of the carbonyl of the adjacent molecule of the saccharinate ligand. The sac(cπ)···sac(π) interaction help stabilize the molecular structure in the 3D lattice observed in Figure 3.13.

3.5 Thermal analysis

The thermal analysis of the saccharinato complexes containing mixed-ligands was performed on selected complexes of (**1**) to (**5**) and (**7**) and (**11**) using the thermal analysis curves (TG, DTA and DTG). See Chapter 2 for experimental details. Results are shown in Table 3.11. From the thermal graphs it was observed that most complexes are stable from 25 to approximately 200 °C at which point they start decomposing.

Table 3. 11 Thermoanalytical data for selected complexes

Complexes	Stage	Temperature range (°C)	DTG_{max} (°C)[a,b]	Mass loss (%)		Total mass loss (%)		Solid residue
				Found	Calc.	Found	Calc.	
1	1	89.9-122.6	112[a]	17.62	17.06			$[Cd(sac)_2(DMSO)$
	2	416.3-445.0	430[b]	39.12	38.90	56.74	55.96	[Cd(sac)]
2	1	104.2-131.9	129[a]	17.41	12.69			$[Co(sac)_2(H_2O)$
	2	148.4-391.4	302[b], 430[b]	3.02	2.93			$[Co(sac)_2]$
	3	414.9-444.8		30.76	29.59	51.19	45.21	[Co(sac)]
3	1	188.8-222.5	190; 214[a]	26.69	26.66			$[Zn(sac)_2]$
	2	450.3-466.9	467[b]	31.17	31.08	58.84	57.83	[Zn(sac)
4	1	60.0-70.0	60.6[a]	2.81	2.72			$[Hg(sac)_2(DMSO)$
	2	135.1-148.0	227, 144[a]	11.62	11.82			$[Hg(sac)_2$
	3	331.7-370.2	223, 307[a]	28.81	27.56			[Hg(sac)]
	4	418.6-441.0	426[a]	33.93	32.40	87.75	87.72	Hg
5	1	128.3-173.44	145[a]	6.83	6.65			$[Cu(sac)_2(DMSO)$
	2	335.7-363.6	347[a], 481[a]	14.56	14.44			$[C(sac)_2]$
	3	463.0-488.9		26.52	27.76	77.16	78.10	[Cu(sac)(O)
7	1	191.7-207.9	57.1[b]	16.10	17.91			$[Cu(sac)_2(MDEA)]$
	2	274.83-352.9	200.7[b]	45.53	45.30	70.24	63.21	[Cu(sac)]
11	1	162.4-179.6	58.4[b]	7.959	10.07			$[Cd(sac)_2(en)]$
	2	302.9-406.3	280[a],328[b]	48.33	40.57			[Cd(sac)]
	3	824.0-914.9	633[a],689[b]	30.36	30.52	86.21	81.16	[Cd]

[a] endothermic, [b] exothermic

The complexes (**1**), (**2**), (**3**), (**4**) and (**5**) consists of aqua- and DMSO ligands. Complex (**3**) does not have aqua ligands coordinated to the metal centre. These complexes show two to four stages of decomposition which appears at different temperature rates depending on the number of present ligands coordinated to the metal centre. Complex (**1**) consists of two decomposition processes in which the complex lose mass. Stage 1 of complex (**1**) on the thermal curve occurs at temperature range of 89.9-122.6°C. The complex decomposes with melting at an endothermic peak at 112°C and this is attributed to the mass loss of two aqua-ligands and one DMSO ligand with a weight loss percentage of 17.60% (calc. 17.06%). The second stage involves the mass loss of saccharinate ion and DMSO with a weight loss mass of 39.12% (calc. 38.90%) which left the solid residue of [Cd(sac)]. This stage takes place at the temperature range of 416.3-445.0°C and it has the exothermic weight loss peak of 430 °C. The total mass lost was 56.74% (calc. 55.96%), see Table 3.11, above

The thermal analysis of complex (**2**) consists of three decomposition stages. The first one occurs at a temperature range of 89.9-122.6°C and it decomposes without melting at the endothermic temperature of 129°C. The mass loss on this stage was 17.41% (calc. 12.69%) and was due to the loss of two DMSO ligands and one aqua-ligand. Stage two shows complex degradation at the temperature range of 148.4-391.4°C and it undergoes two exothermic temperature peaks at 302 and 430°C. This was due to the mass loss of one aqua-ligand losing a mass of 3.02% (calc. 2.93%). Stage three takes place

at the temperature range of 414.9-444.8°C and this shows the mass loss of 30.76% (calc. 28.59%) which is found to be the loss of saccharinate ion. The solid residue was attributed to [Cd(sac)]. The total mass loss was 51.19% (calc. 45.12%).

There are two stages observed for complex (**3**), the first stage shows the mass loss of two DMSO ligands. A 26.69% (calc. 26.66%) weight loss of DMSO ligands was found and it occurs at the temperature range of 188.8-222.5°C with a endothermic melting peak at 190°C and degradation temperature at 214°C. At the temperature range of 450.3-466.9°C the saccharinate ion decomposes with an exothermic peak at 467°C. The mass loss of saccharinate ion was 31.17% (calc. 31.08%). The total mass loss was 58.84% (calc. 57.83%). The solid residue was [Zn(sac)].

Complex (**4**) shows many decomposition stages and some of these were due to the distorted electronic structure of the complex. This results in many melting phases. Those stages which correspond to the complex were identified and matched those of the calculated values. The complex consists of four phases and stage one shows the mass loss of 2.81% (calc. 2.72%) which was attributed to the mass loss of the aqua ligand. This occurs at the temperature range of 60.0-70.0°C with an endothermic peak at 60.6°C. Stage two indicated that the complex melts within the temperature range of 135.1-148.0°C and later decomposes at the endothermic peak of 144 and 227°C. There was a mass loss of 11.62% (calc. 11.82%) this was attributed to a mass loss of DMSO. Stage three of complex (**4**) happens at the temperature range of 331.7-370.2°C and it consists of two endothermic peaks at the temperatures of 223 and 307°C. This stage showed the decomposition of saccharinate ion of the complex. The mass loss of saccharinate ion was 28.81% (calc. 27.56%). The last stage occurred at the temperature range of 418.6-441.0°C and showed the degradation of second saccharinate and its combustion with the weight mass loss of 33.93% (calc. 32.40%). The stages of this complex are all endothermic and the fourth stage shows the peak at 462°C. The total mass loss was 87.75% (Cal. 87.72%). The solid residue was attributed to Hg metal.

Complex (**5**) underwent two stages and the first stage was due to the loss of two aqua-ligands which occurred at the temperature range of 128.3-173.44°C. The complex decomposed without melting with an endothermic temperature peak of 145°C. There was a sub-stage before Stage two which showed a mass loss of 29.25%. Stage 2 was due to mass loss of DMSO at the temperature range of 335.7-363.6°C with an endothermic temperature of 347 and 481°C. The mass loss of 14.65% (calc. 14.44%) was observed. The last stage occurred at the temperature range of 414.9-444.8°C and showed no degradation temperature peak, but the elimination of saccharinate ion ligand with a mass loss of 26.52% (calc. 27.76%) was observed. The total mass loss was 77.16% (calc. 78.10%). The end product was [Cu(sac)(O)].

There are two stages which are observed in complex (**7**), the first stage shows mass loss of two MDEA ligands. A 16.10% (calc. 17.91%) mass loss of MDAE was found and it occurred at a temperature range of 191.7-207.9°C with an exothermic decomposition peak at 57.1°C. At the temperature range of 174.83-352.9°C, the saccharinate anion decomposes together with another MDEA ligand at an exothermic peak of 200.7°C. The mass loss of saccharinate anion and MDEA was found to be 45.53% (calc. 45.30%). The total mass loss was 70.24% (calc. 63.21%). The solid residue was [Cu(sac)]. The same behaviour would have been expected for complex (**8**) since they have similar structural properties.

Complex (**11**) consists of three decomposition temperatures. Complex (**10**) and complex (**11**) are related and therefore the TGA studies were performed only on (**11**). Stage one occurred at a temperature range of 162.4-179.6°C and decomposed without melting at the exothermic temperature of 58.4°C. The mass loss at this stage was 7.959% (calc. 10.07%) and was due to the loss of ethylenediamine (en) of the complex. The solid residue was [$Cd(sac)_2(en)$]. Stage two showed complex degradation at the temperature range of 302.9-406.3°C and it underwent endothermic and exothermic peaks at 208 and 406.3 °C, respectively. This was due to the mass loss of en and sac ligand losing a mass of 48.33% (calc. 240.59%). The solid residue was [Cd(sac)]. Stage three of the complex took place at the temperature range of 824-914.9°C and this showed the mass loss of 30.36% (calc. 30.52%) which was found to be the loss of saccharinate ion. The solid residue was attributed to [Cd]. The total mass loss was 86.21% (calc. 81.16%).

3.6 References:

1. S. Z. Haider and K. M. A. Malik, *J. Bangladesh Acad. Sci.*, 1982, **6**, 119-125.
2. O. Z. Yeşilel, G. Günay and O. Büyükgüngör, *Polyhedron*, 2011, **30**, 364-371.
3. E. J. Baran, *Quim. Nova*, 2005, **28**, 326-328.
4. E. J. Baran and V. T. Yilmaz, *Coord. Chem. Rev.*, 2006, **250**, 1980-1999.
5. Z. Yugeng, *Trans. Met. Chem.*, 1994, **19**, 446-448.
6. V. T. Yilmaz, S. Hamamci and C. Thöne, *Z. Anorg. Allg. Chem.*, 2003, **629**, 711-715.
7. E. B. Miminoshvili, A. N. Sobolev, T. N. Sakvarelidze, K. E. Miminoshvili and E. R. Kutelia, *Acta Cryst.*, 2003, C**59**, m118-m120.
8. S. Z. Haider, K. M. A. Malik, S. Das and M. B. Hursthouse, *Acta Cryst.*, 1984, C**40**, 1147-1150.
9. S. Kirschner, *Inorg. Synth.*, Wiley, 2009, 47-50.
10. A. T. Raad, D. M. Boghaei and H. Reza Khavasi, *J. Coord. Chem.*, 2009, **63**, 273-283.
11. S. M. Teleb, *Quim. Argent.*, 2004, **92**, 31-40.
12. J. Clayden, N. Greeves and S. Warren, *Organic Chemistry*, OUP Oxford, 2012, 56-64.
13. S. Z. Haider, K. M. A. Malik, K. J. Ahmed, G. B. Kauffman and M. Karbassi, in *Inorg. Synth.*, John Wiley & Sons, Inc., 2007, 47-51.
14. S. Guney, V. T. Yilmaz and W. T. A. Harrison, *J. Coord. Chem.*, 2006, **59**, 1123-1130.
15. G. Gliemann, *Ber. Bunsen-Ges. Phys. Chem*, 1978, **82**, 1263-1263.
16. F. A. Cotton, R. Francis and W. D. Horrocks, *J. Phys. Chem.*, 1960, **64**, 1534-1536.
17. M. A. Cinellu, L. Maiore, A. Schier, H. Schmidbaur and D. Rossi, *Z. Naturforsch.*, 2008, **63b**, 1027-1034.
18. S. Z. Haider, K. M. A. Malik, K. J. Ahmed, H. Hess, H. Riffel and M. B. Hursthouse, *Inorg. Chim. Acta*, 1983, **72**, 21-27.
19. L. E. Orgel, *An Introduction to Transition-metal Chemistry Ligand-field Theory*, Methuen, 1963, 392-408.

20. H. Icbudak, H. Olmez, O. Z. Yesilel, F. Arslan, P. Naumov, G. Jovanovski, A. R. Ibrahim, A. Usman, H.-K. Fun, S. Chantrapromma and S. W. Nge, *J. Mol. Struct.*, 2003, **657**, 255-270.

21. I. B. Bersuker, *Electronic Structure and Properties of Transition Metal Compounds: Introduction to the Theory*, John Wiley & Sons, 2010, 393-425.

22. S. A. Shaker, Y. Farina, S. Mahmmod and M. Eskender, *Sains Malaysiana*, 2010, **39**, 957-962.

23. V. T. Yilmaz, Y. Topcu, F. Yilmaz and C. Thoene, *Polyhedron*, 2001, **20**, 3209-3217.

24. C.-C. Wang, W.-C. Lo, C.-C. Chou, G.-H. Lee, J.-M. Chen and S.-M. Peng, *Inorg. Chem.*, 1998, **37**, 4059-4065.

25. O. Andac, Y. Topcu, V. T. Yilmaz and W. T. A. Harrison, *Acta Cryst.*, 2002, C**58**, m14-m16.

26. F. S. W. Potwana and W. E. Van Zyl, *Acta Cryst.*, 2011, E**67**, m1667-m1668.

27. F. S. W. Potwana and W. E. Van Zyl, *Acta Cryst.*, 2011, E**67**, m1635.

28. P. A. M. Williams, E. G. Ferrer, N. Baeza, O. E. Piro and E. J. Baran, *Z. Anorg. Allg. Chem.*, 2006, **632**, 619-623.

29. F. S. W. Potwana, B. E. Shandu and W. E. Van Zyl, *Acta Cryst.*, 2011, E**67**, m1665.

30. V. T. Yilmaz, Y. Topcu, F. Yilmaz and C. Thoene, *Polyhedron*, 2001, **20**, 3209-3217.

31. O. V. Quinzani, S. Tarulli, O. E. Piro, E. J. Baran and E. E. Castellano, *Z. Naturforsch.*, 1997, **52**, 183-187.

32. G. Jovanovski and B. Kamenar, *Acta Cryst.*, 1982, C**11**, 247-255.

33. G. Jovanovski, B. Kamenar, G. Ferguson and B. Kaitner, *Acta Cryst.*, 1988, C**44**, 616-618.

34. V. T. Yilmaz, S. Caglar and W. T. A. Harrison, *Acta Cryst.*, 2004, C**60**, m35-m38.

35. V. T. Yilmaz, V. Kars and C. Kazak, *Z. Naturforsch.*, 2006, **61b**, 555-229.

36. V. T. Yilmaz, S. Caglar and W. T. A. Harrison, *J. Coord. Chem.*, 2005, **58**, 549-558.

37. P. A. M. Williams, E. G. Ferrer, K. A. Pasquevich, E. J. Baran, Z. Chaia, E. E. Castellano and O. E. Piro, *Z. Anorg. Allg. Chem.*, 2000, **626**, 2509-2514.

38. I. Pascual, *Acta Cryst.*, 1995, C**51**, 2028-2030.

39. C. A. Johns, G. M. Golzar Hossain, K. M. Abdul Malik, S. Zahir Haider and U. K. Rowzatur Romman, *Polyhedron*, 2001, **20**, 721-726.

40. V. T. Yilmaz, S. Caglar and W. T. A. Harrison, *Z. Anorg. Allg. Chem.*, 2004, **630**, 1126-1130.

41. F. Nunzi, E. Ruiz, J. Cano and S. Alvarez, *J. Phys. Chem*., 2007, C**111**, 618-621

CHAPTER 4

SCARCE CATIONIC COMPLEXES WITH SACCHARINATE AS ANION

4.1 Introduction

Saccharin, also known as 1,2-benzisothiazoline-3-(2*H*)one 1,1-dioxide or *o*-sulphobenzimide is a very interesting and a diverse polyfunctional ligand in inorganic chemistry.[1] Its alkali and alkali-earth salts are very soluble in water and are used to prepared saccharinato complexes. These salts are used as non-caloric artificial sweeteners and as food additives.[2] The deprotonated form has the ability to bind to the metal centres *via* the amino nitrogen, carbonyl oxygen or the sulfonyl oxygen atoms.[3-5] In the recent past there has been an increasing interest in the synthesis of amine saccharinato complexes due to their ability to modify DNA in order to fight cancer.[6] Sen and Dotson,[7] and Brannon *et al*.[8] have shown that amines readily coordinate to divalent late metal centres.[9] Depending on the type of amine used in the reaction, these can either coordinate in a mono-, bi- or tridentate mode to the metal complexes.[10] The alcohol amines can dissociate and lose the alcoholic proton to form an aminate which can also behave as a strong chelating agent. This behaviour is mostly observed in dimers which are mostly formed by copper(II) cations and cobalt(II) cations. A number of complexes have been reported where the saccharinate anion acts as a counter ion, and this is one of the reasons that saccharin is an interesting ligand because it possesses various possible ligation modes as observed in the following complexes where sac resides in the outer coordination sphere:$[M(dmpy)_2](sac)_2\cdot 2H_2O$, (M =Co),[11] $[Cu(H_2O)_2(pyet)_2](sac)_2$,[12] $[Ni(pyet)_2(H_2O)_2](sac)_2$,[13] $[Ni(dien)_2]\cdot 2(sac)\cdot H_2O$,[14] $[Ni(dmpy)_2](sac)_2\cdot 2H_2O$,[15] and $[M(H_2O)_4(py)_2](sac)_2\cdot 4H_2O$ (M = Co, Ni)[16] except complexes $[Cu_2(dea)_2(sac)_2]$(dea = diethanolamine)[17] and $[Cu_2(pypr)_2(sac)_2]$ (pypr = 2-pyridinepropanoxy anion). The reason saccharin can be a counter ion in a structural complex is that, when a bulky ligands is used in the reaction it might result in one saccharin bonding directly to the metal centre or both the saccharin ligand displacing and forming part of the coordination sphere. The present study demonstrates the characterisation of three structures in which the transition metal centres Ni(II), Cu(II) and Co(II) are coordinated in a variety of denticities. The amines used in this study are: N-methyldiethanolamine (3º), 2-(methylamino)ethanol (2º) and ethylenediamine (1º). These are a class of organic molecules which consists of the moiety of the amine and alcohol groups.

4.2 Results and Discussion

4.2.1 Synthesis of Precursors, $[M(sac)_2(H_2O)_4]\cdot 2H_2O$

The saccharinato complex of the type $[M(sac)_2(H_2O)_4]\cdot 2H_2O$ shown in Scheme 4.1, was prepared according to the preparation procedure outlined by Haider *et al.*[18] see Chapter 3. The reaction produces complexes in good yield of 75 to 85%.

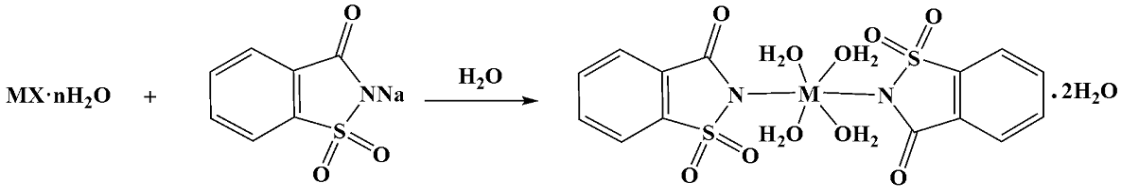

$MX\cdot nH_2O$: $NiCl_2\cdot 6H_2O$, $CuSO_4\cdot 5H_2O$ and $CoCO_3\cdot 6H_2O$

Scheme 4. 1 Synthesis of $[M(sac)_2(H_2O)_4]\cdot 2H_2O$ precursors.

4.2.2 Preparation of Metal Complexes

The following set of amines were used to prepared complexes(**6**), (**9**) and (**12**), respectively: N-methyldiethanolamine (MDEA),2-(methylamino)ethanol (MEA) and ethylenediamine (en). The direct addition of amines in the methanolic solution of $[M(sac)_2(H_2O)_4]\cdot 2H_2O$ at ~80°C yielded a colour change of the solutions to produce complexes (**6**), (**9**) and (**12**). Upon standing for three days, the solution of complex (**6**) yielded violet crystals. The crystals of complex (**9**) were also harvested after three days when the solution was allowed to stand at room temperature (r.t.) to cool down. The crystals of complex (**12**) were obtained after a week of allowing the solution to stand at r.t.. The X-ray crystal analysis indicated that the complex (**12**) contains bicarbonate ion from the starting material of cobalt bicarbonate hexahydrate. This occurred due the strong binding constant of CO_3^{2-} ions to the Co^{2+}cation which could not be removed. Real *et al*. studied cobalt dissolution in a carbonate/ bicarbonate media, and found that when cobalt(II) dissolves in an aqueous media, it forms a Co(OH) as intermediate-adsorbed species and this species participates at some equilibrium reactions with other adsorbed species as $Co(OH)^+$ and $CoCO_3$, making it hard to separate the products.[19] Below is the schematic representation of $[M(sac)_2(H_2O)_4]\cdot 2H_2O$ reacting with amines to replace the labile aqua ligands of the starting material to yield desired products. The yield of the complexes ranged from 75

to 95 %. The CHN micro-analysis confirms the formation of the products, refer to the experimental procedure Chapter 2 and see Scheme 4.2 for chemical properties. Table 4.1 shows a list of physical properties of the complexes.

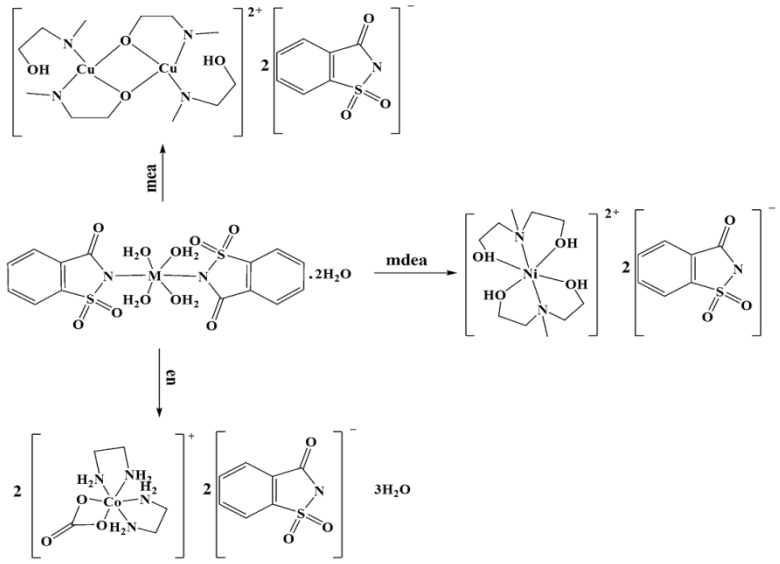

Scheme 4. 2 Reactions showing the formation of saccharinato complexes containing amines

Complexes (**6**) and (**12**) have a decomposition temperature indicating that the metal centres are coordinated to N-methyldiethanolamine for (**6**); and ethylenediamine and carbonate ions for (**12**), respectively, which indicates that they are strongly held together by the ionic bonds of saccharinate counter ions. Complex (**9**) has a sharp melting point temperature which shows high purity and that it is weakly held by the alkoxo-bridging groups of the ligand which collapses when heated causing the molecule to melt easily.

Table 4. 1 Tabulated analytical results of saccharinato complexes

Complexes	Colour	Melting point (°C)	Molecular weight	Yield (%)	Anal. Found (Cal.) (%)		
					C	H	N
6	Violet	225[a]	661.38	75.0	43.0 (43.3)	4.6 (4.8)	8.6 (8.4)
9	Blue	165	789.90	76.0	39.2 (39.5)	5.0 (5.4)	10.2 (10.6)
12	Red	135[a]	896.69	95.0	33.5 (33.2)	4.9 (4.4)	15.3 (15.0)

[a] decomposition temperature

The complexes could not be analysed by Nuclear Magnetic Resonance (NMR) due their paramagnetic nature. This behaviour is common for metal centres like Ni^{2+}, Cu^{2+} and Co^{2+}. In this case the ligands are high-spin and are likely to be drawn towards the strong magnetic field which are positioned in a parallel position to the field lines.

4.3 Spectral Properties

4.3.1 Fourier Transform Infrared spectroscopy (FTIR) Spectral Data of Complexes

The most significant IR bands of the complexes are outlined in Table 4.2. The bands in the range of 3187 to 3485 cm^{-1} show characteristic ν(OH)vibrations which can be attributed to the hydroxyl group of the ethanol group with strong hydrogen bonding for complex (**9**) and to the water of crystallization for complex (**12**). Complexes (**6**), (**9**)and (**12**) showed sharp stretching bands in the range 2823 to 3095 cm^{-1} and 2690 to 2954 cm^{-1}which belong to the ν(NH) and ν(N-CH) of amines, respectively. The distinct strong absorption vibration band of the carbonyl group ν(C=O) for these complexes appears at the range 1577 to 1627 cm^{-1}. The free saccharin has a vibration band of 1720 cm^{-1} [20]. The vibrational stretches at 1289 to 1336 cm^{-1} and 947 to 979 cm^{-1} vibration intensity are assigned to $\nu(CNS)_{sym}$ and $\nu(CNS)_{asym}$ moiety of the saccharin ligand of the counter ion, respectively. There are closely related stretches at a range of 1248 to 1286 and 1141 to 1155 cm^{-1} which are assigned to $\nu_{asym}(O=S=O)$ and $\nu_{sym}(O=S=O)$, respectively. The band which was observed to be in the range of 1456 to 1583$cm^{-1}$was assigned to the ν(C=C) stretch of the saccharin ring. For pure saccharin, this band occur at 1462 to 1600 cm^{-1} [20]. The wavenumbers in the range 300 to 550 cm^{-1} are due to M-O and M-N vibration bands.[21]

Table 4. 2 IR spectral data for the metal complexes

Complexes	ν(OH)	ν(NH)/ N-CH	ν(C=O)	$\nu(SO_2)$		ν(CNS)		ν(C=C)
				asym	sym	asym	Sym	
6	–	2917, 2690	1613	1286	1155	979	1336	1580
9	3187	2823, 2876	1627	1255	1147	947	1330	1583, 1456
12	3458	3095, 2954	1577	1248	1141	949	1289	1457

The bands obtained in the experimental data lie very close to those of the $[M(sac)_2(H_2O)_4]\cdot 2H_2O$ complex whereby M(II) = Ni, Cu and Co. The spectral frequencies of the $[M(sac)_2(H_2O)_4]\cdot 2H_2O$ was previously reported.[22] The current complexes have been shown to possess similar infrared properties.

The important infrared peaks are observed at the following wavenumbers: 3500 to 3100 cm^{-1} for different types of the aqua ligands ; 1610cm^{-1} for carbonyl group; 1280 cm^{-1} for $\nu(SO_2)_{asym}$; 1150 cm^{-1} for $\nu(SO_2)_{sym}$;1570 to 1479 cm^{-1} for C=C and 942 cm^{-1} for $\nu(CNS)_{asym}$ and 1327 cm^{-1} for $\nu(CNS)_{sym}$.[23, 24]

4.3.2 UV-Vis spectroscopy

The UV-Vis spectroscopy data for complexes (**6**), (**9**) and (**12**) are reported in Table 4.3, together with the λ_{max} values and molar absorptiviy in parenthesis. The λ_{max} values of complexes (**6**), (**9**) and (**12**) are compared with those that have been previously reported for sodium saccharin which exhibits two absorption bands at λ_{max} = 220 nm, ε = 10166 L mol^{-1} cm^{-1} and at λ_{max} = 268nm, ε = 1628 L mol^{-1} cm^{-1}. This was assigned as a ligand-to-ligand charge-transfer intraligand L-L* transition[25], and $[M(sac)_2(H_2O)_4]\cdot 2H_2O$ complexes at λ_{max} = 525 nm and 280 nm where M(II) =Co, λ_{max} = 680 nm, 400 nm and 280 nm where M(II) =Ni and λ_{max} = 780 nm and 355 nm where M(II) =Cu.[18, 22] Not too much information is known about the UV-Vis spectroscopy of complexes that contain saccharinate counter ion.

Table 4. 3 Electronic spectra results of saccharinato complexes

Complexes	λ_{max} (nm), ε (M^{-1} cm^{-1})^x		
	ligands		d–d
6	275(28266)	–	419(164), 783(127)
9	270(5223)	370(5010)	652(77.8)
12	276(4142)	–	379(69.7),527(74.5)

The UV spectrum of complex **(6)** consists of three absorption bands which appeared at 275 nm for complex **(6)** which are close to the values of those reported previously. The d-d transition state of these two octahedral coordination geometries are in the range 419 to 783 nm. The values of λ_{max} of (**6**) are red-shifted compared to the starting $[M(sac)_2(H_2O)_4]\cdot 2H_2O$. Molar absorptivities of the ligands that participate in the charge-transfer absorption are normally larger than 10,000 L mol^{-1} cm^{-1}in Table 4.3. The area which indicates the presence of intraligand L-L* transition is greater than 500 $M^{-1}cm^{-1}$ and less than 10, 000 $M^{-1}cm^{-1}$ which indicates the formation of the sacharinato complexes. The UV spectrum of the saccharinato complex **(9)** reported herein consists of three absorption bands. The bands at 270and 370 nm corresponds to the saccharinate anion of the complexes. These absorption peaks are correspond with intraligand L-L* transition due to LMCT arising from an un occupied ligand π -orbital to the empty d-orbital of Cu(II). The low energy intensity at 652 nm resulting from the d-d transition are noticed due to MLCT transition which occurs when the saccharinato complexes and other related complexes are in a low oxidation state and this shows the

activity whereby the ligands are easily reduced in solution. Complex **(12)** containing Co(II) showed distinct UV-visible absorption behaviour at a different region of the spectra. This complex's UV spectrum displays three absorption bands. The intraligand L-L* transition observed appeared to be red shifted compared to the values of those observed in saccharin anion and the $[M(sac)_2(H_2O)_4]\cdot 2H_2O$ complex.[18, 20, 26] The intraligand L-L* transition of the saccharinate anion of the complexes are observed at 276 nm.

4.4 Description of the Crystal Structures of Saccharinato Complexes

4.4.1 X-ray Structure Determination of the Complexes

The instruments, conditions and programs in which the crystal structures were solved are outlined in Chapter 2, the experimental section. Herein is the summary of the crystallographic data of complexes which is given in Table 4.4.

Table 4. 4 Crystal data and structure refinement for complexes (**6**), (**9**) and (**12**)

	6	**9**	**12**
Formula	$(C_{10}H_{26}N_2NiO_4).2(sac)$	$(C_{12}H_{34}N_2Cu_2N_4O_4).2(sac)$	$C_{24}\ H_{46}\ Co_2\ N_{10}\ O_{15}\ S_2$
M_r	661.38	789.90	896.69
Crystal system	Triclinic	Triclinic	Triclinic
Space group	*P-1 (No.2)*	*P-1 (No.2)*	*P-1 (No.2)*
a, Å	8.5680(5)	8.9048(13)	8.8000(2)
b, Å	9.0490(7)	10.6791(8)	11.9050(3)
c, Å	10.5720(9	10.7255(7)	17.9938(4)
α, deg	106.139(3)	118.4340(10)	74.3790(10)
β, deg	94.681(4)	107.640(2)	88.4700(10)
γ, deg	111.196(4)	111.196(4)	78.4910(10)
V	718.76(10)	821.46(15)	1778.24(7)
Z	1	1	2
ρcalcd, g cm^{-3}	1.528	1.597	1.675
M, mm^{-1}	0.881	1.484	1.133
F(000)	346	410	932
Crystal size (mm^3)	0.18x0.22x0.28	0.12x0.18x0.22	0.41x0.20x0.14
Θ Range (º)	2.6,25.0	2.4,28.3	1.8,28.4
Index range (*h,k,l*)	0/10, -10/10, -12/12	-11/11, -12/13, -13/7	-11/11, -15/15, -24/21
T, K	173(2)	173(2)	100(2)
Reflections collected	20824	10027	46448
Independent reflections	2538	3365	8818
R_{int}	0.048	0.027	0.0427
Completeness to	Θ = 25.0º 100%	Θ = 26.4º 100%	Θ = 28.4º 99.1%
Goodness-of-fit on *F*2	1.12	1.06	1.046
Final *R* indices [I > 2σ(*I*)]	*R*1 = 0.03719, w*R*2 = 0.0711	*R*1 = 0.0344 w*R*2 = 0.0893	*R*1 = 0.0416 w*R*2 = 0.1151
R indices (all data)	*R*1 = 0.03719 wR2 = 0.0711	*R*1 = 0.0344 w*R*2 = 0.0893	*R*1 = 0.0501 w*R*2 = 0.1230
Largest diff. peak and hole, e / Å	-0.42 and -0.36	-0.56 and -1.25	1.370 and -1.170

w = 1/[\s^2^(Fo^2^)+(0.0204P)^2^+0.7574P] where P=(Fo^2^+2Fc^2^)/3 for complex(**6**), w = 1/[\s^2^(Fo^2^)+(0.0366P)^2^+1.1365P] where P=(Fo^2^+2Fc^2^)/3 for complex (**9**)

4.4.2 Crystal structures

4.4.2.1 [Ni(*N,O,O*-mdea)$_2$]·2(sac) (**6**)

The ORTEP view of the molecular structure of complex (**6**) is shown in Figure 4.1, together with the atom labeling. The selected bond distances and angels are tabulated in Table 4.5. The unit cell dimensions of the crystal structure are shown in Table 4.4, above.

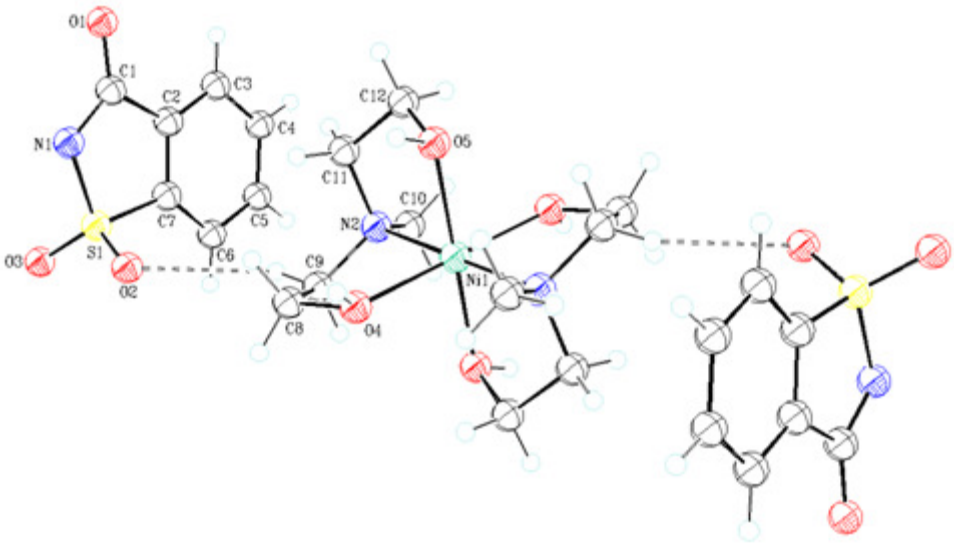

Figure 4. 1 Molecular structure of (**6**) showing the atom labelling scheme. The atom displacement ellipsoids are drawn at 50% probability level. Only atoms in the asymmetric unit are labelled and the other half of the complex was generated *via* symmetry code -x, -y, 2-z. The dashed lines indicate hydrogen bonding.

The $[Ni(MDEA)_2]^{2+}$complex and two saccharinate anions acts as counter ions. From the starting material, the four aqua ligands were expected to be displaced by the N-methyldiethanolamine without breaking the covalent bond between the metal centre and the N atom of the saccharin anion, hence the result was unexpected. Amines are known to have a strong chelating effect. The single X-ray crystal analysis of complex (**6**) shows that the molecule crystallizes in a triclinic system within the space group of P-1. The metal centre is coordinated to a tridentate ligand which occupies a six-coordination site resulting in an octahedral coordination geometry. The amine is coordinated *via* the nitrogen atom and the two oxygen atoms of the ligand. Complex (**6**) has these selected bond distances: for Ni1-O4 is 2.0657(18), Ni1-O5 is 2.0822(16) and Ni1-N2 is 2.0845(18)Å. These are the bond lengths obtained for the known complex of the starting materials: Ni1-O4 is 2.042(1), Ni1-O5 is 2.096(2) and Ni1-N2 is 2.154(1)Å. The bond angles for O-Ni-O is 91.3,O-Ni-N is 91.6 and O-Ni-N is 91.7(1)º.[27] The

average bond distances of the Ni-N of different ligands range from 2.094–2.119Å for complexes $[Ni(pyet)_2(H_2O)_2](sac)_2$, $[Ni(dien)_2]\cdot 2(sac)\cdot H_2O$ and $[Ni(dmpy)_2](sac)_2\cdot 2H_2O$ and their Ni-Nsac bond distances are 2.262(2) and 2.2874(19)Å[28, 29]. These bond lengths and bond angles agree with the bond lengths and bond angles of $[Ni(pyet)_2(H_2O)_2](sac)_2$ and others.

4.4.2.2 $[Cu_2(\mu\text{-}O)_2(mea)_4]\cdot 2(sac)$ (**9**)

A view of the molecular structure of complex (**9**) is shown in Figure 4.2, together with selected bond distances and bond angles in Table 4.5.

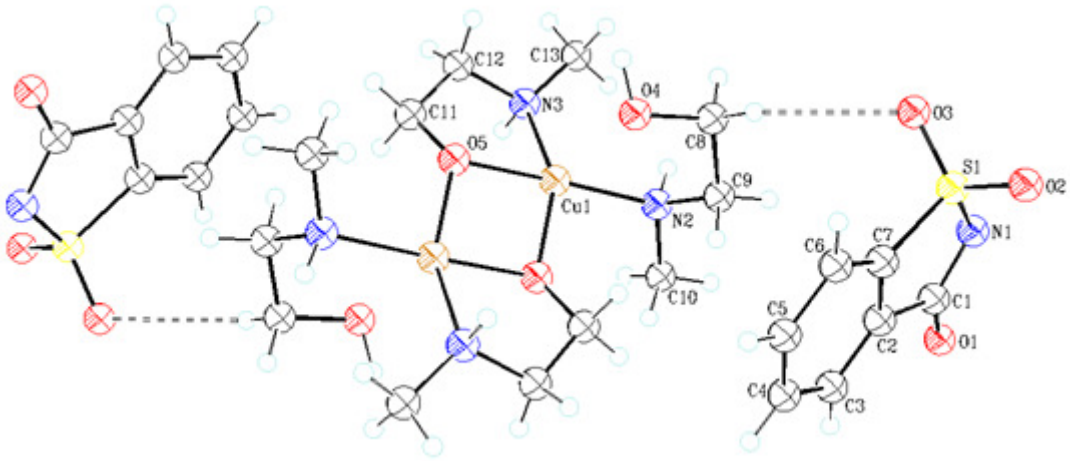

Figure 4. 2 The ORTEP crystal structure of (**9**) showing the labelling scheme. The atom displacement ellipsoids are drawn at 50% probability level. The atoms in the asymmetric unit are labelled and the other half of the complex was generated via symmetry code 1-x, 1-y, 1-z. The dashed interactions show hydrogen bonding of the complex.

The unit cell dimensions of the crystal structure are shown in Table 4.4. The molecular structure of (**9**) shows that 2-(methylamino)ethanol is a bidentate chelating ligand *via* the N and O-atoms. This amine is a neutral ligand and is coordinated to the two copper(II) metal centres forming a binuclear molecular complex in which the saccharinate anions acts as a counter ion. The crystallographic data indicates that the single X-ray structure of complex (**9**) crystallises in a triclinic system with the space group of P-1 whereby the metal centre is are positioned at the inversion centre of the four amine ligands. The coordination geometry of complex (**9**) is a distorted square planar around each copper centre. This complex is formed by two alkoxo-bridges whereby the two copper centres are connected by the deprotonated oxygen atoms of the 2-(methylamino)ethanol. The loss of one hydrogen atom from both ligands of ethanol resulted in 2-(methylamino)ethanol acting as a bidentate donor via the

oxygen and nitrogen atoms which bridge the two copper atoms. This geometry resulted from the addition of the strong amine ligand to the precursor complex, which caused the covalent bond of the staring material to be broken and replaced by the stronger covalent bonding of the amines. The distance between the Cu···Cu atoms is 3.016Å which falls within the Cu···Cu interaction distance of 2.99(2)Å for $[Cu_2(sac)_2(\mu\text{-dea})_2]$ and 3.0404(7)Å for $[Cu_2(sac)_2(\mu\text{-pypr})_2]$ and other observed alkoxo-the bridged copper(II) dimeric structures.[17,31] There are many examples of the closely related complex which illustrate the ranges of bond distances and angles that could be used to compare with those of the complexes. From Table 4.5, the bond distance of Cu1-O4 is 2.290(2), Cu1-O5 is 1.942(2), Cu1-N2 is 2.017(3), Cu1-N3 is 2.026(3) and Cu1-O5a is 1.959(2)Å for complex (**9**). In previously reported complexes of dinuclear copper(II) complexes, the Cu-N saccharinate bond distance is 1.9792(13)Å and it is shorter than these average bond distances 2.032(2), 2.033, 2.073 and 2.1776(16)Å found in the following complexes: $[Cu(H_2O)(py)_2(sac)_2]$[30], $[Cu(H_2O)_2(pyet)_2](sac)_2$, $[Cu(sac)_2(bzim)(H_2O)(EtOH)]\cdot 2EtOH$[31] and $[Cu(dipyr)_2(sac)]sac\cdot 0.25H_2O$[31].

4.4.2.3 Hydrogen bonding of the complexes

The atoms which are most likely to participate in hydrogen bonding interactions are O, H, N and some short interaction which result from the S-atoms and the π···π stacking interactions as a result of the rich electronic system. There are two significant hydrogen bonding interactions which can help stabilise the molecule: intra-and intermolecular hydrogen bonding.

Table 4. 5 Tabulated selected bond lengths (Å) and angles (°) for complexes (**6**) and (**9**) and hydrogen bonding coordination geometry for complexes (**6**)[b] and (**9**)[e]

Ni1-O4	2.0657(18)
Ni1-O5	2.0822(16)
Ni1-N2	2.0845(18)

O4-Ni1-O5	94.92(7)
O4-Ni1-N2	82.15(7)
O4-Ni1-O4a	180.00
O4-Ni1-O5a	85.09(7)
O4-Ni1-N2a	97.85(7)
O5-Ni1-N2	83.70(7)
O4a-Ni1-O5	85.09(7)
O5-Ni1-O5a	180.00

Cu1-O4	2.290(2)
Cu1-O5	1.942(2)
Cu1-N2	2.017(3)
Cu1-N3	2.026(3)
Cu1-O5a	1.959(2)

O4-Cu1-O5	100.24(8)	O5a-Cu1-N3	151.71(12)
O4-Cu1-N2	79.71(9)	Cu1-O4-C8	106.95(15)
O4-Cu1-N3	104.88(11)	Cu1-N2-H2N	110(2)
O4-Cu1-O5a	100.49(8)	Cu1-N2-H3N	107(2)
O5-Cu1-N2	178.20(10)	Cu1a-O5-C11	112.7(2)
O5-Cu1-N3	84.60(12)	Cu1-O5-C11	112.7(2)
O5-Cu1-O5a	78.72(9)	Cu1-N3-C12	107.0(2)
O5a-Cu1-N2	99.51(10)	–	–

D-H···A	d(D-H) (Å)	d(H···A) (Å)	d(D···A) (Å)	<(DHA) (°)
O(4)-H(4O)···O(1)	0.97(3)	1.64(3)	2.601(2)	170(3)
O(5)-H(5O)···N(1)	0.97(3)	1.72(3)	2.679(3)	176(3)
C(4)-H(4)···O(3)[m]	0.9500	2.5100	3.421(3)	162.00
C(6)-H(6)···O(2)[h]	0.9500	2.5700	3.383(3)	144.00
C(8)-H(8B)···O(1)[c]	0.9900	2.4400	3.291(3)	144.00
C(9)-H(9A)···O(3)[e]	0.9900	2.5900	3.428(3)	143.00

[b] Translation of Symmetry Code: (m) 1+x,y,z ; (h) 1-x,1-y,1-z; (c) 1-x,-y,2-z; (e) x,y,1+z

D-H···A	d(D-H) (Å)	d(H···A) (Å)	d(D···A) (Å)	<(DHA) (°)
N(2)-H(2N)···N(1)[d]	0.97(2)	2.15(2)	3.005(4)	147(3)
N(3)-H(3N)···O(2)[b]	0.97(4)	2.21(4)	3.036(4)	142(3)
O(4)-H(4O)···O(1)	0.97(4)	1.72(4)	2.671(4)	166(4)
C(8)-H(8B)···O(1)[d]	0.9900	2.4900	3.411(4)	154.00
C(10)-H(10B)···O(2)[b]	0.980	2.5000	3.376(4)	149.00

[e] Translation of Symmetry Code: (d) -1+x,y,-1+z; (d) 1-x,-y,1-z

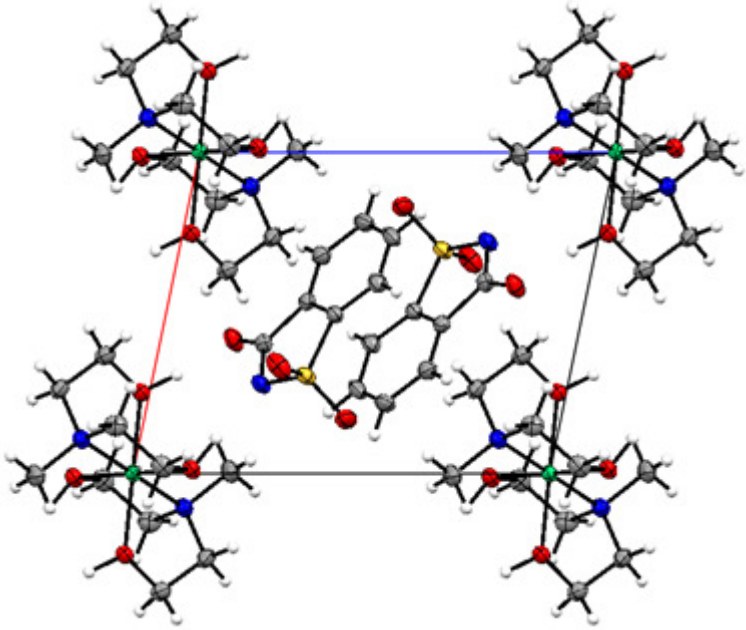

Figure 4. 3 The ORTEP crystal unit cell packing of (**6**) viewed along the crystallographic b axis. The elements are shown as (C = dark grey, H = light grey, S = yellow, O = red, N = blue and Ni = green).

The hydrogen bonding of complexes (**6**) and (**9**) are shown in Table 4.5 and presented as *dash lines* in Figure 4.1 and Figure 4.2, respectively. This shows that the crystal packing of the complex is stabilised throughout by intermolecular hydrogen bonding together with weak van der Waals interactions which result in 3D framework lattice of the complexes. Complex (**6**) shows that the CH and OH of the N-methyldiethanolamine have a strong intermolecular hydrogen bonding with the N atom of the saccharinate counter ions and the S atoms of the sulfonyl group and the O atom of the carbonyl group. The N-methyldiethanolamine ligand H atoms of the OH and CH groups, carbonyl

oxygen atoms and the oxygen sulfonyl atoms form a mono-, bi- and trifurcated intermolecular hydrogen bonding with the hydrogen of the phenyl from the adjacent saccharinate counter ions, see Table 4.5. Therefore these bonds helps in forming a 3D infinite network for complex (**6**) in Figure 4.3.

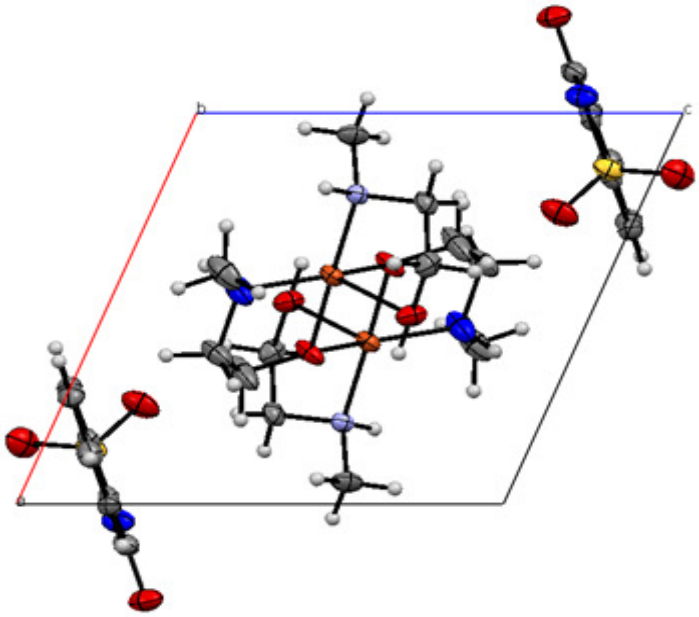

Figure 4. 4 The ORTEP crystal packing of (**9**) view down along the crystallographic b axis. The elements are shown as (C = dark grey, H = light grey, S = yellow, O = red, N = blue and Cu = orange).

The 3D framework of complex (**9**) is stabilised by the hydrogen bonding caused by OH, .i.e. (N-H···O) of the 2-(methylamino)ethanol forming a intermolecular interaction with the oxygen atom of the saccharinate counter ions and the N-H··N of the amine also participating in forming the intermolecular hydrogen bonding with the oxygen atom of the sulfonyl atoms, see Table 4.5. This is accompanied by the hydrogen atoms of the benzene ring interacting with the OH of the amine and the methylene hydrogen atoms interacting with the oxygen atom of the sulfonyl group. The hydrogen bonding interactions help to stabilise the complex into an infinite 3D network structure, see Figure 4.4.

4.4.2.4 $Co_2(en)_4(CO_3)_2]\cdot 2(sac)3H_2O$ (12)

The ORTEP crystal structure of complex $[Co_2(en)_4(CO_3)_2]$ 2(sac)$3H_2O$ (**12**) is shown in Figure 4.5. This information is accompanied by Table 4.6 which shows selected bond distances and bond angles. The crystal data and structural refinement data is listed in Table 4.4.

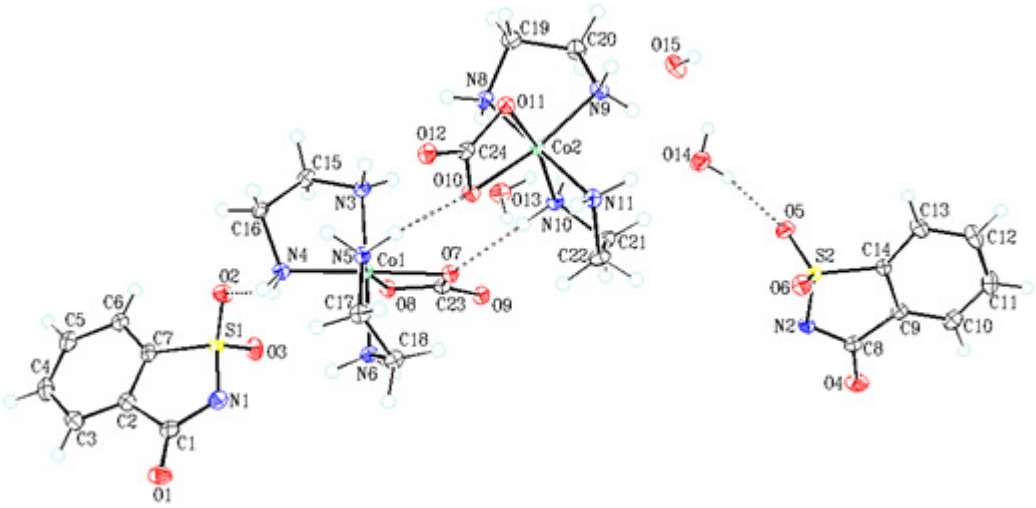

Figure 4. 5 The ORTEP crystal structure of (**12**) showing the labeling scheme. The atom displacement ellipsoids are drawn at 50% probability level. The dashed interactions show hydrogen bonding of the complex.

The molecular structure shows that the complex is made up of $[Co_2(en)_4(CO_3)_2]^{2+}$cation and two non coordinating saccharinate counter ions. The structure consists of two bidentate neutral ligand of ethylenediamine and an ionic bidentate ligand of bicarbonate which are both coordinated to the Co^{2+} metal centre which lies at the complex centre of inversion and this is accompanied by three waters of crystallization. The crystallographic data indicate that the single X-ray structure of complex (**12**) crystallizes in a triclinic system with the space group P-1. The complex has an octahedral coordination geometry. The positive charge of the complexes is counter balanced by two non-bonding saccharinate anion ligands. The Co-N and the Co-O bond distances of the $[Co(TEA)_2](sac)_2$,[32]$[Co(meaH)_3][Co(mea)(meaH)_2](SCN)_3$ are in the range of 1.928(3) to 1.949(3) and 1.899(3) to 1.915(3)Å, respectively. The Co-O bond length of complex (**12**) is slightly shorter than that observed for $[Co(meaH)_3][Co(mea)(meaH)_2](SCN)_3$ because of the delocalization of the electrons on the CO_3 atoms.[33]

Table 4. 6 Tabulated selected bond lengths (Å) and bond angles (°) for complex (**12**) and hydrogen bonding coordination geometry for complex (**12**)[k]

Co1-O7	1.9303(15)
Co1-O8	1.9207(15)
Co1-N6	1.9404(17)
Co1-N5	1.9525(17)
Co1-N3	1.9596(18)
Co1-N4	1.9465(18)
C23-O9	1.244(3)
Co2-O11	1.9256(15)
Co2-O10	1.9231(15)
Co2-N11	1.9395(18)
Co2-N8	1.9473(18)
Co2-N9	1.9418(18)
Co2-C24	2.332(2)
Co2-C23	2.336(2)
Co2-N10	1.9485(17)

N8-Co2-N11	178.47(8)
O1-Co2-N11	167.63(7)
O16-Co2-N9	97.38(7)
N6-Co2-N3	178.58(8)
N4-Co1-O7	167.73(7)
N5-Co1-O8	167.08(7)
N6-Co1-N4	93.89(8)
O7-Co1-N5	98.82(7)

D-H···A	d(D-H) (Å)	d(H···A) (Å)	d(D···A) (Å)	<(DHA) (°)
N(3)-H(3A)···O(12)[b]	0.92	2.08	2.990(2)	168
N(3)-H(3B)···O(9)[a]	0.92	2.03	2.934(2)	166
N(4)-H(4A)···O(2)	0.92	2.19	2.996(2)	145
N(4)-H(4B)···O(14)	0.92	2.11	2.999(3)	162
N(5)-H(5A)···O(10)	0.92	1.92	2.839(2)	174
N(5)-H(5B)···O(11)[b]	0.92	2.27	3.101(2)	150
N(6)-H(6A)···O(15)	0.92	1.91	2.818(2)	170
N(6)-H(6B)···O(4)	0.92	1.98	2.855(3)	158
N(8)-H(8A)···O(9)[a]	0.92	2.05	2.966(2)	175
N(8)-H(8B)···O(12)[b]	0.92	2.00	2.922(2)	175
N(9)-H(9A)···O(5)[e]	0.92	2.24	3.088(3)	153
N(9)-H(9B)···O(3)[a]	0.92	2.08	2.855(3)	141
N(10)-H(10A)···O(7)	0.92	2.04	2.962(2)	175
N(10)-H(10B)···O(8)[a]	0.92	2.11	2.950(2)	151
N(11)-H(11A)···N(2)[e]	0.92	1.93	2.841(2)	173
N(11)-H(11B) ···O(13)[f]	0.92	2.16	2.960(3)	145
O(13)-H(13A)···O(12)	0.86(4)	2.04(4)	2.875(2)	168(3)
O(13)-H(13B)···O(6)[g]	0.90(4)	2.24(3)	3.091(2)	156(4)
O(14)-H(14A)···O(5)[e]	0.80(4)	1.99(4)	2.780(3)	170(4)
O(14)-H(14B)···O(1)[h]	0.87(4)	2.04(4)	2.884(3)	165(4)
O(15)-H(15C)···O(1)[h]	0.77(4)	2.03(5)	2.762(3)	160(4)
O(15)-H(15D)···N(1)	0.85(4)	2.00(4)	2.829(3)	166(3)
C(16)-H(16A)···O(11)[b]	0.99	2.55	3.482(3)	156
C(17)-H(17A)···O(14)	0.99	2.44	3.295(3)	144
C(18)-H(18B)···O(2)[g]	0.99	2.56	3.433(3)	148
C(22)-H(22B)···O(9)[e]	0.99	2.46	3.423(3)	163

[k] Translation of Symmetry Code:(a) 1-x,1-y,1-z; (b) 1-x,-y,1-z;(c) 1+x,-1+y,z; (d) -1+x,y,z; (e) -x,1-y,1-z; (f)-x,-y,1-z; (h) x,-1+y,z; (i) 1-x,1-y,-z.

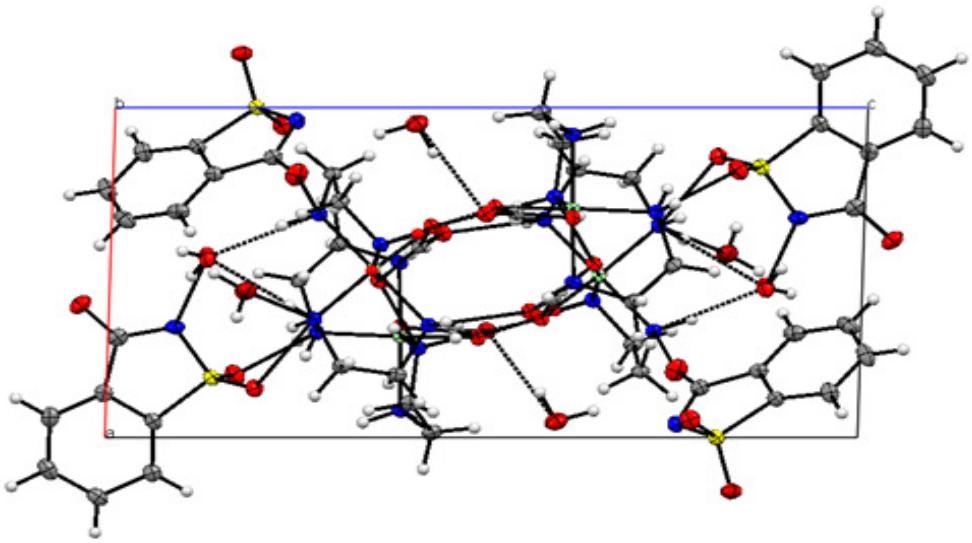

Figure 4. 6 The ORTEP crystal packing of (**12**) viewed down along crystallographic b axis. The elements are shown as (C = dark grey, H = light grey, S = yellow, O = red, N = blue and Co = light green).

4.5 Thermal analysis

The thermal analysis of the saccharinato complexes of (**6**), (**9**) and (**12**) were performed according to the experimental conditions outlined on Chapter 2. The complexes start decomposing at temperatures between 180 to 230°C where degradation process start occurring with an increase in temperature.

Table 4. 7 Thermoanalytical data for the selected metal complexes

Complexes	Stage	Temperature range (°C)	DTG_{max} (°C)[a,b]	Mass loss (%)		Total mass loss (%)		Solid residue
				Found	Calc.	Found	Calc.	
6	1	243.1-261.4	57.09[b],268.6[a]	28.11	27.63			$[Ni(MDEA)_2]$
	2	321.2-351.6	–	43.90	36.03	72.26	63.66	[Ni]
9	1	172.4-177.0	57.1[b], 180.1[a]	39.35	38.13			$[Cu(sac)_2]$
	2	465.1-521.2	–	40.14	46.38	79.53	84.51	[Cu]
12	1	117.5-143.7	139.1[a]	6.95	6.03			$[Co_2(en)_4(CO_3)_2]\cdot 2sac$
	2	204.7-221.2	216[a]	13.09	13.69			$[Co_2(en)_4]\cdot 2sac$
	3	293.4-329.3	306.3[a]	30.14	27.08			$[Co_2(en)_2]\cdot sac$
	4	402.1-420.6	–	6.15	6.69			$[Co_2]\cdot sac$
	5	443-825	645[b], 822.3[a]	20.49	20.38	77.46	73.87	$[Co_2]$

[a] endothermic, [b] exothermic

Complex (**6**) is a salt complex which does not melt but begins to decomposes at 243.1 to 261.4°C. This decomposition process leads to the degradation step which was the first stage in which the complex loses its weak counter ions. The process occurs at the two exothermic DTA peaks at 57.09 and 268.6°C. The experimental mass loss is 28.11% (calc. 27.63%). This leaves behind the solid residue of the complex $[Ni(MDEA)_2]$ which later decomposes at 321.2 to 351.6°C losing a mass of 43.90% (calc. 36.03%) with no observable endothermic-or exothermic TDA peaks. The total mass loss was 72.26% (63.66%).

Complex **(9)** is a dimeric structure in which the ligands were lost in two stages. Stage one involves the melt phase of the four 2-(methylamino)ethanol with a mass loss of 39.35% (calc. 38.13%). This stage takes place at the temperature range of 172.4-177.0°C with an exothermic TDA peak at 57.1°C and endothermic DTA peak at 180.1°C. The DTA peak at 180.1°C is a melt phase temperature which occurs in the vicinity of the melting temperature of the complex. At the temperature range of 465.1 to 521.2°C, the complex completely decomposes, losing the two saccharin counter ions to leave residue metallic copper losing 40.14% (calc. 46.38%) with no observed endothermic-or exothermic TDA peaks. The residual solids that was lost was79.53% (calc. 84.51%).

Complex (**12**) is a molecular complex which undergoes five stages of decomposition. The first decomposition temperature starts at 117.5 to 143.7°C. This decomposition is attributed to the three waters of crystallization, 6.95%, (calc. 6.02%). It occurs at an exothermic DTA peak of 139.1°C leaving a solid residue of $[Co_2(en)_4(CO_3)_2]\cdot 2sac$. Stage one was followed by stage two which took place at the DTA peak of 216.4°C, and it was exothermic. The decomposition temperature proceeds at 204.7 to 221.5°C. This process eliminates the two carbonate ions. The weight loss of these ions was 13.09% (calc. 13.69%). The solid residue was $[Co_2(en)_4]\cdot 2sac$. The third stage was assigned to the weight loss of two (en) ligand and sac ligand at the DTA peak of 306.4°C. The decomposition temperature was exothermic and it occurred in the temperature range of 293.4 to 329.3°C. The weight loss was 30.14% (calc. 27.08%) with the solid residue of $[Co_2(en)_2]\cdot sac$. Stage four took place in the temperature range of 402.1 to 420.6°C and it occurred without any endothermic or exothermic DTA temperature peaks. This implies the loss of the two en ligands, which was found to be 6.15% (calc. 6.69%) and it leaves the solid residue of $[Co_2]sac$. The last stage happens in the temperature range of 443 to 825°C. It has two DTA peaks, one at 645°C (exothermic) and the other one at 822.3°C (endothermic). The degradation loses the sac ion and leaves the solid residue of $[Co_2]$ metal. The sac ion lost had a weight loss of 20.49% (calc. 20.38%).

4.6 References

1. D. P. P. David J. Ager, Scott A. Henderson, Alan R. Katritzky, Indra Prakash, D. Eric Walters, *Angew. Chem. Int. Ed.*, 1998, **37**, 1802-1817.

2. G. Jovanovski and B. Kamenar, *Acta Cryst.*, 1982, C**11**, 247-255.

3. S. Z. Haider, K. M. A. Malik and K. J. Ahmed, *J. Bangladesh Acad. Sci.*, 1981, **5**, 81-90.

4. S. Z. Haider and K. M. A. Malik, *J. Bangladesh Acad. Sci.*, 1982, **6**, 119-125.

5. V. T. Yilmaz, S. Guney, O. Andac and W. T. A. Harrison, *Polyhedron*, 2002, **21**, 2393-2402.

6. O. Z. Yeşilel, C. Darcan and E. Şahin, *Polyhedron*, 2008, **27**, 905-913.

7. B. Sen and R. L. Dotson, *J. Inorg. Nucl. Chem.*, 1970, **32**, 2707-2716.

8. D. G. Brannon, R. H. Morrison, J. L. Hall, G. L. Humphrey and D. N. Zimmerman, *J. Inorg. Nucl. Chem.*, 1971, **33**, 981-990.

9. A. Karadag, V. T. Yilmaz and C. Thoene, *Polyhedron*, 2001, **20**, 635-641.

10. N. S. Poonia, N. Chhabra, W. S. Sheldrick, G. Hundal, S. Obrai and M. S. Hundal, *Acta Cryst.*, 1999, C**55**, 24-26.

11. O. Andac, S. Guney, Y. Topcu, V. T. Yilmaz and W. T. A. Harrison, *Acta Cryst.*, 2002, C**58**, m17-m20.

12. V. T. Yilmaz, S. Hamamci and C. Thöne, *J. Coord. Chem.*, 2003, **56**, 787-795.

13. S. Hamamci, V. T. Yilmaz and C. Thone, *Acta Cryst.*, 2002, E**58**, m700-m701.

14. C. A. Johns and K. M. Abdul Malik, *Polyhedron*, 2002, **21**, 395-401.

15. V. T. Yilmaz, S. Guney, O. Andac and W. T. A. Harrison, *J. Coord. Chem.*, 2003, **56**, 21-32.

16. G. Jovanovski, P. Naumov, O. Grupcče and B. Kaitner, *Eur. J. Solid State Inorg. Chem.*, 1998, **35**, 579-590.

17. V. T. Yilmaz, Y. Topcu, F. Yilmaz and C. Thoene, *Polyhedron*, 2001, **20**, 3209-3217.

18. S. Z. Haider, K. M. A. Malik, S. Das and M. B. Hursthouse, *Acta Cryst.*, 1984, C**40**, 1147-1150.

19. S. G. Real, S. B. Ribotta and A. J. Arvia, *Corros. Sci.*, 2008, **50**, 463-472.

20. Z. Yugeng, L. Jianmin, W. Jing, W. Xingtao and D. Shaowu, *Cryst. Res. Technol.*, 1994, **29**, 975-980.

21. K. Nakamoto, in *Handbook of Vibrational Spectroscopy*, John Wiley & Sons, Ltd, 2006.

22. S. Z. Haider, K. M. A. Malik, K. J. Ahmed, G. B. Kauffman and M. Karbassi, in *Inorg. Synth.*, John Wiley & Sons, Inc., 2007, 47-51.

23. S. Kirschner, *Inorg. Synth.*, Wiley, 2009, 47-50.

24. S. Guney, V. T. Yilmaz and W. T. A. Harrison, *J. Coord. Chem.*, 2006, **59**, 1123-1130.

25. M. A. Cinellu, L. Maiore, A. Schier, H. Schmidbaur and D. Rossi, Z.Naturforsch., 2008, **b63**, 1027-1034.

26. Z. Yugeng, *Trans. Met. Chem.*, 1994, **19**, 446-448.

27. S. Z. Haider, K. M. A. Malik, K. J. Ahmed, H. Hess, H. Riffel and M. B. Hursthouse, *Inorg. Chim. Acta*, 1983, **72**, 21-27.

28. I. Bulut, H. Pasaoglu, G. Kastas and A. Bulut, *Acta Cryst.*, 2007, E**63**, m2409-m2410.

29. J. Bernstein, R. E. Davis, L. Shimoni and N.-L. Chang, *Angew. Chem. Int. Ed.*, 1995, **34**, 1555-1573.

30. O. V. Quinzani, S. Tarulli, O. E. Piro, E. J. Baran and E. E. Castellano, *Z. Naturforsch.*, 1997, **52**, 183-187.

31. P. A. M. Williams, E. G. Ferrer, K. A. Pasquevich, E. J. Baran, Z. Chaia, E. E. Castellano and O. E. Piro, *Z. Anorg. Allg. Chem.*, 2000, **626**, 2509-2514.

32. Y. Topcu, O. Andac, V. Yilmaz and W. Harrison, *J. Coord. Chem.*, 2002, **55**, 805-815.

33. V. T. Yilmaz, O. Andac, A. Karadag and W. T. A. Harrison, *J. Mol. Struct.*, 2002, **641**, 119-124.

CHAPTER 5

CONCLUSION AND FUTURE PROSPECTS

5.1 CONCLUSION

This study focused on the synthesis and characterization of saccharinato complexes of various group 9 to group 12 metals using dimethyl sulfoxide and ethylenediamine, N-methyldiethanolamine and 2-(methylamino)ethane as auxiliary ligands. The ligands were coordinated to the common starting complexes $[M(sac)_2(H_2O)_4]\cdot 2H_2O$. The study successfully demonstrated the synthesis and characterization of 12 new saccharinato complexes using the following metal centres: Cd^{2+}, Zn^{2+}, Co^{2+}, Ni^{2+}, Hg^{2+} and Cu^{2+}. A number of complexes were characterized by solution NMR, i.e. complexes (**1**), (**3**), (**4**) and (**11**), supporting their proposed molecular structures. All complexes in the study were analysed by IR and have distinctive peak stretches owing to the presence of coordinated ligands. Micro-analysis performed on the complexes proved useful in demonstrating bulk purity. The complexes all had good to excellent percentage yields ranging from 75 to 95%. Melting points were sharp, further indicating sample purity. Some of the complexes decomposed at various temperature ranges. The thermal behaviour of the complexes were studied using DTA and TG in nitrogen atmosphere, and showed complex stability up to 200 °C. Single crystals of suitable quality for X-ray studies were grown for eight of the twelve complexes. All complexes containing DMSO were successfully solved by single crystal X-ray diffraction. Interestingly, this study reports on synthesis methods for complexes ((**6**), (**9**) and (**12**)) whereby saccharine acts as a weak counter ion, i.e. not in the first coordination sphere of the metal centre. Complex (**9**) also had a weak cuprophilic Cu···Cu interaction of 3.016 Å. The UV-vis spectroscopy showed λ_{max} for ligand-to-ligand charge-transfer intraligand for d^{10} complexes and λ_{max} for metal-to ligand charge transfer (MLCT) transition at very low energy intensities.

5.2 FUTURE PROSPECTS

The saccharinato ligand has been successfully applied to transition-metal coordination chemistry. Most such complexes coordinate to metal centres in a number of different coordination modes via the N-donor atom, O-donor atoms of sulfonyl and carbonyl group. The chemistry of sulfonyl coordination through the O-donor atom needs further development. Removal of one sulfonyl O atom leading to sulfinyl type derivatives can also be interesting as it could lead to isomers as chirality is introduced. Another branch of unexplored coordination chemistry is possible ring-opening reactions of saccharin.

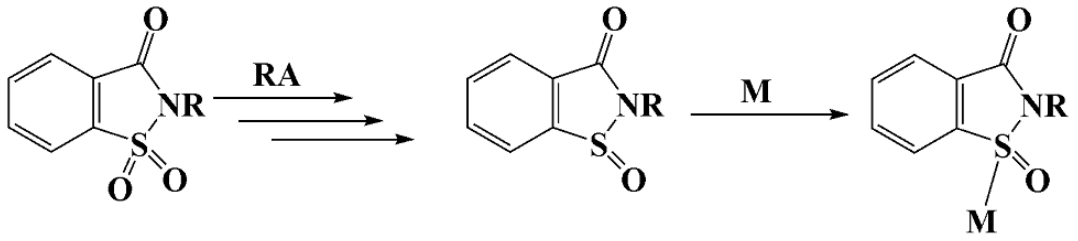

Scheme 5. 1 Reduction of sulfonyl O-donor atom leading to sulfinyl type derivative which can be further coordinated to metals, RA is a reducing agent

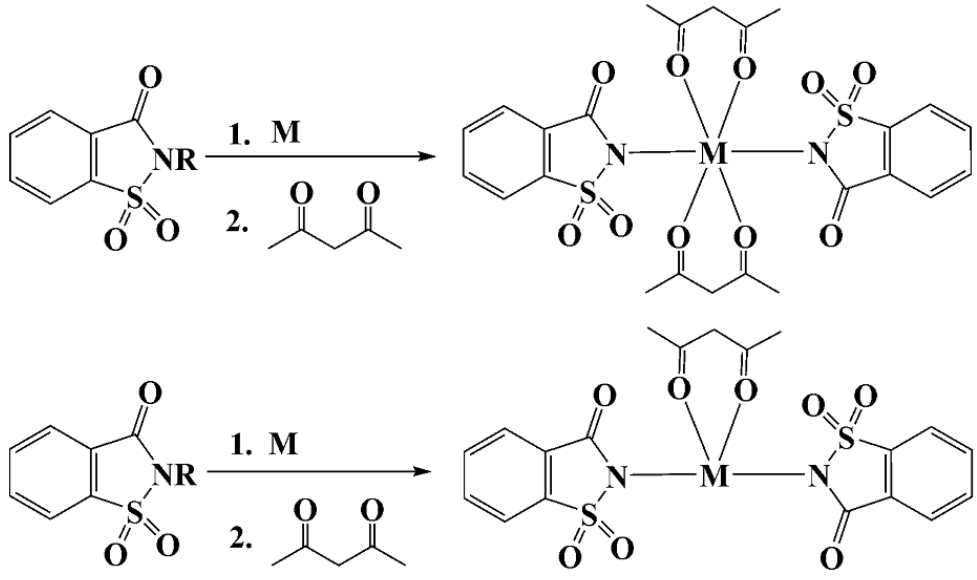

Scheme 5. 2 A possible ring-opening reaction of saccharin

APPENDIX

The work on this dissertation is supported by the spectral data, TGA graphs and the (*cif* file) which include the X-ray crystallographic data. All this appendix is attached on the CD.